Model-based Estimation of State of Charge of Lithium Cells

Nimitt Bhatt

Master of Science Thesis

TU Delft Delft University of Technology

Delft Center for Systems and Control

Model-based Estimation of State of Charge of Lithium Cells

Master of Science Thesis

For the degree of Master of Science in Systems and Control at Delft University of Technology

Nimitt Bhatt

June 27, 2011

Faculty of Mechanical, Maritime and Materials Engineering (3mE) · Delft University of Technology

Abstract

Lithium ion (Li-ion) batteries have been used extensively in mobile electronic devices and lately the focus has been shifted to more demanding applications like Hybrid and Electric vehicles. In these applications a battery pack may consist of hundreds of individual cells delivering the required electrical energy and power. As battery sizes and usage increase, we need new battery control and management strategies to improve the performance, safety, reliability and to improve the lifetime of the battery pack. The State of Charge (SoC) of each individual cell is one of the most important parameters for control. Roughly speaking it indicates how much energy is stored in the cell. It is represented from 0% to 100% describing the available energy left as a percentage of full capacity. Internally each cell can be viewed as a dynamic system governed by diffusive mass transport processes leading to a parabolic partial differential equation (PDE) system. The SoC can be viewed as an internal state of this system. The goal here is to estimate this state considering the cell as a SISO system with dis/charge current as the input and terminal voltage as the measurable output. In the case of mobile electronic devices, the low magnitude almost constant dis/charge current does not excite all the dynamics inside the cell and thus a simplified electric equivalent model with 2-3 states or a black box approach yield satisfactory results. However electric traction applications combined with regenerative braking, excite the cells at high frequency with high magnitude transient peaks of both discharge and charge currents. Since the cell is inherently an infinite dimensional PDE system, it responds at a wide range of time scales and thus simplified electric equivalent models or black box models do not provide satisfactory estimates of SoC. While discretization of PDEs and online solution of the resulting set of ordinary differential equations can result into an accurate SoC estimate, it is highly computationally expensive, slow and possibly non-convergent due to implicit relationships and thus prohibiting its real-time implementation. On the other hand, model order reduction techniques can be used on this high order discretized model but in this case, to incorporate non-linearities becomes difficult and again the SoC estimates are poor. Here we present an innovative technique wherein the order of the discretized model is kept high but it is considered as a spatially distributed string interconnected system. Each element after discretization is modeled as an explicit non-linear state space model of comparatively lower order. These elements are string interconnected to form the high order cell model. An efficient state-estimation algorithm is

developed for this interconnected system which exploits the structure of the system to reduce the computational cost. Using this approach, an RMS SoC estimation error of around 2% was obtained with transient dis/charge current profiles as high as 300A with a reasonable computational cost. The computation time per step required by this algorithm was found to be less than 0.15sec. From the literature, it is found that iterative algorithms can take as high as 2.8sec of computation time in order to obtain the SoC at a particular time. Thus we achieved significant improvement in computational cost without compromising accuracy using this efficient technique. Further, the algorithm is parallelizable upto 6 times thus enabling a real time implementation possible upto 40Hz using parallel processing. Moreover the algorithm does not suffer from convergence issues since an explicit state-space model has been developed. Apart from this application, the efficient state-estimation algorithm developed in this thesis can be used for many other PDE systems or systems which are inherently spatially distributed in a string interconnected form. The gain in computational cost will be higher as the number of sub-systems N grows, since this algorithm using a structured approach has $O(N)$ computational complexity while traditional unstructured algorithm yields $O(N^3)$ computational complexity.

Table of Contents

List of Figures

Acknowledgements

About an year ago, I started working on my graduation project at the Delft University of Technology. I got introduced to the topic of State of Charge estimation of a battery during the first introductory meeting with my supervisors. I found this research topic very interesting since it had scope for both fundamental and application oriented research. During the first phase of literature review, I was able to identify the important challenges faced by the research community in this field. Subsequently I started working towards a new innovative approach and was able to achieve significant improvement over current methodologies.

This has only become possible due to the exceptional supervision that I received during this entire project. I would like to thank my immediate supervisor dr.ir. Matteo Corno for his constant help, support and encouragement. I would also like to thank my other supervisor Prof.dr.ir. Michel Verhaegen for the thorough guidance that he provided me. All the meetings and discussions with both of them were very fruitful and thought-provoking. I always got motivated to try something new. I would also like to sincerely thank Corrado Locati for being a part of the thesis committee as an external member.

In addition, I would like to thank the developers of the Sequentially Semi-Separable Matrix Toolbox at the DCSC which I have used during my project. Also thanks to all the friends at DCSC for their important comments and suggestions during the colloquiums and monthly workshops. I would also like to thank all the professors who taught me during the last two years of my master's study program in Systems and Control. The fundamentals learned during the coursework helped a lot while performing research. Also special thanks to the program coordinators, the international office, DCSC secretariat and the service desk.

Many thanks to all my friends here, who made my stay a lot of fun! It was very nice discussing about my research with them too. I would also like to thank my friends and relatives abroad for being in touch over Skype.

Finally I would like to wholeheartedly thank my parents and sister for constantly supporting and encouraging me from half way around the world.

Delft, University of Technology — Nimitt Bhatt
June 27, 2011

"When the five senses fail to provide direct information, human beings rely on post-sensory cognitive function of the brain to interpret sensory inputs to derive new information. Fortunately for dynamic systems, this can be done more mathematically using modeling and state-estimation."

Chapter 1

Introduction

Lithium ion (Li-ion) cells are all around us; in cell phones, digital cameras, laptop computers and in many other mobile electronic devices. Recently they have been considered for more demanding applications like Hybrid and Electric vehicles. As battery sizes and usage increases, we need new battery control and management strategies to improve the performance, safety, reliability and to improve the lifetime of the battery pack. Particularly in the case of hybrid and electric vehicles where the battery is subjected to sudden peaks of both drawn and recharge power compared to almost constant discharge current in the case of mobile electronic devices. The State of Charge (SoC) of the battery is one of the most important parameters for control. Roughly speaking it indicates how much energy the battery is left with. Apart from control, accurate knowledge of this quantity is also very important from the driver's point of view especially when electric energy inside a battery is the only source of power for the vehicle. The main problem is that it is not possible to physically measure this quantity. This opens up the application of estimation theory where this quantity can be estimated using other physically measurable quantities in a Li-ion cell. This thesis work is a research in this direction, developing new accurate estimation technique to estimate the SoC of a Li-ion cell using a model-based approach.

In this chapter, we'll first overview the motivations of accurate SoC estimation, the difficulties associated and a brief summary of findings from the Literature survey. In section 1-2 we'll describe our own approach to this problem, and outline the specific goals and contributions of this thesis. Following that in section 1-3 we'll describe the organization of the chapters that follow and an outline of this thesis.

1-1 Motivations and State of Art

The major motivation driving research in this field is the sharp increase of Hybrid and Electric vehicles. In conventional vehicles, the measurement of remaining gasoline available is a fairly simple problem solved by measuring the level of fluid in the tank. However, when a battery is used as an energy source in vehicles the estimation of the remaining useful capacity commonly

known as the SoC is non-trivial. Especially in these **high transient applications** where the battery is subjected to high transient peaks of discharge and charge currents which arise from sudden acceleration and regenerative braking maneuver. We'll explain what happens during this scenario using a simplified diagram of a cell Figure 1-1.

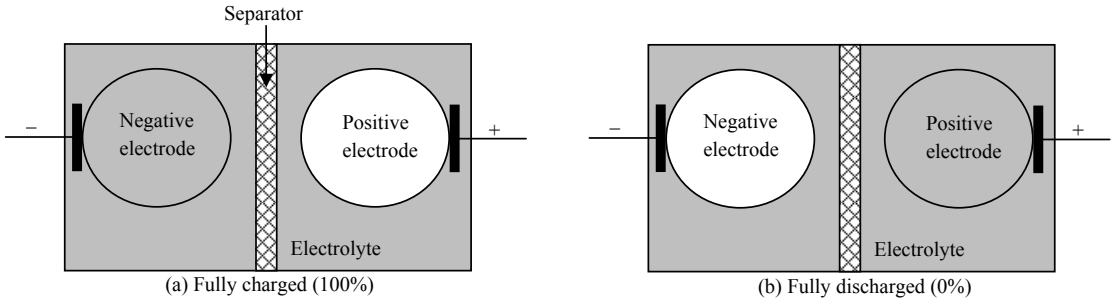

Figure 1-1: Simplified Li-ion cell schematic showing fully charged and fully discharged conditions

As shown, the cell consists of a negative electrode and a positive electrode immersed in an electrolyte. The electrolyte regions of the negative and the positive electrode are separated by a separator. Since this is a simplified diagram, the electrodes are shown lumped, as spheres. When the cell is fully charged, the negative electrode is fully lithiated i.e. the concentration of Li ions is maximum, represented by gray color in the figure. The electrolyte solution will have nominal concentration of Li ions, while the positive electrode is fully deprived of Li ions. As the cell discharges, the Li ions convert from solid phase to liquid phase at the surface of the negative electrode. They travel through the electrolyte across the separator and reach the positive electrode. At the surface of the positive electrode, they again convert from liquid phase to solid phase and slowly the positive electrode gets lithiated. Thus during discharge, the concentration of Li ions decreases at the negative electrode while it increases at the positive electrode and finally becomes maximum. The exact opposite process happens during charging. End of dis/charge is nothing but saturation or depletion of Li ion concentration at either electrode. These values of saturation / depletion of concentration can now be considered as 0% and 100% SoC and the whole intermediate range can provide a measure of SoC in percentage.

Since it is not possible to measure the concentration of Li ions and obtain this quantity directly, we need to estimate it using the Terminal Voltage of the cell. This terminal voltage is directly correlated to Li ion concentration at the surface of the electrodes. As can be seen from the Figure 1-1, the terminal contacts can only give information of the surface concentration, not the bulk concentration. During charge and discharge currents of very low magnitude, the surface concentration is almost equal to the bulk concentration and the terminal voltage can provide a measure of the SoC directly and there is no need of dynamic models. As the dis/charge current severity increases, **gradients** start forming in the electrodes as shown in Figure 1-2 in which the discharge condition is shown. This happens because the transport of Li ions from the inner regions to the surface happens by means of diffusion and if the current is high, the diffusion is not able to match up with the reaction rate at the surface and the concentration at the surface becomes lower compared to the inner regions at the negative electrode. The exact opposite happens at the positive electrode. Moreover the transport of Li ions through the electrolyte again by diffusion can also prove to be sluggish and resulting

into gradients as shown in Figure 1-2. Thus the cell can now be considered as a dynamic system, with current as the input, terminal voltage as the measurable output and the internal dynamics governed by these diffusion phenomena. The SoC can be considered as an internal state of the system which is nothing but the bulk concentration which needs to be estimated using the Terminal voltage which is statically correlated to the surface concentration.

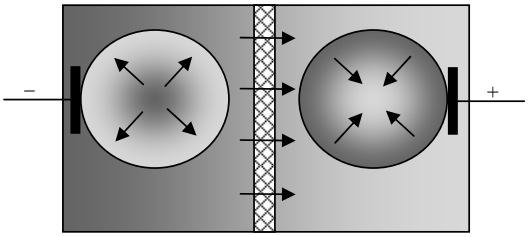

Figure 1-2: Simplified Li-ion cell schematic showing concentration gradients during high rate discharge

For mobile electronic devices, the dis/charge current is almost always direct current of low magnitude which does not excite all the dynamics of a cell and thus simplified electric equivalent circuit models with 2-3 states or black box models fitted to data or empherical models can give satisfactory results. However when it comes to electric vehicle application, due to high magnitude transient current profiles, severe gradients are formed inside the cell. For instance, with a very high continuous discharge current, the surface of negative electrode can become totally depleted of Li ions only in a few seconds. The terminal voltage correlated to the surface concentration will show that the cell is empty though it does not mean that the cell is actually empty. If kept at rest for some time, the Li ions will diffuse from the inner regions to the surface and further current can be drawn from the cell. In this situation, a battery management system should accurately know at what time and what magnitude of current can be further drawn from the cell. This requires an accurate model along with a state estimator which can provide accurate results with high rate transient current profiles. It is argued in [1] that diffusive mass transport processes, with an infinite number of negative real eigenvalues, cause batteries to respond across a range of time scales, equivalent circuit models with just 2-3 states cannot be expected to predict accurately the current/voltage behavior across such disparate time scales.

Several techniques using **electric equivalent circuit models** have been tried in the literature like the mixed-algorithm proposed in [2] or electric equivalent model combined with an extended kalman filter algorithm in [3] however results with high dis/charge current profiles are not shown. Results are shown only with less than 1C of dis/charge current profiles. Note that here C-rate is used as a standard way to represent the current with respect to the cell capacity. For instance if the cell capacity is 6Ah then 1C of current is 6A, similarly 10C is 60A. For a vehicle application sudden peaks of dis/charge currents can reach as high as 50C. A very detailed algorithm with electric equivalent circuit model is found in [4] using an extended kalman filter along with a noise model and data rejection algorithm. However, accurate results ($\pm 2\%$ SoC error) have been shown only with a scaled down automotive current profile, 5 times smaller than the actual profile.

Many **black box models** have also been tried in the literature like a rule based fuzzy logic model is used in [5] however an accuracy of around 5% has been shown only with low magnitude constant currents. Results with a Radial Basis Function model have been shown in [6] and [7] and a maximum absolute error in SoC estimation is found to be approximately 3% at ±4C rate. Though it exhibited unreliable performance when ported to the battery management system of the pack with a different test data. This is a major shortcoming with black box models. Since the black box models lack any physical insights, they may not be considered very reliable. It is difficult to understand and argue why the model is working and why not in different scenarios. The main problem is that they predict system behaviour best when the system is operating in the same regime where data was collected to train the model. If they are trained with sequence of transient currents, they fail to work well in constant current or rest scenario which may be encountered in practice.

The need arises for the most accurate physics based **white box models**. Apart from high accuracy another advantage of these models is that the variables have physical meaning, facilitating a constraint management system based on estimation of these physical variables. This can prove to be extremely beneficial in terms of full utilization of the battery. The electrochemical processes inside the cell are described by partial differential equations. The best method would be spatial discretization and numerical solution of the set of coupled ordinary differential equations online. However this method would be highly computationally expensive, slow and possibly non-convergent and thus prohibiting its real-time implementation. There is a need to develop reduced order models without significant compromise in the accuracy. The model developed in [1] is an attempt in this direction. Quite accurate as well as lower order but since the reduced order model is generated numerically, it loses its analytical form and thus it is observed that treating non-linearities becomes difficult. An estimator based on a linear model is shown in [8] and is found to be accurate (±5%) only in the middle SoC range of 30-70% with 10C pulse discharge currents. The major challenge is that due to the coupled nature of the non-linear partial differential equations, obtaining an explicit non-linear state-space form of the whole system is not trivial. There are estimation algorithms which do not need this explicit representation like the sigma point kalman filter. In [9], the model is not explicitly formulated as a state-space model. The algorithm solves the system of non-linear differential algebraic model equations which are based on the fundamental equations at each sigma point. It is shown that this method gives accurate SoC estimates (±2%) in high rate operation upto 20C. However transformation at each sigma point is required which involves high computational cost and it increases as the number of sigma points chosen gets higher for better accuracy.

We can conclude that only the models based on fundamental electrochemical equations can provide accurate estimation results in the presence of high rate current profiles. We also conclude that only a little research has been done with very high rate current profiles typical for electric vehicles and there are some pros and cons with each approach. In the last approach discussed, the accuracy is high only because the algorithm solves non-linear fundamental equations for each sigma point at each time instant. As a result the computational cost involved is very high. Thus the major challenge here is to develop new estimation algorithms based on fundamental model equations which are computationally efficient.

1-2 Scope and Contributions of this Thesis

In the approach presented in this thesis, we utilize the fundamental electrochemical equations and form an explicit non-linear state-space representation of the system. First we start with the procedure that is utilized while solving the PDEs online, that is discretization. The second step would be to solve these huge number of discretized equations with implicit relationships which is the main cause of slow and perhaps non-reliable solution time due to convergence issues. Instead we use a different approach. We obtain lower order non-linear state-space representation of each finite element. Some assumptions need to be made to make the model explicit. Then we consider the whole model as spatially distributed string interconnected system formed of these elements as sub-systems. An efficient state-estimation algorithm is developed for this type of interconnected system which exploits the structure of the model to reduce the computation time. That is, the whole system is of high order but composed of lower order sub-systems. Moreover the algorithm is parallelizable and computation time can be further reduced by using parallel processing. Since it is in explicit form, the computation time is always constant, reliable and convergence issues are not encountered. Thus we gain accurate SoC estimation with reasonable computation time. Apart from this, since the model is based on spatial discretization of fundamental equations, all variables have physical meaning. The model can accurately estimate the gradient of different variables along space and can be very useful for a battery management system, to increase the life of the cell without compromising on the usable capacity range. Since normally what is done is to increase the life of the battery, its use is limited from say 25% to 90% SoC, which underutilizes a significant part of an expensive battery. We enumerate the contributions of this thesis as follows,

1. An **efficient Extended Kalman Filter (EKF)** is developed for spatially distributed string interconnected system using a structured approach. Using the Li-ion cell as an example, it is shown that the computational complexity of this algorithm is of $O(N)$ where N is the number of sub-systems in this interconnected scheme. Note that here with $O(\cdot)$ we represent how the computational cost grows as a function of the size of the problem [1].
2. A Lithium ion cell is discretized along spatial dimensions and **modeled as a spatially distributed string interconnected system**. Explicit non-linear state-space model for each sub-system of this interconnected system is derived. The validity of this model is shown.
3. An **efficient SoC estimation algorithm** is developed using this model and the efficient EKF after solving some observability issues of the model. Results of accurate SoC estimation with high magnitude dis/charge current profiles are shown.

1-3 Thesis Outline

We first start with some fundamentals of Spatially distributed string interconnected system in Chapter 2. It deals with the issue of well posedness of interconnected systems, Sequentially

[1] Formally, a positive function $f(N) \in O(N^{\alpha})$ if there exist finite positive constants, $\infty > c, \kappa > 0$ such that $f(N) < cN^{\alpha}, \forall N > \kappa$ [10].

Semi Separable (SSS) structured matrix approach and efficient SSS arithmetic. These fundamentals are utilized in Chapter 3 to develop an efficient state-estimation algorithm for these interconnected systems. Each step of a traditional algorithm will be taken and modified to make it efficient having $O(N)$ computational complexity.

In Chapter 4, a Li-ion cell is modeled as spatially distributed string interconnected system based on spatial discretization of fundamental electrochemical equations. Validation of newly developed model is also done. Using this model and the efficient algorithm of Chapter 3, an SoC estimator is developed in Chapter 5. After solving some observability issues, SoC estimation results are presented.

Chapter 2

Spatially Distributed Interconnected Systems

2-1 Introduction

Many physical, chemical or biological processes can be described by Partial Differential Equations (PDE). These equations describe the phenomena distributed in one or more spatial dimensions with time. Spatial discretization of these equations lead to a special class of system known as Spatially distributed interconnected system. These are the systems consisting of finite or infinite number of sub-systems which directly interact with their nearest neighbors. Though spatial discretization of a PDE is not the only way of arriving at such a system. Some systems are inherently in this form as enlisted in [11] like for example highway traffic control and vehicle platooning, iterative circuit networks, building anti-earthquake systems, aircraft and satellite formation flight, large adaptive telescope mirrors, image processing, paper processing, irrigation networks, etc. The references to these applications can be found in [11].

These interconnected systems can be distributed in one, two or even three spatial dimensions with finite or infinite number of building blocks. They can be string interconnected or can even have periodic interconnections [12] as shown in Figure 2-1. These systems can be spatially invariant meaning that the system dynamics of each sub-system is exactly the same or they can be spatially varying. In this work, we will only focus on string interconnected spatially varying systems distributed in one dimension with finite number of building blocks as shown in Figure 2-2 where, Σ_1 to Σ_N are dynamic systems interconnected by interconnecting variables v_2^m to v_N^m and v_1^p to v_{N-1}^p. This choice has been made since spatial discretization of One Dimensional (1D) PDEs with spatially varying coefficients and boundary conditions give rise to such kind of systems. The same will be the case of a Lithium ion (Li-ion) cell model which is illustrated in Chapter 4.

Further each building block of the system can be linear or non-linear, time invariant or time varying. In the following section, we will first start with analysis of a non-linear interconnected system. The property of spatially strictly properness of the interconnected system

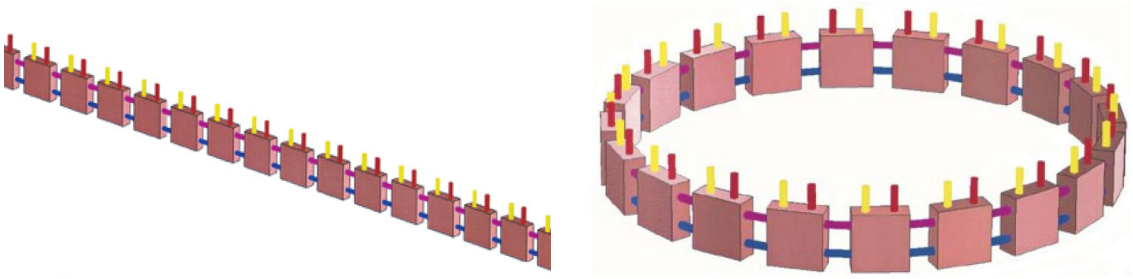

(a) String interconnected system in 1D

(b) Periodic interconnected system in 1D

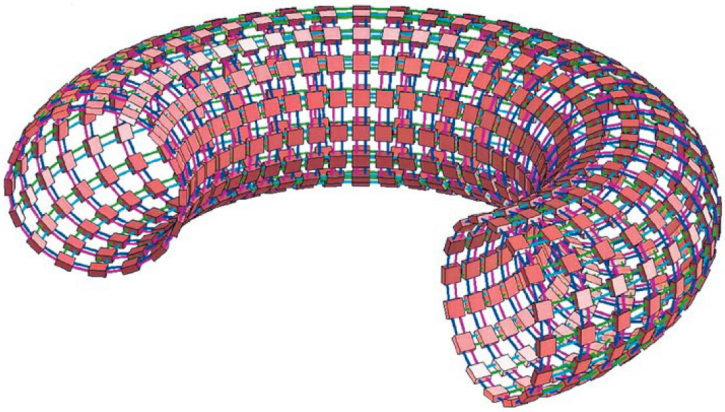

(c) Periodic interconnected system in 2D

Figure 2-1: Different forms of spatially distributed interconnected systems [12]

is introduced and the issue of "well posedness" of the system is discussed. In section 2-3 only linear state-space representation of each sub-system is considered and a special structure of the system as a whole (lifted system) is shown. This structured matrix has a closed form efficient arithmetic of its own which will be discussed in section 2-4. The theoretical and mathematical base of this chapter will be utilized in developing efficient state-estimation algorithms in Chapter 3.

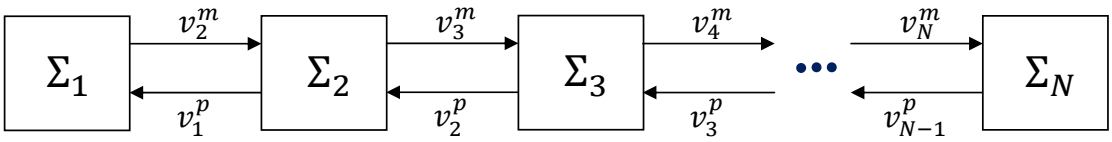

Figure 2-2: String interconnected system with interconnecting variables (Exogenous inputs and outputs are not shown)

2-2 Well Posedness

Consider a string interconnected system with only two building blocks as shown in Figure 2-3.

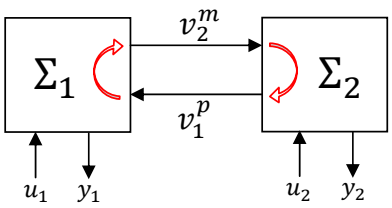

Figure 2-3: String interconnected system with only two sub-systems

First let us assume that the system is spatially strictly proper meaning that there is no direct feed-through between the interconnecting variables on the same side of a building block, shown as red colored arrows in the Figure 2-3. Though it does not mean that there is no direct feedthrough between interconnecting variables on the opposide sides of a building block. Direct feedthrough is allowed say between signals entering on left hand side of a building block and leaving on right hand side of the same block. It can be clearly seen from the figure that due to these red colored feedthrough terms, algebraic loops are formed and a general closed form representation of the system as a whole becomes difficult. This will be more clear with some mathematical treatment.

In the case of spatially strictly proper system, the non-linear dynamic equations of each building block can be written as,

$$\begin{aligned} \dot{x}_1 &= f_1\left(x_1, v_1^p, u_1\right) \\ v_2^m &= g_{12}\left(x_1, u_1\right) \\ y_1 &= h_1\left(x_1, v_1^p, u_1\right) \end{aligned} \tag{2-1}$$

Similarly for the second sub-system,

$$\begin{aligned} \dot{x}_2 &= f_2\left(x_2, v_2^m, u_2\right) \\ v_1^p &= g_{21}\left(x_2, u_2\right) \\ y_2 &= h_2\left(x_2, v_2^m, u_2\right) \end{aligned} \tag{2-2}$$

where x_s is the state vector of the sub-system Σ_s. v_s^p and v_s^m are the interconnecting variables and u_s and y_s are the exogenous inputs and outputs. Each sub-system Σ_s is allowed to be arbitrarily different from every other, even having different state, input, and output dimensions, as long as the interconnections are of correct size.

In this case, it can be clearly seen that a closed form representation of the whole system is possible by eliminating the interconnecting variables from the equations above as,

$$\begin{aligned} \dot{x}_1 &= f_1\left(x_1, g_{21}\left(x_2, u_2\right), u_1\right) \\ \dot{x}_2 &= f_2\left(x_2, g_{12}\left(x_1, u_1\right), u_2\right) \\ \text{Say, } \ \dot{\bar{x}} &= f\left(\bar{x}, \bar{u}\right) \end{aligned} \tag{2-3}$$

where the state vector $\bar{x}$ is obtained by stacking the individual state vectors of sub-systems, same for exogenous inputs $\bar{u}$ and outputs $\bar{y}$. Similarly the non-linear output equations of the lifted system are,

$$\begin{aligned} y_1 &= h_1\left(x_1, g_{21}\left(x_2, u_2\right), u_1\right) \\ y_2 &= h_2\left(x_2, g_{12}\left(x_1, u_1\right), u_2\right) \\ \text{Say, } \ \bar{y} &= h\left(\bar{x}, \bar{u}\right) \end{aligned} \tag{2-4}$$

However now let us look at the interconnected system that is not spatially strictly proper. The non linear equations can be written as,

$$\begin{aligned} \dot{x}_1 &= f_1\left(x_1, v_1^p, u_1\right) \\ v_2^m &= g_{12}\left(x_1, v_1^p, u_1\right) \\ y_1 &= h_1\left(x_1, v_1^p, u_1\right) \end{aligned} \tag{2-5}$$

For the second sub-system,

$$\begin{aligned} \dot{x}_2 &= f_2\left(x_2, v_2^m, u_2\right) \\ v_1^p &= g_{21}\left(x_2, v_2^m, u_2\right) \\ y_2 &= h_2\left(x_2, v_2^m, u_2\right) \end{aligned} \tag{2-6}$$

With these set of equations, it is not possible to eliminate the inter-connecting variables and arrive at a closed form representation of the whole system, since we run into an infinite recursion.

A particular assumption has to be made here to proceed further. We assume that the inter-connecting variables are linearly related. Non-linear state and exogenous input dependency is allowed. With this assumption, we arrive at the following equations,

$$\begin{aligned} \dot{x}_1 &= f_1\left(x_1, v_1^p, u_1\right) \\ v_2^m &= g_{12}\left(x_1, u_1\right) + Z_1^p v_1^p \\ y_1 &= h_1\left(x_1, v_1^p, u_1\right) \end{aligned} \tag{2-7}$$

For the second sub-system,

$$\begin{aligned} \dot{x}_2 &= f_2\left(x_2, v_2^m, u_2\right) \\ v_1^p &= g_{21}\left(x_2, u_2\right) + Z_2^m v_2^m \\ y_2 &= h_2\left(x_2, v_2^m, u_2\right) \end{aligned} \tag{2-8}$$

With this linearity assumption, we can now solve the system of linear equations,

$$\begin{bmatrix} I & -Z_1^p \\ -Z_2^m & I \end{bmatrix} \begin{bmatrix} v_2^m \\ v_1^p \end{bmatrix} = \begin{bmatrix} g_{12}\left(x_1, u_1\right) \\ g_{21}\left(x_2, u_2\right) \end{bmatrix} \tag{2-9}$$

Say,

$$E \begin{bmatrix} v_2^m \\ v_1^p \end{bmatrix} = \begin{bmatrix} g_{12}\left(x_1, u_1\right) \\ g_{21}\left(x_2, u_2\right) \end{bmatrix} \tag{2-10}$$

$$\begin{bmatrix} v_2^m \\ v_1^p \end{bmatrix} = E^{-1} \begin{bmatrix} g_{12}\left(x_1, u_1\right) \\ g_{21}\left(x_2, u_2\right) \end{bmatrix} \tag{2-11}$$

It is clear that the system is solvable if and only if the matrix E is invertible. This condition is known as "Well posedness" of the interconnected system. If the system is well posed, we can solve for the interconnecting variables using equation (2-11) and arrive at relations,

$$\begin{aligned} v_2^m &= j_1\left(x_1, u_1, x_2, u_2\right) \\ v_1^p &= j_2\left(x_1, u_1, x_2, u_2\right) \end{aligned} \tag{2-12}$$

and thus arrive at the closed form representation of the whole system,

$$\begin{aligned} \dot{x}_1 &= f_1\left(x_1, j_2\left(x_1, u_1, x_2, u_2\right), u_1\right) \\ \dot{x}_2 &= f_2\left(x_2, j_1\left(x_1, u_1, x_2, u_2\right), u_2\right) \\ &\text{Say, } \; \dot{\bar{x}} = f\left(\bar{x}, \bar{u}\right) \end{aligned} \tag{2-13}$$

Similarly for the output equations,

$$\begin{aligned} y_1 &= h_1\left(x_1, j_2\left(x_1, u_1, x_2, u_2\right), u_1\right) \\ y_2 &= h_2\left(x_2, j_1\left(x_1, u_1, x_2, u_2\right), u_2\right) \\ &\text{Say, } \; \bar{y} = h\left(\bar{x}, \bar{u}\right) \end{aligned} \tag{2-14}$$

Further it can be observed that a spatially strictly proper system is always well posed [12]. Here we explained the concept of well posedness in a very simplified manner however for a

detailed mathematical analysis the reader is referred to [12] and the references therein. We will observe later in the case of a Li-ion cell model that certain assumption has to be made in order to make the model well posed. Apart from that, some fundamentals illustrated in this section will be utilized in section 3-2 to develop efficient non-linear simulator for the interconnected system.

2-3 SSS Structure

In the previous section we investigated some issues of interconnected systems by considering non-linear sub-systems. However for many systems and control applications like optimal control design algorithms or estimation algorithms we need to linearize the system and work with linearized state-space representation of systems. Here in this section, we will deal with string interconnected systems which have linear / linearized state-space representation of each sub-system.

Consider the following linear state-space realization of a sub-system,

$$\Sigma_s : \begin{bmatrix} \dot{x}_s \\ v^p_{s-1} \\ v^m_{s+1} \\ y_s \end{bmatrix} = \begin{bmatrix} A_s & B^p_s & B^m_s & B^2_s \\ C^p_s & W^p_s & Z^m_s & V^p_s \\ C^m_s & Z^p_s & W^m_s & V^m_s \\ C^2_s & H^p_s & H^m_s & D^{22}_s \end{bmatrix} \begin{bmatrix} x_s \\ v^p_s \\ v^m_s \\ u_s \end{bmatrix} \tag{2-15}$$

These sub-systems are connected in series to form a string interconnected system. Again we observe that due to non-zero terms Z^m_s and Z^p_s terms, the system is not spatially strictly proper. For linear systems which are well posed, techniques are available to convert the system into spatially strictly proper form. For instance the change of variables technique shown in [11] where the interconnecting variables are transformed to eliminate the terms Z^m_s and Z^p_s. Further this technique has an $O(N)$ computational complexity. An extension to this technique with exogenous inputs and outputs is illustrated in Appendix A.

After converting to spatially strictly proper form, the system as a whole (lifted system) can be found by eliminating the interconnecting variables. It is simply a series connection of bilaterally coupled systems. The lifted system is represented by a bar on top of variables and matrices,

$$\bar{\Sigma} : \begin{bmatrix} \dot{\bar{x}} \\ \\ \bar{y} \end{bmatrix} = \begin{bmatrix} \bar{A} & \bar{B}_2 \\ \\ \bar{C}_2 & \bar{D}_{22} \end{bmatrix} \begin{bmatrix} \bar{x} \\ \\ \bar{u} \end{bmatrix} \tag{2-16}$$

Now consider an example of N sub-systems interconnected to form the lifted system, the matrix $\bar{A}$ will look like,

$$\bar{A} = \begin{bmatrix} A_1 & B_1^p C_2^p & B_1^p W_2^p C_3^p & B_1^p W_2^p W_3^p C_4^p & \ddots & \vdots \\ B_2^m C_1^m & A_2 & B_2^p C_3^p & B_2^p W_3^p C_4^p & \ddots & \vdots \\ B_3^m W_2^m C_1^m & B_3^m C_2^m & A_3 & B_3^p C_4^p & \ddots & \vdots \\ B_4^m W_3^m W_2^m C_1^m & B_4^m W_3^m C_2^m & B_4^m C_3^m & A_4 & \ddots & \vdots \\ \ddots & \ddots & \ddots & \ddots & \ddots & B_{N-1}^p C_N^p \\ \dots & \dots & \dots & \dots & B_N^m C_{N-1}^m & A_N \end{bmatrix} \tag{2-17}$$

This matrix has a special structure, called Sequentially Semi Separable (SSS). We follow the following notation for this type of structured matrix as,

$$\bar{A} = SSS\left(B_s^m, W_s^m, C_s^m, A_s, B_s^p, W_s^p, C_s^p\right) \tag{2-18}$$

where the arguments of $SSS\left(\right)$ are called the 'generator' matrices of $\bar{A}$. In the case of N interconnected systems shown above, the generator matrices are the system matrices of each part. Similar structure is observed in the other lifted matrices as well,

$$\begin{aligned} \bar{B}_2 &= SSS\left(B_s^m, W_s^m, V_s^m, B_s^2, B_s^p, W_s^p, V_s^p\right) \\ \bar{C}_2 &= SSS\left(H_s^m, W_s^m, C_s^m, C_s^2, H_s^p, W_s^p, C_s^p\right) \\ \bar{D}_{22} &= SSS\left(H_s^m, W_s^m, V_s^m, D_s^{22}, H_s^p, W_s^p, V_s^p\right) \end{aligned} \tag{2-19}$$

Thus we observed that the lifted system matrices of a spatially distributed string interconnected system has a particular structure known as Sequentially Semi Separable (SSS). We will exploit this structure while developing efficient state-estimation algorithm in Chapter 3 using the efficient SSS arithmetic illustrated in the next section.

2-4 SSS Arithmetic

The SSS matrix is a special type of data sparse matrix and the most interesting thing about them is that there exist algorithms of only $O\left(N\right)$ computational complexity for SSS matrix-matrix addition and multiplication, inversion, LU, and QR factorization, and further, that the class of SSS matrices is closed under these operations, that is, they are structure preserving. A detailed analysis of SSS structured matrix has been done in [10] and this structured matrix approach is used in developing efficient algorithms for distributed control. Here we'll show how SSS arithmetic works using a simple addition operation first.

To add together two conformably sized SSS matrices, $X = SSS\left(P_s^X, R_s^X, Q_s^X, D_s^X, U_s^X, W_s^X, V_s^X\right)$ and $Y = SSS\left(P_s^Y, R_s^Y, Q_s^Y, D_s^Y, U_s^Y, W_s^Y, V_s^Y\right)$ and obtain the SSS generator form of their sum: $X+Y = Z = SSS\left(P_s^Z, R_s^Z, Q_s^Z, D_s^Z, U_s^Z, W_s^Z, V_s^Z\right)$, simply perform the following computations,

$$\begin{gathered} P_s^Z = \begin{bmatrix} P_s^X & P_s^Y \end{bmatrix},\ D_s^Z = D_s^X + D_s^Y,\ U_s^Z = \begin{bmatrix} U_s^X & U_s^Y \end{bmatrix}, \\ V_s^Z = \begin{bmatrix} V_s^X \\ V_s^Y \end{bmatrix},\ Q_s^Z = \begin{bmatrix} Q_s^X \\ Q_s^Y \end{bmatrix},\ W_s^Z = \begin{bmatrix} W_s^X & 0 \\ 0 & W_s^Y \end{bmatrix},\ R_s^Z = \begin{bmatrix} R_s^X & 0 \\ 0 & R_s^Y \end{bmatrix} \end{gathered} \tag{2-20}$$

The derivation can be found in [10] and is based on simply treating the SSS matrices as the input output matrices of two Linear Time Varying (LTV) systems put in parallel. We can clearly observe from this SSS addition that the computation is $O(N)$. From the interconnected systems point of view, say N systems each of order n are interconnected and we perform addition operation on their lifted system matrices. If we increase the number of blocks N keeping n constant, the computational cost will grow linearly with N. While without any structured approach it will grow with $O(N^2)$. Exactly similar $O(N)$ computation techniques are available for multiplication and inverse operations. In those cases the advantage is much more since without structure the computational cost grows with $O(N^3)$. These computation techniques can be found in [10]. To develop efficient state-estimation algorithms we'll exploit the SSS arithmetic of these three operations; matrix addition, multiplication and inverse.

Looking carefully at the addition operation, we observe that the size of generator matrices of the result of addition is higher than the size of generator matrices of its operands. In iterative algorithms, like state-estimation algorithms, the size will keep on increasing. Fortunately there exist order reduction techniques to reduce the size of matrices with little loss of accuracy and the loss of accuracy can be controlled by means of setting a tolerance value. An $O(N)$ technique for order reduction of SSS matrices using balanced truncation method has been shown in [10]. All these computation techniques and reduction techniques have been used to develop a complete SSS toolbox at the Delft Center for Systems and Control (DCSC) [13]. This toolbox will be used to perform efficient calculations with SSS matrices in this thesis. A brief illustration of some functions of this toolbox which will be used here is provided below,

1. The function "sss" is used to build an SSS matrix from its generators, each of compatible size.

2. All the matrix operators '+', '−', '×', '$(\cdot)^T$' and '$(\cdot)^{-1}$' are overloaded with the standard matrix operators. Thus these operations with SSS matrices can easily be applied using standard Matlab syntax.

3. The function "construct" is used to construct an SSS matrix from any real unstructured matrix. If the matrix has no sequentially semi-separable structure, the size of generators will be large precluding any speed-ups. Dimensions of the required SSS matrix must be specified as inputs to this function.

4. The function "reduce", returns a compact SSS representation of matrix. After addition or multiplication a check is automatically applied to the SSS matrix, to see if a reduction is necessary. If this is true, this function is called automatically. It can also be called explicitly along with specifying a tolerance value. With this tolerance as additional input, the function compresses a given SSS representation to a prespecified tolerance.

Chapter 3

Efficient State Estimator

We discussed some fundamentals of Spatially distributed string interconnected systems in the last chapter. For many applications, we need to estimate the states of each sub-system of this interconnected system using limited number of available measurement signals. These available measurements can be from each sub-system or can be even from only a limited number of sub-systems or in some cases as a linear combination of outputs from different sub-systems. For instance, we will observe that in the case of a Lithium ion (Li-ion) cell modeled as spatially distributed string interconnected system (Chapter 4), the measurable signal is the difference between the output from the last block to that of the first block (Terminal voltage). A centralized state-estimator can be developed which takes the inputs and the measurement signals and estimates the states of all sub-systems. However as the number of sub-systems grows; the computation cost per time step grows very fast and it becomes infeasible to implement the algorithm online. In this chapter we'll develop an efficient state estimation algorithm based on Extended Kalman Filter (EKF) with a computational complexity of $O(N)$. First the basic three steps of an EKF are illustrated in section 3-1 and subsequently, techniques to make each step efficient are shown. The idea is to exploit the structure of the whole system which is of very high order but formed by interconnection of lower order sub-systems in a particular form. This efficient estimation algorithm is then applied in Chapter 5 to estimate the State of Charge (SoC) of a Li-ion cell modeled as spatially distributed string interconnected system.

3-1 Extended Kalman filter

The Kalman filter is a computational scheme to reconstruct the state of a given linear state-space model in a statistically optimal manner, which is generally expressed as the minimum variance of the state-reconstruction error conditioned on the acquired measurements [14]. Basically, a Kalman filter runs in parallel with the system and uses all the inputs and measurement outputs of the system at a given point in time to find the minimum mean squared error estimate $\hat{x}_k$ of the true state x_k in the presence of process noise w_k and measurement

noise v_k. This is only possible if the system is observable. A system is observable if for any time $T > 0$ it is possible to uniquely estimate the states for $t \in [0, T]$ based on knowledge of inputs and outputs for $t \in [0, T]$ [15]. For systems which are not fully observable, sometimes a milder condition of detectability is used. A system is detectable if the eigenvalues corresponding to the unobservable states are asymptotically stable and thus the difference between the real states and the estimated states go to zero as $k \to \infty$. If not detectable also, then a Kalman filter cannot be designed for that system. For the noise, it is assumed that the process noise and the measurement noise are additive, white and Gaussian, with zero mean and covariance matrices Σ_w and Σ_v respectively. An Extended Kalman Filter is simply an extension to the linear Kalman Filter wherein the algorithm runs by linearizing the non-linear state-space model of the system at each time step.

Consider a non-linear state-space representation of a system as,

$$\begin{aligned} \dot{x} &= f(x, u) + w_k \\ y &= h(x, u) + v_k \end{aligned} \tag{3-1}$$

The goal is to estimate x based on the complete history of inputs u and y at any time instant k. For the case of interconnected system the states x, inputs u and the outputs y are obtained by stacking the states, inputs and outputs of each individual system, similar to equations (2-3), (2-4) or (2-13), (2-14). Note that here for simplicity the bar on top of lifted system variables and matrices is not used, a variable x or a matrix A without the subscript s should be considered as lifted.

An algorithm of EKF is shown in Figure 3-1. The filter is first initialized with the best available information on the state $\hat{x}_0^+$ and error covariance $\Sigma_{\tilde{x},0}^+$. Following initialization, the EKF repeatedly performs three steps. Time update, linearization and measurement update.

1. Using the model of the system, input signal and the initial condition as the estimate of the state in the previous step $\hat{x}_{k-1}^+$, it predicts the value of the next state $\hat{x}_k^-$ and the system output $\hat{y}_k$. This step requires non-linear simulation which can be done accurately using an ODE solver.

2. The next step is linearization in which the non-linear state-space model of the system is linearized to obtain the system matrices $\hat{A}_k$ and $\hat{C}_k$. Since the state transition matrix is obtained from a continuous time model, we need to perform a continuous to discrete time conversion using Tustin approximation as,

$$\hat{\Phi}_k = \left(I + \frac{\hat{A}_k h}{2}\right)\left(I - \frac{\hat{A}_k h}{2}\right)^{-1} \tag{3-2}$$

   where, h is the sampling time at which the measurements are taken.

3. After obtaining the system matrices, first the initial state error covariance matrix is obtained which is the error covariance of the initial estimate of the state $\hat{x}_k^-$. Then the Kalman gain L_k is obtained which is used to correct the initial estimate of the state using the difference between the actual measured output y_k and the predicted output $\hat{y}_k$. Subsequently the error covariance of this corrected state is obtained as $\Sigma_{\tilde{x},k}^+$.

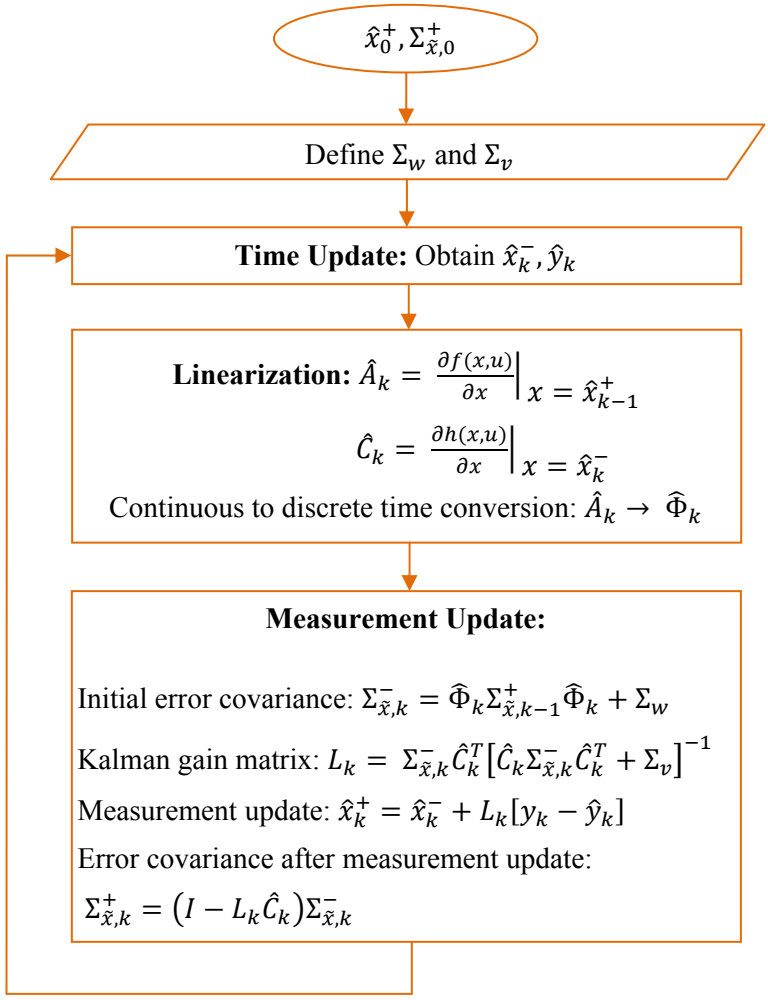

Figure 3-1: Extended Kalman Filter Algorithm

Thus an EKF runs iteratively, every time refining the estimate of the state from all the available input and output information up to that point in time. After having explained the three steps of an EKF, in the next sections we will utilize the structure of the interconnected system to make all these steps efficient with $O(N)$ computational complexity.

3-2 Simulation / Time Update

In the time update step, the system is simulated using an ODE solver for the time interval h to predict the value of next state and the output. The time required for this simulation grows very fast with the order of the system. In the plot Figure 3-2, we show the mean simulation time required by linear systems of different orders from 25 to 700 for a time interval $h = 0.05$.

This plot is obtained by simulation of systems represented by randomly generated system matrices of the required size and randomly generated initial conditions as well as inputs.

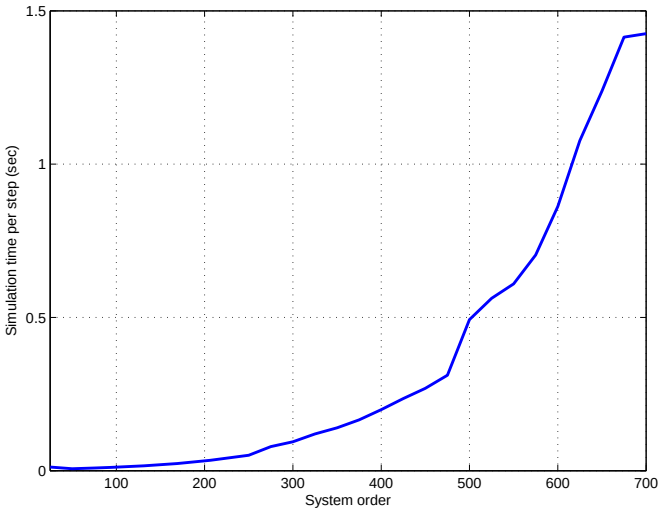

Figure 3-2: Simulation time required by systems of different orders for a time interval of $h = 0.05$

From the plot it is observed that the simulation time grows roughly with $O\left(N^3\right)$ complexity. Thus as the system order grows, it becomes infeasible to perform the simulation in real time. For the case of an interconnected system, the lifted system order is very high however it consists of sub-systems whose order is low. If we can decouple the systems so that they can be simulated independently, then we can achieve significant gain in terms of efficiency. For instance consider 10 systems each of order 50 interconnected to form the lifted system. From the Figure 3-2, simulation time for this lifted system is 0.5 sec while simulation time for a sub-system is 0.006 sec. It the sub-systems are independently simulated, sequentially on a single core processor, the total time for 10 systems is 0.06 sec which is 7.8 times less than the lifted system. Further, the simulation can be parallelized using a multi-core processor up to 10 times. Thus the idea is to decouple the sub-systems and remove interdependencies. Here it is achieved by sampling and zero order hold of interconnecting variables. Consider the non-linear state-space representation of a sub-system Σ_s as,

$$\begin{aligned} \dot{x}_s &= f_s\left(x_s, v_s^p, v_s^m, u_s\right) \\ v_{s-1}^p &= g_{s1}\left(x_s, u_s\right) + W_s^p v_s^p + Z_s^m v_s^m \\ v_{s+1}^m &= g_{s2}\left(x_s, u_s\right) + Z_s^p v_s^p + W_s^m v_s^m \\ y_s &= h_s\left(x_s, v_s^p, v_s^m, u_s\right) \end{aligned} \tag{3-3}$$

Here we consider the system not to be in spatially strictly proper form but having linear dependency between the interconnecting variables. It was shown in section 2-2 that the interconnecting variables can be represented as a function of states and exogenous inputs only, equation (2-11). What is done here is, all the linear interconnecting variables dependent

part of all the output equations is casted in a matrix E while all the state and input dependent terms are casted into a vector b and all the interconnecting variables are combined in the vector i thus forming,

$$\begin{aligned} Ei &= b \\ i &= E^{-1}b \end{aligned} \tag{3-4}$$

where,

$$i = \begin{bmatrix} v_1^p \\ v_2^m \\ v_2^p \\ \vdots \\ v_{N-1}^m \\ v_{N-1}^p \\ v_N^m \end{bmatrix} \quad b = \begin{bmatrix} g_{12}\left(x_1, u_1\right) \\ g_{21}\left(x_2, u_2\right) \\ g_{22}\left(x_2, u_2\right) \\ \vdots \\ g_{(N-1)1}\left(x_{(N-1)}, u_{(N-1)}\right) \\ g_{(N-1)2}\left(x_{(N-1)}, u_{(N-1)}\right) \\ g_{N1}\left(x_N, u_N\right) \end{bmatrix} \tag{3-5}$$

$$E = SSS\left(L_s, M_s, N_s, O_s, P_s, Q_s, R_s\right) \tag{3-6}$$

where,

$$L_s = \begin{bmatrix} I \\ 0 \end{bmatrix} \ \forall s \in \{2, 3, \cdots, N-1\}, \ L_N = I$$

$$M_s = 0 \ \forall s \in \{2, 3, \cdots, N-1\}$$

$$N_1 = I, \ N_s = \begin{bmatrix} 0 & I \end{bmatrix} \ \forall s \in \{2, 3, \cdots, N-1\}$$

$$O_1 = -Z_1^p, \ O_s = \begin{bmatrix} -Z_s^m & -W_s^p \\ -W_s^m & -Z_s^p \end{bmatrix} \ \forall s \in \{2, 3, \cdots, N-1\}, \ O_N = -Z_N^m \tag{3-7}$$

$$P_1 = I, \ P_s = \begin{bmatrix} 0 \\ I \end{bmatrix} \ \forall s \in \{2, 3, \cdots, N-1\}$$

$$Q_s = 0 \ \forall s \in \{2, 3, \cdots, N-1\}$$

$$R_s = \begin{bmatrix} I & 0 \end{bmatrix} \ \forall s \in \{2, 3, \cdots, N-1\}, \ R_N = I$$

At any time instant k the current state and exogenous inputs are used to evaluate the interconnecting variables in a centralized block Figure 3-3. Here, the centralized block is implemented to achieve two goals. First, to eliminate the problem of algebraic loops formed because of the non-spatially strictly proper form of the system. Second, to remove interdependencies between sub-systems and thus be able to perform the simulation at the sub-system level independently for one time interval. During this time interval, zero order hold is assumed for the interconnecting variables and thus their values are assumed to remain constant from time

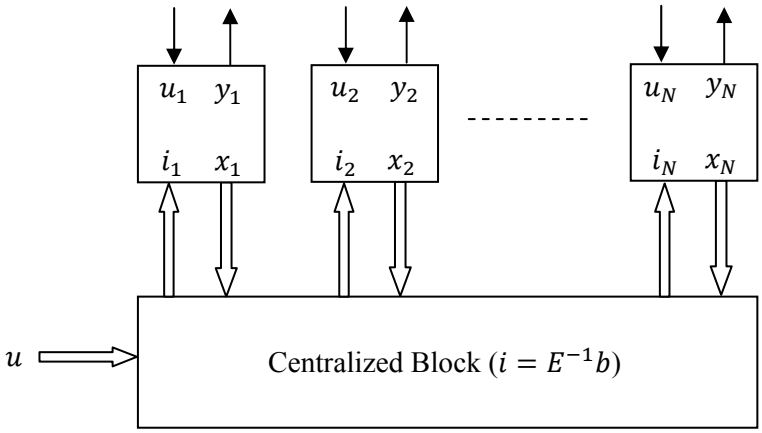

Figure 3-3: Block diagram of efficient simulator of a string interconnected system

instant k to $k+1$. Their values are fed to individual sub-system blocks, wherein simulation takes places at the sub-system level to obtain the value of new state at time $k+1$, i.e. integrating the equation,

$$\dot{x}_s = f_s\left(x_s, v_s^p, v_s^m, u_s\right) \tag{3-8}$$

Again this new state at time $k+1$ and the exogenous inputs at time $k+1$ are used to obtain the vector b and subsequently i for the next round of simulations. Using this technique, the sub-systems can be simulated independently for each time interval. Also the matrix inverse operation in the centralized block can be done using efficient SSS arithmetic thus resulting into the whole simulation scheme with $O(N)$ computational complexity. This is validated using Li-ion cell as an example in section 4-6-5. Though there will be some loss of accuracy due to sampling and zero order hold of interconnecting variables as h goes higher. This will be investigated using Li-ion cell as example in section 4-6.

3-3 Linearization

At the second step of an EKF, we need to obtain the linearized system matrices by evaluating the Jacobians as shown in Figure 3-1. This calculation could be very much simplified if we do the linearization at the sub-system level since we have to deal with systems of lower order and then lift to obtain the lifted linearized system matrices. In the following illustration, it will be proved that lifting and linearization operations are commutative, using a string interconnected system with only two sub-systems Figure 2-3 which can be easily extended to N sub-systems.

First consider a spatially strictly proper non-linear system described by equations (2-3) and (2-4). Lets linearize these lifted equations and obtain the system matrix A using chain rule of differentiation, we obtain,

$$A = \begin{bmatrix} \frac{\partial f_1}{\partial x_1} & \frac{\partial f_1}{\partial g_{21}} \frac{\partial g_{21}}{\partial x_2} \\ \\ \frac{\partial f_2}{\partial g_{12}} \frac{\partial g_{12}}{\partial x_1} & \frac{\partial f_2}{\partial x_2} \end{bmatrix} \tag{3-9}$$

Now if we linearize the two sub-systems individually, we obtain the sub-system matrices as,

$$\begin{aligned} A_1 = \tfrac{\partial f_1}{\partial x_1}, \quad B_1^p = \tfrac{\partial f_1}{\partial v_1^p} = \tfrac{\partial f_1}{\partial g_{21}} \quad (v_1^p = g_{21}(\cdot)), \quad C_1^m = \tfrac{\partial g_{12}}{\partial x_1} \\ A_2 = \tfrac{\partial f_2}{\partial x_2}, \quad B_2^m = \tfrac{\partial f_2}{\partial v_2^m} = \tfrac{\partial f_2}{\partial g_{12}} \quad (v_2^m = g_{12}(\cdot)), \quad C_2^p = \tfrac{\partial g_{21}}{\partial x_2} \end{aligned} \tag{3-10}$$

Then Lifting to obtain the lifted matrix A similar to equation (2-17) we obtain,

$$A = \begin{bmatrix} A_1 & B_1^p C_2^p \\ \\ B_2^m C_1^m & A_2 \end{bmatrix} \tag{3-11}$$

Clearly the equations (3-9) and (3-11) are equivalent. The equivalence of matrix C can also be proved on similar lines.

Now for the case of non-linear systems which are not spatially strictly proper, described by equations (2-13) and (2-14), linearization results into,

$$\begin{aligned} A = \begin{bmatrix} \frac{\partial f_1}{\partial x_1} + \frac{\partial f_1}{\partial j_2} \frac{\partial j_2}{\partial x_1} & \frac{\partial f_1}{\partial j_2} \frac{\partial j_2}{\partial x_2} \\ \\ \frac{\partial f_2}{\partial j_1} \frac{\partial j_1}{\partial x_1} & \frac{\partial f_2}{\partial x_2} + \frac{\partial f_2}{\partial j_1} \frac{\partial j_1}{\partial x_2} \end{bmatrix} \\ \text{Where,} \quad \tfrac{\partial j_2}{\partial x_1} = \left(\tfrac{Z_2^m}{1 - Z_1^p Z_2^m}\right) \tfrac{\partial g_{12}}{\partial x_1}, \quad \tfrac{\partial j_2}{\partial x_2} = \left(\tfrac{1}{1 - Z_1^p Z_2^m}\right) \tfrac{\partial g_{21}}{\partial x_2}, \\ \tfrac{\partial j_1}{\partial x_1} = \left(\tfrac{1}{1 - Z_1^p Z_2^m}\right) \tfrac{\partial g_{12}}{\partial x_1}, \quad \tfrac{\partial j_1}{\partial x_2} = \left(\tfrac{Z_1^p}{1 - Z_1^p Z_2^m}\right) \tfrac{\partial g_{21}}{\partial x_2} \end{aligned} \tag{3-12}$$

Note that here all variables like Z_1^p and Z_2^m are assumed scalar, this proof can be extended to matrices also using inverse of block matrices. Now, sub-system level linearization will result into following matrices,

$$\begin{aligned} A_1 = \tfrac{\partial f_1}{\partial x_1}, \quad B_1^p = \tfrac{\partial f_1}{\partial v_1^p} = \tfrac{\partial f_1}{\partial j_2} \quad (v_1^p = j_2(\cdot)), \quad C_1^m = \tfrac{\partial g_{12}}{\partial x_1} \\ A_2 = \tfrac{\partial f_2}{\partial x_2}, \quad B_2^m = \tfrac{\partial f_2}{\partial v_2^m} = \tfrac{\partial f_2}{\partial j_1} \quad (v_2^m = j_1(\cdot)), \quad C_2^p = \tfrac{\partial g_{21}}{\partial x_2} \end{aligned} \tag{3-13}$$

In this case, the system is not spatially strictly proper and thus can not be lifted directly using equation (2-17). It needs to be converted to spatially strictly proper form using the technique shown in [11] illustrated in Appendix A. After this transformation and lifting, we obtain,

$$A = \begin{bmatrix} A_1 + B_1^p \left(\frac{Z_2^m}{1-Z_1^p Z_2^m}\right) C_1^m & B_1^p \left(\frac{1}{1-Z_1^p Z_2^m}\right) C_2^p \\ \\ B_2^m \left(\frac{1}{1-Z_1^p Z_2^m}\right) C_1^m & A_2 + B_2^m \left(\frac{Z_1^p}{1-Z_1^p Z_2^m}\right) C_2^p \end{bmatrix} \tag{3-14}$$

Clearly the equations (3-12) and (3-14) are equivalent. Thus, linearization at the sub-system level can be done followed by lifting without losing the validity of the algorithm.

3-4 Correction / Measurement Update

We observed that the lifted system matrices A and C have SSS structure. Also from equation (3-2), the matrix Φ has SSS structure, due to structure preserving SSS inverse and multiplication operations. The idea is to initialize the matrix $\Sigma^+_{\tilde{x},0}$ in the SSS form and also define the matrices Σ_w and Σ_v in the SSS form. As a result, all the steps of measurement update, Figure 3-1 can be performed using efficient SSS arithmetic having $O(N)$ computational complexity. At the last step the state error covariance matrix $\Sigma^+_{\tilde{x},k}$ obtained will be in the SSS form which is then used in the next iteration and thus the SSS structure is preserved through all iterations.

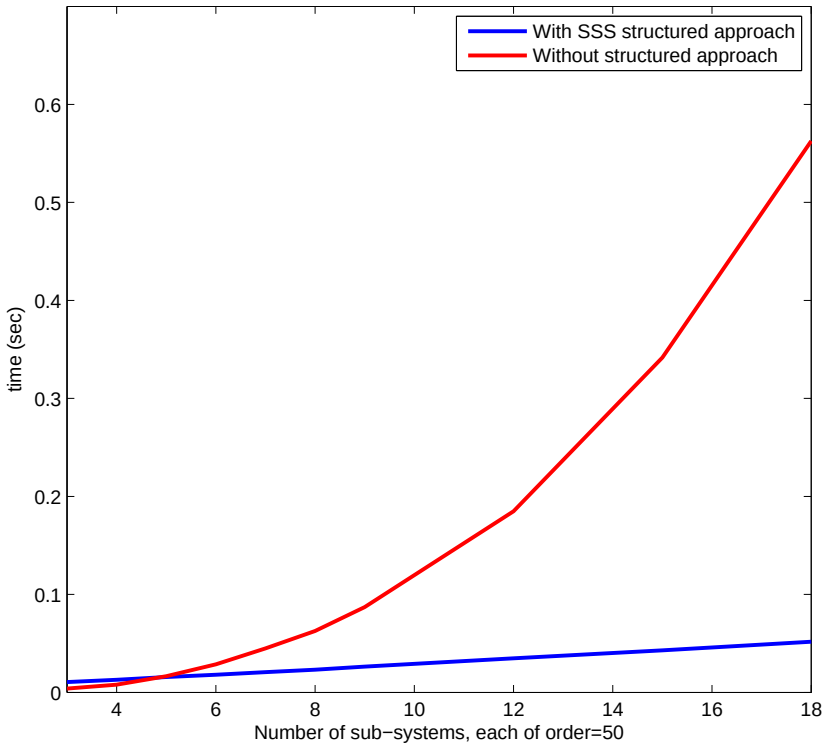

Figure 3-4: Simulation time for one set of measurement update matrix computations with and without SSS structured approach

To check the efficiency of this structured matrix approach, an interconnected system is considered with each sub-system of order 50. The sub-system matrices are then generated randomly in Matlab and all matrix computations of measurement update are performed using the SSS arithmetic as well as traditional matrix arithmetic. A comparison of the mean time required by both these approaches for one set of measurement update matrix computations is shown as the number of sub-systems N grows in Figure 3-4. Clearly with the SSS structured approach, due to efficient SSS arithmetic, the computational complexity is $O(N)$. In the beginning, we observe that the computation time required by the structured approach is higher than the traditional approach. This is due to the fact that the gain in the computation time is very less and the cost of other overheads while performing SSS arithmetic is higher. Thus leading to a cut-off point of '5' sub-systems in this case. Below that point, it is not beneficial to use SSS arithmetic, on the other hand, the gain in computational cost will be higher as the number of sub-systems N grows. Even for 6 sub-systems, the gain in computation time is 37%. With this we achieved $O(N)$ computational complexity for the measurement update step also.

Chapter 4

Lithium-ion Cell Modeling

In this chapter, we will develop a model of Lithium ion (Li-ion) cell based on fundamental electrochemical equations. The model will be developed as spatially distributed string interconnected system in One Dimension (1D) exactly in the form discussed in previous chapters, thus enabling efficient simulation and state-estimation. We'll start with a brief description of working of the cell followed by explanation of fundamental electrochemical equations which describe the processes inside the cell by means of Partial Differential Equations (PDE). In section 4-3 we'll discretize this cell in 1D and correspondingly discretize the PDEs. However this leads to a very high order non-linear system with implicit relationships. Simulation of such a system is highly computationally expensive, slow and possibly non-convergent and thus prohibiting its real-time implementation. Hence in section 4-4, an explicit non-linear state-space model for each discretized part of the cell is developed and the system as a whole is considered as spatially distributed string interconnected system consisting of these parts as building blocks, which are of lower order. Based on this model, an efficient simulator is developed in section 4-5 and finally the simulation results are shown in section 4-6.

4-1 Li-ion Cell Basics

This section explains the basic working of a Li-ion cell. In this entire work, a 6Ah capacity Li-ion cell for a Hybrid Electric Vehicle application has been chosen. The parameters and constant values for this cell have been taken from [1] and can be found in Appendix B. A schematic diagram of this cell is shown in Figure 4-1.

As shown in the Figure 4-1, a Li-ion cell consists of three domains: the negative composite electrode (anode), separator and positive composite electrode (cathode). The working of the cell is based on Redox (shorthand for Reduction-Oxidation) reaction. In brief, oxidation occurs at the anode resulting into cations (positively charged ions) into the electrolyte and free electrons. These electrons travel through the external circuit (load current) to reach the cathode and internally within the cell, the cations travel through the electrolyte across the

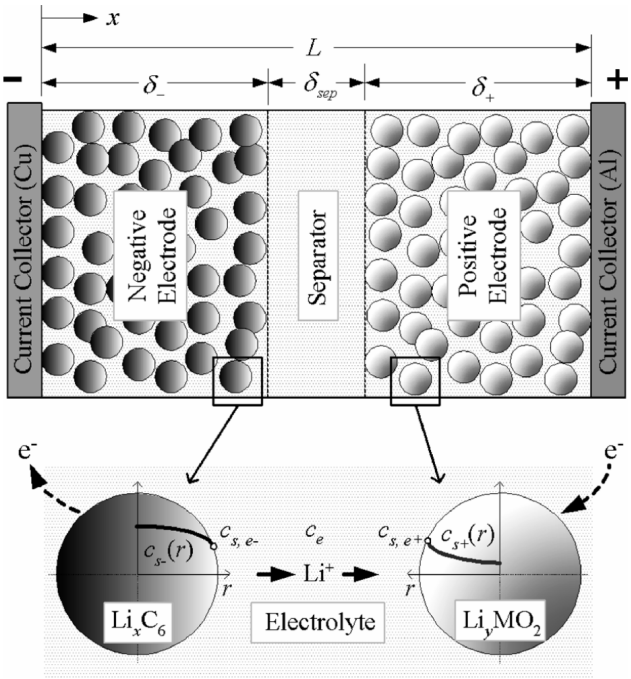

Figure 4-1: Schematic diagram of Li-ion cell [1]

separator to reach the cathode. At the cathode, reduction reaction occurs consuming these electrons and cations from the electrolyte.

Normally the composite electrodes are made porous (Figure 4-1) to increase the active area between the electrolyte and the electrode; made of active material particles. For instance in this case, the negative active material particle is Li_xC_6 while the positive active material particle is Li_yMO_2. These electrodes can be seen as consisting of spherical active material particles held together with a binder and a suitable filler material to enhance electron transport forming a solid matrix. The Li ions intercalate or deintercalate into these active electrodes. During discharge, Li ions diffuse to the surface of Li_xC_6 active material particles (solid phase) in the negative electrode where they undergo electrochemical reaction (oxidation) and transfer into a liquid or gelled electrolyte solution (electrolyte phase). The positively charged ions then travel through the electrolyte solution via diffusion and ionic conduction to the positive electrode active material particles where they react (reduction) and diffuse towards the inner regions of these metal oxide active material particles (solid phase). The porous separator serves as an electronic insulator, forcing electrons to follow an opposite path through an external circuit or load. End of discharge/charge, occurs when the solid phase Li concentrations at either electrode become saturated or depleted, or electrolyte phase Li^+ concentration becomes depleted at either electrode [1].

Thus as a measure of available capacity, the bulk electrode averaged concentration of a single electrode, $c_{s,avg}(t)$ at time t can be taken as reference and the State of Charge (SoC) can be defined as,

$$SoC\,(t) = \frac{c_{s,avg}\,(t) - \ c_{s,0\%}}{c_{s,100\%} - \ c_{s,0\%}} \tag{4-1}$$

where,
$c_{s,0\%}$ and $c_{s,100\%}$ are the reference values of concentration at 0% and 100% SoC respectively.

Hence this definition is based on the fraction of concentration available in the solid phase for further reaction. With this, we have explained the electrochemistry based working of the Li-ion cell and developed the physical definition of the SoC which finally needs to be estimated. All these phenomena can be described using partial differential equations as will be explained in the next section.

4-2 Fundamental Equations

Referring to Figure 4-1 the electrodes are modeled using porous electrode theory, meaning that the solid and electrolyte phases are treated as superimposed continua without regard to microstructure and the electrode is assumed to be composed of spherical particles. The simplest model would be One Dimensional (1D) along the x-direction and assuming lumped behaviour over other dimensions. The starting point of all 1D control oriented electrochemical models is based on equations originally derived in [16] and compactly written in [1, 17, 18]. The equations that follow are based on charge and mass conservation laws. All equations are thoroughly explained stating their physical meaning with respect to the working of the cell, however the reader is strongly recommended to follow the next section 4-3 wherein a discretized version of these equations are described for clear understanding.

Charge balances: The entire external current enters / leaves the cell in the solid spherical active material particles only at the terminals. Then the current flows through this solid matrix. The current flowing per unit area in this solid phase, i_s is thus simply given by Ohm's law as,

$$i_s(x) = -\sigma^{eff}\overrightarrow{\nabla}_x\phi_s \tag{4-2}$$

here, σ^{eff} is the effective conductivity and ϕ_s is the potential in the solid phase. At each spherical particle, the current gets diverged due to reaction taking place between the electrode and the electrolyte. This current is now in the form of flow of Li^+ ions. The magnitude of this diverged current is related to the volumetric rate of electrochemical reaction taking place at the solid/ electrolyte interface (j^{Li}) as,

$$\overrightarrow{\nabla}_x i_s(x) = -j^{Li} \tag{4-3}$$

this diverged current gets added to the current already flowing through the electrolyte at that point given by,

$$\overrightarrow{\nabla}_x i_e(x) = j^{Li} \tag{4-4}$$

this current in the electrolyte phase, i_e follows modified Ohm's law which includes an extra term to account for concentration variations,

$$i_e(x) = -\kappa^{eff}\overrightarrow{\nabla}_x\phi_e - \kappa_D^{eff}\overrightarrow{\nabla}_x lnc_e \tag{4-5}$$

here κ^{eff} is the effective ionic conductivity, κ_D^{eff} is the effective diffusion conductivity, ϕ_e is the electrolyte phase potential and c_e is the Li ion concentration in the electrolyte phase.

The boundary conditions of these equations are,

$$-\sigma_-^{eff}\overrightarrow{\nabla}_x\phi_s\Big|_{x=0} = \sigma_+^{eff}\overrightarrow{\nabla}_x\phi_s\Big|_{x=L} = \frac{I}{A} \tag{4-6}$$

$$\overrightarrow{\nabla}_x\phi_e\Big|_{x=0} = \overrightarrow{\nabla}_x\phi_e\Big|_{x=L} = 0 \tag{4-7}$$

these equations say that all the current flowing at the battery terminals is through the electrode (solid phase) only.

$$\overrightarrow{\nabla}_x\phi_s\Big|_{x=\delta_-} = \overrightarrow{\nabla}_x\phi_s\Big|_{x=\delta_-+\delta_{sep}} = 0 \tag{4-8}$$

According to this boundary condition, no current flows through the electrode at the separator since physically the electrode ends there and the separator begins.

Further, there is no divergence of current within the separator and the entire terminal current flows through the separator in the form of Li^+ ions given by equations,

$$\overrightarrow{\nabla}_x i_e\,(x) = 0 \tag{4-9}$$

$$-\kappa^{eff}\overrightarrow{\nabla}_x\phi_e - \kappa_D^{eff}\overrightarrow{\nabla}_x lnc_e = \frac{I}{A}. \tag{4-10}$$

Mass balances: These are the equations that relate the concentration of Li ions with space and time. In the case of solid spherical active material particle,

$$\frac{\partial c_s}{\partial t} = \frac{D_s}{r^2}\overrightarrow{\nabla}_r\left(r^2\overrightarrow{\nabla}_r c_s\right) \tag{4-11}$$

this equation represents the conservation of Li ions in a single active material particle assuming it to be spherical of radius R_s, described by Flicks law of diffusion. Here D_s is the solid phase diffusion coefficient and r is the radial distance. The boundary conditions are,

$$\overrightarrow{\nabla}_r c_s\Big|_{r=0} = 0; \quad D_s\overrightarrow{\nabla}_r c_s\Big|_{r=R_s} = \frac{-j^{Li}}{a_s F} \tag{4-12}$$

which say that at the surface of the sphere, the concentration of Li ions is related to the volumetric rate of electrochemical reaction, j^{Li}. Further, $c_{s,e}\,(x,t) = c_s(x,\ R_s,t)$, that is the concentration at the surface of the spherical active material particle.

For the case of electrolyte,

$$\frac{\partial\epsilon_e c_e}{\partial t} = \overrightarrow{\nabla}_x\left(D_e^{eff}\overrightarrow{\nabla}_x c_e\right) + \frac{1-t_+^0}{F}j^{Li} \tag{4-13}$$

this equation represents conservation of Li ions in the electrolyte phase, assuming the species transport by diffusion and migration only. Here D_e^{eff} is the effective diffusion coefficient, t_+^0 is the transference number of Li^+ ions with respect to the velocity of solvent which is assumed to be constant. The boundary conditions are,

$$\overrightarrow{\nabla}_x c_e\Big|_{x=0} = \overrightarrow{\nabla}_x c_e\Big|_{x=L} = 0 \tag{4-14}$$

thus it is assumed that the gradient of electrolyte concentration at the battery terminals is zero which is related to the boundary condition which says that the gradient of electrolyte potential at the battery terminals is zero.

Kinetics: The volumetric rate of electrochemical reaction at the solid/ electrolyte interface (j^{Li}) which is coupling the equations of charge balance and material balance is given by,

$$j^{Li}(x) = a_s j_0 \left[exp\left(\frac{\alpha_a F}{RT}\eta\right) - exp\left(-\frac{\alpha_c F}{RT}\eta\right) \right] \tag{4-15}$$

$$j_0 = k(c_e)^{\alpha_a}(c_{s,max} - c_{s,e})^{\alpha_a}(c_{s,e})^{\alpha_c} \tag{4-16}$$

where the overpotential η is obtained as,

$$\eta = \phi_s - \phi_e - U(c_{s,e}). \tag{4-17}$$

The equilibrium (open circuit) voltage $U(c_{s,e})$ is evaluated as a non linear empirical function of the surface stoichiometry θ. This highly non-linear function is taken from [1] as,

$$\begin{gathered} U_-(\theta_-) = 8.00229 + 5.0647\theta_- - 12.578\theta_-^{1/2} - 8.6322\times10^{-4}\theta_-^{-1} + 2.1765\times10^{-5}\theta_-^{3/2} \\ -0.46016exp[15.0(0.06-\theta_-)] - 0.55364exp[-2.4326(\theta_- - 0.92)] \\ \\ U_+(\theta_+) = 85.681\theta_+^6 - 357.70\theta_+^5 + 613.89\theta_+^4 - 555.65\theta_+^3 \\ +281.06\theta_+^2 - 76.648\theta_+ - 0.30987exp(5.657\theta_+^{115}) + 13.1983 \end{gathered} \tag{4-18}$$

where,

$$\theta_-(x) = \frac{c_{s,e-}}{c_{s,max}^{anode}}; \qquad \theta_+(x) = \frac{c_{s,e+}}{c_{s,max}^{cathode}}. \tag{4-19}$$

Note that ϕ_s has only one spatial dependence x while c_s is dependent on x and also the radial dimension r. On the other hand $c_{s,e}$ which is the surface concentration is given by: $c_{s,e}(x,t) = c_s(x,\ R_s,t)$ thus has only one spatial dependence x.

Here the reaction rate is assumed to follow Butler-Volmer equation (4-15). Where α_a and α_c are the anodic and cathodic transfer coefficients of electrode reaction, F is the Faraday's constant, R the universal gas constant, T the absolute temperature in Kelvin, k is the kinetic rate constant and a_s is the specific interfacial area of an electrode which is zero in the separator region (leading to no divergence of current).

Measurable quantity: Finally the cell potential which is measured is given as,

$$V = \phi_s(x = L) - \phi_s(x = 0) - \frac{R_f}{A} I \tag{4-20}$$

where R_f is the film resistance on the electrodes surface.

Further, temperature information can be incorporated in the model by adding energy balances as shown in [18]. Also the parameters can be adapted with ageing of the cell i.e. with the State of Health (SoH) of the cell [19]. However in this work, constant temperature of 298K is assumed and cell ageing is not considered.

4-3 Discretized Model

From the previous section it is clear that the system is described by a set of coupled partial differential equations. In this section we perform spatial discretization in 1D to obtain a discretized model of the cell consisting of a set of ordinary differential equations and static relationships. The cell is discretized along the x and r dimensions as shown in Figure 4-2. The model input is considered as the dis/charge current I.

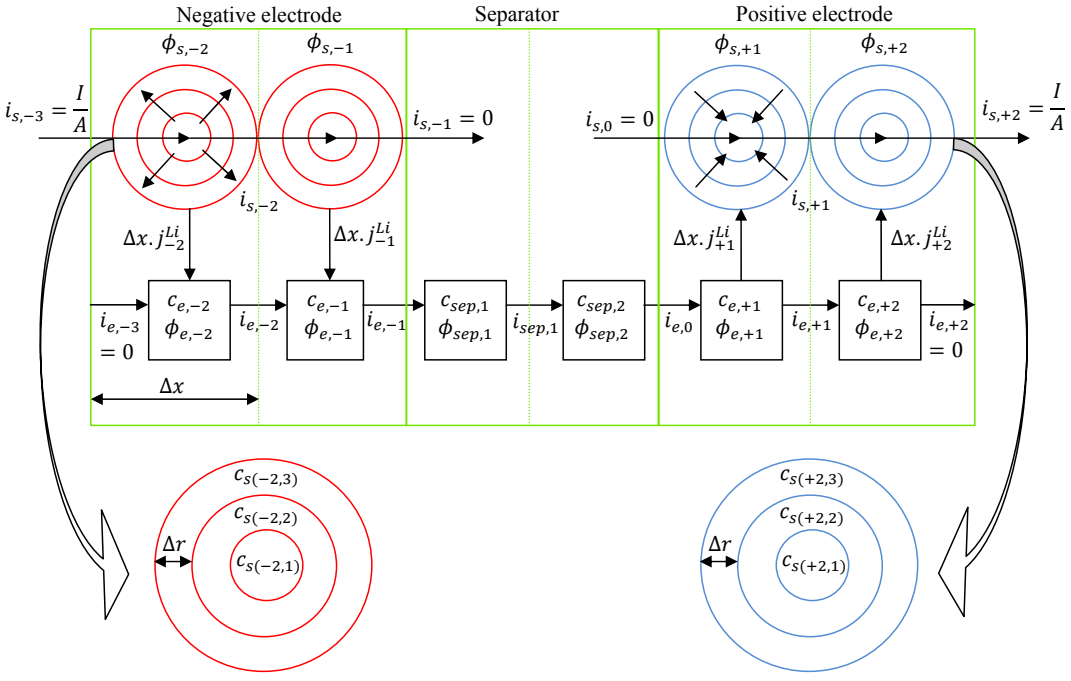

Figure 4-2: Discretization of Li-ion cell along x and r dimensions

As a first step, finite element method is used to discretize the electrolyte region. In the Figure 4-2, the positive electrode region, the negative electrode region and the separator region each is divided only into two slices simply to explain the concept, however it can be extended to more finely discretized schemes. In the positive and negative regions, each

discretized slice consists of one spherical electrode particle. Thus the positive and negative electrodes are assumed to be formed of spherical active material particles in series whose centers are connected by a fictitious wires of finite resistance. Each spherical active material particle is further discretized along the radial dimension r into three regions here, which can again be extended to more finely discretized schemes. Each discretized region has a lumped electrolyte phase Li^+ ion concentration c_e and electrolyte phase potential ϕ_e or c_{sep} and ϕ_{sep} respectively in the case of separator. Each sphere has a lumped solid phase potential ϕ_s while the solid phase Li ion concentration is different at each discretized slice along r. The volumetric rate of electrochemical reaction at the solid/electrolyte interface, j^{Li} is lumped in a particular discretized region and it is zero in the separator regions. Further the current flowing in the solid region, i_s by means of electrons and in the electrolyte region i_e or i_{sep} by means of Li ions are shown in the Figure 4-2. Note that here we have considered one spherical active material particle in each positive and negative discretized slice. As a result, Δx in those regions represent the average distance between spherical active material particles. Its approximate calculation based on the geometry of the cell and active material volume fraction is shown in Appendix B. Further, based on the fraction of actual length of these regions to the chosen number of discretized parts times Δx, the interfacial surface area a_s needs to be scaled, Appendix B.

Now we start discretizing the Partial Differential Equations using first order finite difference method and at the same time also explain the various phenomena inside the cell mathematically. Consider the cell discharge situation, where the load current enters the center of the first spherical particle of the negative electrode. A part of this current gets diverged into the sphere and the current can be considered as flowing in all the directions away from the centre. In fact this phenomena is nothing but the diffusion of Li ions from the inner regions towards the surface i.e. the Li ions are travelling away from the centre (direction of the current) while electrons are travelling towards the centre of the sphere (opposite to the direction of current). The part of the current which is not diverged, flows through the fictitious wire interconnecting the spheres. Similarly divergence of a part of the current takes place at the second sphere and so on. Finally by the last sphere, all the current has to get diverged. The current flowing in the solid phase, i.e. in the fictitious wires connecting the spheres is obtained by discretizing the equation (4-2) and the boundary condition (4-6) and (4-8),

$$-\sigma_-^{eff}\left(\frac{\phi_{s,-2}-\phi_{s,-3}}{\Delta x_-}\right)=\frac{I}{A} \tag{4-21}$$

$$-\sigma_-^{eff}\left(\frac{\phi_{s,-1}-\phi_{s,-2}}{\Delta x_-}\right)=i_{s,-2} \tag{4-22}$$

$$-\sigma_-^{eff}\left(\frac{\phi_{s,-0}-\phi_{s,-1}}{\Delta x_-}\right)=0 \tag{4-23}$$

Similarly at the positive electrode,

$$-\sigma_+^{eff}\left(\frac{\phi_{s,+1}-\phi_{s,+0}}{\Delta x_+}\right)=0 \tag{4-24}$$

$$-\sigma_+^{eff}\left(\frac{\phi_{s,+2}-\phi_{s,+1}}{\Delta x_+}\right)=i_{s,+1} \tag{4-25}$$

$$-\sigma_{+}^{eff}\left(\frac{\phi_{s,+3}-\phi_{s,+2}}{\Delta x_{+}}\right)=\frac{I}{A} \tag{4-26}$$

From these equations, we have 10 unknown variables $(\phi_{s,-3},\phi_{s,-2},\phi_{s,-1},\phi_{s,-0},\phi_{s,+0},\phi_{s,+1},\phi_{s,+2},\phi_{s,+3},i_{s,-2},i_{s,+1})$ and 6 equations so far. Note that the variables $\phi_{s,-3},\phi_{s,-0},\phi_{s,+0}$ and $\phi_{s,+3}$ are fictitious and are resolved by using one of the boundary conditions above.

Now the diverged current at each spherical particle is related to the volumetric rate of electrochemical reaction at the solid/electrolyte interface (j^{Li}). This is because of the oxidation / reduction reaction taking place at the interface which either generates or consumes Li^{+} ions and electrons. Simply applying Kirchhoff's current law (same as discretizing equation (4-3)),

$$i_{s,-2}-\frac{I}{A}=-\Delta x_{-}j_{-2}^{Li} \tag{4-27}$$

$$0-i_{s,-2}=-\Delta x_{-}j_{-1}^{Li} \tag{4-28}$$

Similarly at the positive electrode,

$$i_{s,+1}-0=-\Delta x_{+}j_{+1}^{Li} \tag{4-29}$$

$$\frac{I}{A}-i_{s,+1}=-\Delta x_{+}j_{+2}^{Li} \tag{4-30}$$

Note that the value of j^{Li} is negative in the positive electrode. Here we added 4 new variables $(j_{-2}^{Li},j_{-1}^{Li},j_{+1}^{Li},j_{+2}^{Li})$ and 4 new equations.

The diverged current now flows in the electrolyte by means of Li^{+} ions and gets added to the already flowing electrolyte phase current. Again applying Kirchhoff's current law (same as discretizing equations (4-4) and (4-9)) and using boundary conditions (4-7),

$$i_{e,-2}-0=\Delta x_{-}j_{-2}^{Li} \tag{4-31}$$

$$i_{e,-1}-i_{e,-2}=\Delta x_{-}j_{-1}^{Li} \tag{4-32}$$

$$i_{sep,1}-i_{e,-1}=0 \tag{4-33}$$

$$i_{e,0}-i_{sep,1}=0 \tag{4-34}$$

$$i_{e,+1}-i_{e,0}=\Delta x_{+}j_{+1}^{Li} \tag{4-35}$$

$$0-i_{e,+1}=\Delta x_{+}j_{+2}^{Li} \tag{4-36}$$

Here we added 5 new unknowns $(i_{e,-2},i_{e,-1},i_{sep,1},i_{e,0},i_{e,+1})$ and 6 new equations.

The flow of current in the electrolyte phase follows modified ohm's law, discretizing equation (4-5) and boundary conditions (4-7),

$$\phi_{e,-2} - \phi_{e,-3} = 0 \tag{4-37}$$

$$-\kappa_{-}^{eff}\left(\frac{\phi_{e,-1}-\phi_{e,-2}}{\Delta x_{-}}\right) - \kappa_{D_{-}}^{eff}\left(\frac{lnc_{e,-1}-lnc_{e,-2}}{\Delta x_{-}}\right) = i_{e,-2} \tag{4-38}$$

$$-\kappa_{-}^{eff}\left(\frac{\phi_{sep,1}-\phi_{e,-1}}{\Delta x_{-}}\right) - \kappa_{D_{-}}^{eff}\left(\frac{lnc_{sep,1}-lnc_{e,-1}}{\Delta x_{-}}\right) = i_{e,-1} \tag{4-39}$$

$$-\kappa_{sep}^{eff}\left(\frac{\phi_{sep,2}-\phi_{sep,1}}{\Delta x_{sep}}\right) - \kappa_{D_{sep}}^{eff}\left(\frac{lnc_{sep,2}-lnc_{sep,1}}{\Delta x_{sep}}\right) = i_{sep,1} \tag{4-40}$$

$$-\kappa_{+}^{eff}\left(\frac{\phi_{e,+1}-\phi_{sep,2}}{\Delta x_{+}}\right) - \kappa_{D_{+}}^{eff}\left(\frac{lnc_{e,+1}-lnc_{sep,2}}{\Delta x_{+}}\right) = i_{e,0} \tag{4-41}$$

$$-\kappa_{+}^{eff}\left(\frac{\phi_{e,+2}-\phi_{e,+1}}{\Delta x_{+}}\right) - \kappa_{D_{+}}^{eff}\left(\frac{lnc_{e,+2}-lnc_{e,+1}}{\Delta x_{+}}\right) = i_{e,+1} \tag{4-42}$$

$$\phi_{e,+3} - \phi_{e,+2} = 0 \tag{4-43}$$

With these equations, we added 8 unknowns ($\phi_{e,-3}, \phi_{e,-2}, \phi_{e,-1}, \phi_{sep,1}, \phi_{sep,2}, \phi_{e,+1}, \phi_{e,+2}, \phi_{e,+3}$) and 7 new equations. Again the variables $\phi_{e,-3}$ and $\phi_{e,+3}$ are fictitious and are resolved using one of the boundary conditions above.

All the equations above are static equations. The dynamic equations arise from the mass balances. The Li ions intercalate or deintercalate into these active spherical material particles of the electrodes. For instance, during discharge, Li ions diffuse to the surface of active material particles in the negative electrode where they undergo electrochemical reaction and transfer into a liquid or gelled electrolyte solution. We have discretized the sphere along radial distance and thus the diffusion phenomenon is approximated by discretized Flicks law of diffusion equation. Consider the first spherical active material particle of the negative electrode, discretizing equation (4-11) and the boundary conditions (4-12) we get,

$$\dot{c}_{s(-2,1)} = \frac{D_{s_{-}}}{r_1^2}\left[2r_1\left(\frac{c_{s(-2,2)}-c_{s(-2,1)}}{\Delta r_{-}}\right) + r_1^2\left(\frac{c_{s(-2,0)}-2c_{s(-2,1)}+c_{s(-2,2)}}{\Delta r_{-}^2}\right)\right] \tag{4-44}$$

$$\dot{c}_{s(-2,2)} = \frac{D_{s_{-}}}{r_2^2}\left[2r_2\left(\frac{c_{s(-2,3)}-c_{s(-2,2)}}{\Delta r_{-}}\right) + r_2^2\left(\frac{c_{s(-2,1)}-2c_{s(-2,2)}+c_{s(-2,3)}}{\Delta r_{-}^2}\right)\right] \tag{4-45}$$

$$\dot{c}_{s(-2,3)} = \frac{D_{s_{-}}}{r_3^2}\left[2r_3\left(\frac{c_{s(-2,4)}-c_{s(-2,3)}}{\Delta r_{-}}\right) + r_3^2\left(\frac{c_{s(-2,2)}-2c_{s(-2,3)}+c_{s(-2,4)}}{\Delta r_{-}^2}\right)\right] \tag{4-46}$$

$$c_{s(-2,1)} - c_{s(-2,0)} = 0 \tag{4-47}$$

$$D_{s_-}\left(\frac{c_{s(-2,4)} - c_{s(-2,3)}}{\Delta r_-}\right) = \frac{-j^{Li}_{-2}}{a_{s_-}F} \tag{4-48}$$

The last equation here quantify the transfer of Li ions from the surface of the sphere to the liquid phase due to electrochemical reaction whose volumetric rate is j^{Li}. Here r_1, r_2 and r_3 are the radial distances of each discretized slice from the origin of the sphere. With these equations, we added 5 unknowns $(c_{s(-2,0)}, c_{s(-2,1)}, c_{s(-2,2)}, c_{s(-2,3)}, c_{s(-2,4)})$ and 5 equations. Again the variables $c_{s(-2,0)}$ and $c_{s(-2,4)}$ are fictitious, they are resolved using one of the boundary conditions above. Similar equations can be written for each spherical active material particle leading to total of 20 unknowns and 20 equations in this case. Note that in the case of positive electrode, opposite process takes place, i.e. for instance during discharge, Li ions get added from the liquid phase into the solid particles at the surface and then they diffuse towards the inner regions of the sphere.

Once in the liquid phase, these Li^+ ions travel through the electrolyte across the separator. Discretizing equation (4-13) and the boundary conditions (4-14) we get,

$$\dot{c}_{e,-2} = \frac{D^{eff}_{e_-}}{\epsilon_{e_-}}\left(\frac{c_{e,-3} - 2c_{e,-2} + c_{e,-1}}{\Delta x^2_-}\right) + \frac{1 - t^0_+}{F} j^{Li}_{-2} \tag{4-49}$$

$$\dot{c}_{e,-1} = \frac{D^{eff}_{e_-}}{\epsilon_{e_-}}\left(\frac{c_{e,-2} - 2c_{e,-1} + c_{sep,1}}{\Delta x^2_-}\right) + \frac{1 - t^0_+}{F} j^{Li}_{-1} \tag{4-50}$$

$$\dot{c}_{sep,1} = \frac{D^{eff}_{e_{sep}}}{\epsilon_{e_{sep}}}\left(\frac{c_{e,-1} - 2c_{sep,1} + c_{sep,2}}{\Delta x^2_{sep}}\right) \tag{4-51}$$

$$\dot{c}_{sep,2} = \frac{D^{eff}_{e_{sep}}}{\epsilon_{e_{sep}}}\left(\frac{c_{sep,1} - 2c_{sep,2} + c_{e,+1}}{\Delta x^2_{sep}}\right) \tag{4-52}$$

$$\dot{c}_{e,+1} = \frac{D^{eff}_{e_+}}{\epsilon_{e_+}}\left(\frac{c_{sep,2} - 2c_{e,+1} + c_{e,+2}}{\Delta x^2_+}\right) + \frac{1 - t^0_+}{F} j^{Li}_{+1} \tag{4-53}$$

$$\dot{c}_{e,+2} = \frac{D^{eff}_{e_+}}{\epsilon_{e_+}}\left(\frac{c_{e,+1} - 2c_{e,+2} + c_{e,+3}}{\Delta x^2_+}\right) + \frac{1 - t^0_+}{F} j^{Li}_{+2} \tag{4-54}$$

$$c_{e,-2} - c_{e,-3} = 0 \tag{4-55}$$

$$c_{e,+3} - c_{e,+2} = 0 \tag{4-56}$$

With this we added 8 unknowns $(c_{e,-3}, c_{e,-2}, c_{e,-1}, c_{sep,1}, c_{sep,2}, c_{e,+1}, c_{e,+2}, c_{e,+3})$ and 8 equations. Again the variables $c_{e,-3}$ and $c_{e,+3}$ are fictitious, they are resolved using one of the boundary conditions above.

The volumetric rate of electrochemical reaction at the solid/ electrolyte interface (j^{Li}) is obtained by The Butler-volmer kinetic expression (equation (4-15))which is a static equation and can be written for each discretized slice at the positive and negative electrode.

$$\begin{aligned} j^{Li}_{-2} = \; & a_{s\_} j_{0\_} \left[exp\left(\frac{\alpha_a F}{RT}\eta_{-2}\right) - exp\left(-\frac{\alpha_c F}{RT}\eta_{-2}\right) \right] \\ & \text{where,} \;\; \eta_{-2} = \phi_{s,-2} - \phi_{e,-2} - U_{-}\left(c_{s(-2,3)}\right) \end{aligned} \tag{4-57}$$

$$\begin{aligned} j^{Li}_{-1} = \; & a_{s\_} j_{0\_} \left[exp\left(\frac{\alpha_a F}{RT}\eta_{-1}\right) - exp\left(-\frac{\alpha_c F}{RT}\eta_{-1}\right) \right] \\ & \text{where,} \;\; \eta_{-1} = \phi_{s,-1} - \phi_{e,-1} - U_{-}\left(c_{s(-1,3)}\right) \end{aligned} \tag{4-58}$$

$$\begin{aligned} j^{Li}_{+1} = \; & a_{s_+} j_{0_+} \left[exp\left(\frac{\alpha_a F}{RT}\eta_{+1}\right) - exp\left(-\frac{\alpha_c F}{RT}\eta_{+1}\right) \right] \\ & \text{where,} \;\; \eta_{+1} = \phi_{s,+1} - \phi_{e,+1} - U_{+}\left(c_{s(+1,3)}\right) \end{aligned} \tag{4-59}$$

$$\begin{aligned} j^{Li}_{+2} = \; & a_{s_+} j_{0_+} \left[exp\left(\frac{\alpha_a F}{RT}\eta_{+2}\right) - exp\left(-\frac{\alpha_c F}{RT}\eta_{+2}\right) \right] \\ & \text{where,} \;\; \eta_{+2} = \phi_{s,+2} - \phi_{e,+2} - U_{+}\left(c_{s(+2,3)}\right) \end{aligned} \tag{4-60}$$

With these we added no new variables and 4 new equations. This essentially concludes the equations describing this model.

Lastly, the measurable quantity of the cell which is the terminal voltage is simply given by the solid phase potential difference of the last sphere and the first sphere, less the potential drop at the film resistance, equation (4-20).

$$V = \phi_{s,+2} - \phi_{s,-2} - \frac{R_f}{A} I \tag{4-61}$$

In the whole discretized model, we have 55 equations and 55 unknown variables, thus the system is solvable. We have 18 dynamic equations which is the order of the system and 37 static equations. The terms j^{Li}_s couples the dynamic and static equations. The dynamic equations can be solved using numerical integration however at each time instant, we need to evaluate for the terms j^{Li}_s by solving the whole set of coupled non-linear static equations using iterative techniques. With only two discretized parts each at negative electrode, separator and positive electrode, and only three discretized parts for each sphere, we observe that the order of the system is 18. This order grows quickly with finer discretization schemes and thus prohibiting real-time implementation of this model. With N_n number of discretized parts in the negative electrode, N_s number of discretized parts in the separator, N_p number discretized parts in the positive electrode and N_r number of discretized parts along the radius of each sphere we obtain a system of order $N_n\,(N_r + 1) + N_s + N_p\,(N_r + 1)$.

4-4 Model as String Interconnected System

We observed that the real-time simulation of high order non-linear Li-ion cell model is difficult. Thus in this section a new approach will be shown where the cell is modeled as spatially distributed string interconnected system as shown in Figure 4-3 where $N = N_n + N_s + N_p$. An explicit state-space model for each discretized part of the cell will be developed.

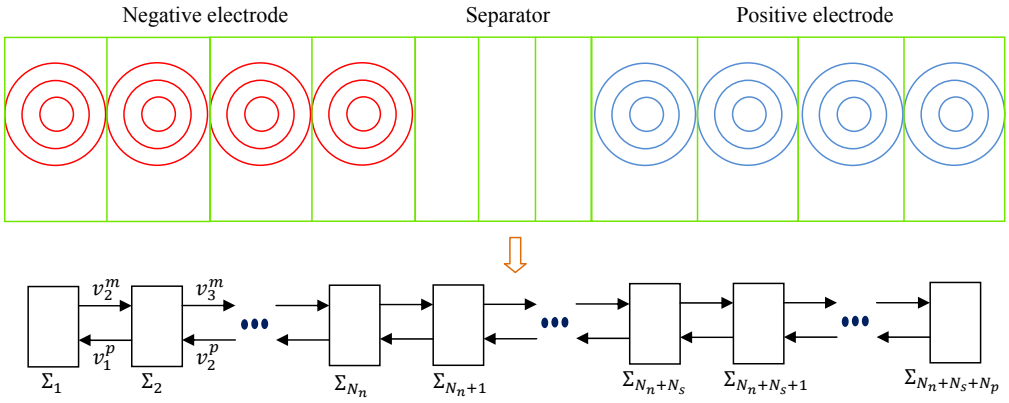

Figure 4-3: Li-ion cell as spatially distributed string interconnected system

4-4-1 Positive and Negative Electrodes

A single discretized part of positive / negative electrode (Σ_2 to Σ_{N_n-1} and $\Sigma_{N_n+N_s+2}$ to $\Sigma_{N_n+N_s+N_p-1}$) is shown in Figure 4-4 with neighboring parts shown dotted. Here, we are modeling the discretized parts of positive / negative electrode which have neighboring parts on both sides. The boundary parts will be delt with separately in section 4-4-3. For simplicity of notations, subscript 1 is assigned to the variables of the part whose model Σ_s is being developed. For instance, ϕ_{e1} is the electrolyte phase potential of the discretized part Σ_s under consideration, while ϕ_{e0} is the electrolyte phase potential of its neighboring block Σ_{s-1} to the left and ϕ_{e2} is the electrolyte phase potential of its neighboring block Σ_{s+1} to the right, Figure 4-4. For the variables which are inbetween the discretized parts i.e. currents, a simple rule is used; the currents leaving the block under consideration, Σ_s are assigned with subscript 1, while the currents entering the block under consideration are assigned with subscript 0. These rules are used while developing models of all discretized parts in the following sections. Further, with inputs and outputs here we mean the interconnecting inputs and outputs from neighboring blocks. The exogenous input and output which are terminal current per unit area $\frac{I}{A}$ and terminal voltage V respectively appear only at the discretized boundary parts shown in section 4-4-3.

We derive a non-linear state space model for a part of positive / negative electrode. We first obtain the state equations for the model which arise from the dynamic equations. As shown in 4-3 we have 3 dynamic equations for the solid spherical active material particle. Using equations, (4-44), (4-45) and (4-46) and eliminating the fictitious variables using boundary conditions (4-47) and (4-48) we obtain in this case,

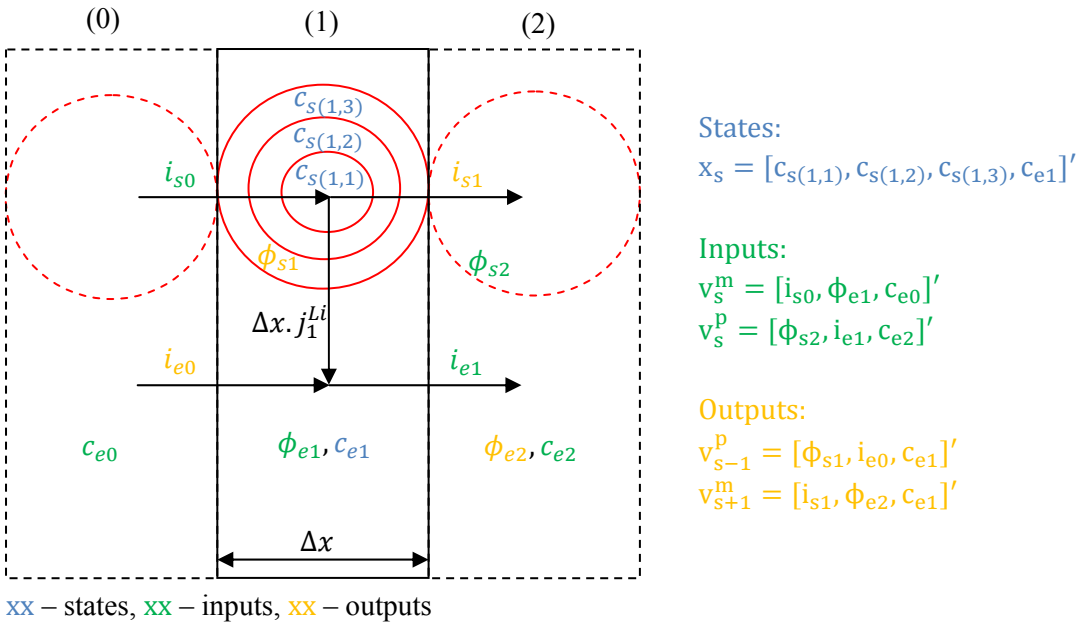

Figure 4-4: A single discretized part of positive / negative electrode interconnected with neighboring blocks shown as dotted

$$\dot{c}_{s(1,1)} = -\left(\frac{2D_s}{r_1\Delta r} + \frac{D_s}{\Delta r^2}\right) c_{s(1,1)} + \left(\frac{2D_s}{r_1\Delta r} + \frac{D_s}{\Delta r^2}\right) c_{s(1,2)} \tag{4-62}$$

$$\dot{c}_{s(1,2)} = \left(\frac{D_s}{\Delta r^2}\right) c_{s(1,1)} - \left(\frac{2D_s}{r_2\Delta r} + \frac{2D_s}{\Delta r^2}\right) c_{s(1,2)} + \left(\frac{2D_s}{r_2\Delta r} + \frac{D_s}{\Delta r^2}\right) c_{s(1,3)} \tag{4-63}$$

$$\dot{c}_{s(1,3)} = \left(\frac{D_s}{\Delta r^2}\right) c_{s(1,2)} - \left(\frac{D_s}{\Delta r^2}\right) c_{s(1,3)} - \left(\frac{2}{r_3 a_s F} + \frac{1}{\Delta r a_s F}\right) j_1^{Li} \tag{4-64}$$

Note that subscripts $-$ or $+$ need to be added for the parameters at the negative and positive electrode respectively.

There is one more dynamic equation for the electrolyte concentration,

$$\dot{c}_{e1} = -\frac{2D_e^{eff}}{\epsilon_e \Delta x^2} c_{e1} + \frac{D_e^{eff}}{\epsilon_e \Delta x^2} c_{e0} + \frac{D_e^{eff}}{\epsilon_e \Delta x^2} c_{e2} + \frac{1 - t_+^0}{F} j_1^{Li} \tag{4-65}$$

Thus we have 4 dynamic equations, corresponding to each state. By observing these equations, it is clear that the derivative of state is a function of states and j_1^{Li}. We want it to be a function of states and inputs, thus the next task is to obtain j_1^{Li} as a function of states and inputs.

We have the following discretized static equations,

$$i_{e1} = -\kappa^{eff}\left(\frac{\phi_{e2}-\phi_{e1}}{\Delta x}\right) - \kappa_D^{eff}\left(\frac{lnc_{e2}-lnc_{e1}}{\Delta x}\right) \tag{4-66}$$

$$i_{s1} = -\sigma^{eff}\left(\frac{\phi_{s2}-\phi_{s1}}{\Delta x}\right) \tag{4-67}$$

$$i_{e1} - i_{e0} = \Delta x j_1^{Li} \tag{4-68}$$

$$i_{s1} - i_{s0} = -\Delta x j_1^{Li} \tag{4-69}$$

$$\begin{aligned} j_1^{Li} = \ & a_s j_0 \left[exp\left(\tfrac{\alpha_a F}{RT}\eta_1\right) - exp\left(-\tfrac{\alpha_c F}{RT}\eta_1\right) \right] \\ \text{where,} \ & \eta_1 = \phi_{s1} - \phi_{e1} - U\left(c_{s(1,3)}\right) \end{aligned} \tag{4-70}$$

If we eliminate ϕ_{s1} from equation (4-70) by using equation (4-67) and then eliminate i_{s1} using equation (4-69) we get j_1^{Li} as a function of states, inputs but also j_1^{Li} itself. This leads to an implicit expression and thus prohibiting the state equations to be written in standard form. To bring this expression to explicit form, we need to use the linearized version of equation (4-70). Referring to [1] we write the linearized version of Butler-volmer kinetic expression,

$$\begin{aligned} j_1^{Li} &= \tfrac{a_s}{R_{ct}}\left[\phi_{s1} - \phi_{e1} - U\left(c_{s(1,3)}\right)\right] \\ \text{where,} \ & R_{ct} = \tfrac{RT}{j_0 F(\alpha_a+\alpha_c)} \end{aligned} \tag{4-71}$$

The validity of this linearization is investigated in the range of interest (based on high rate dis/charge current profiles). Taking the 6Ah Li-ion cell parameters, it is found that even in the range of $\pm 20 A/cm^3$ the maximum linearization error is only 0.8503% in the case of positive electrode and 0.3070% in the case of negative electrode as shown in Figure 4-5.

Now combining (4-67) and (4-69) we get,

$$\phi_{s1} = -\frac{\Delta x^2}{\sigma^{eff}} j_1^{Li} + \phi_{s2} + \frac{\Delta x}{\sigma^{eff}} i_{s0} \tag{4-72}$$

Substituting (4-72) in (4-71),

$$\begin{aligned} j_1^{Li} &= \tfrac{a_s}{\beta R_{ct}}\phi_{s2} + \tfrac{a_s}{\beta R_{ct}}\tfrac{\Delta x}{\sigma^{eff}} i_{s0} - \tfrac{a_s}{\beta R_{ct}}\phi_{e1} - \tfrac{a_s}{\beta R_{ct}} U\left(c_{s(1,3)}\right) \\ \text{where,} \ & \beta = 1 + \tfrac{\Delta x^2}{\sigma^{eff}}\tfrac{a_s}{R_{ct}} \end{aligned} \tag{4-73}$$

Thus we obtained j_1^{Li} as a function of states and inputs. Now substituting this expression in the dynamic equations (4-62), (4-63), (4-64) and (4-65) we obtain the following state equation,

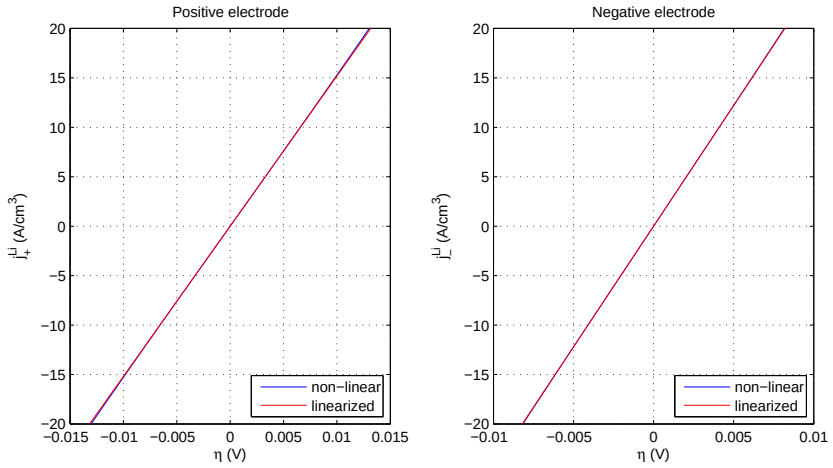

Figure 4-5: Non-linear versus Linearized Butler-volmer kinetic expression in the range of interest

$$\dot{x}_s = \begin{bmatrix} -\left(\frac{2D_s}{r_1\Delta r}+\frac{D_s}{\Delta r^2}\right) & +\left(\frac{2D_s}{r_1\Delta r}+\frac{D_s}{\Delta r^2}\right) & 0 & 0 \\ \frac{D_s}{\Delta r^2} & -\left(\frac{2D_s}{r_2\Delta r}+\frac{2D_s}{\Delta r^2}\right) & \left(\frac{2D_s}{r_2\Delta r}+\frac{D_s}{\Delta r^2}\right) & 0 \\ 0 & \frac{D_s}{\Delta r^2} & -\frac{D_s}{\Delta r^2} & 0 \\ 0 & 0 & 0 & -\frac{2D_e^{eff}}{\epsilon_e\Delta x^2} \end{bmatrix} x_s$$
$$+ \begin{bmatrix} 0 \\ 0 \\ -\Omega\, U\left(x_s\left(3\right)\right) \\ -\gamma\, U\left(x_s\left(3\right)\right) \end{bmatrix} + \begin{bmatrix} 0 & 0 & 0 \\ 0 & 0 & 0 \\ \Omega & 0 & 0 \\ \gamma & 0 & \frac{D_e^{eff}}{\epsilon_e\Delta x^2} \end{bmatrix} v_s^p + \begin{bmatrix} 0 & 0 & 0 \\ 0 & 0 & 0 \\ \Omega\frac{\Delta x}{\sigma^{eff}} & -\Omega & 0 \\ \gamma\frac{\Delta x}{\sigma^{eff}} & -\gamma & \frac{D_e^{eff}}{\epsilon_e\Delta x^2} \end{bmatrix} v_s^m \tag{4-74}$$
$$\text{where,}\quad \Omega = -\frac{1}{\beta R_{ct}}\left(\frac{2}{r_3 F}+\frac{1}{\Delta r F}\right) \quad \gamma = \frac{a_s}{\beta R_{ct}}\left(\frac{1-t_+^0}{F}\right)$$

From this equation, the linear and non-linear state dependent parts can be seen separately and there is no non-linear input dependency.

Now we derive the output equations for a discretized part of positive / negative electrode. Defining some constants,

$$M_1 = \frac{\Delta x a_s}{\beta R_{ct}} \quad M_2 = \frac{\Delta x^2}{\sigma^{eff}}\frac{a_s}{\beta R_{ct}}$$
$$M_3 = \frac{\Delta x}{\sigma^{eff}} \quad M_4 = -\frac{\Delta x}{\kappa^{eff}} \quad K_d K = \frac{\kappa_D^{eff}}{\kappa^{eff}} \tag{4-75}$$

Using equations (4-72) and (4-73) we get ϕ_{s1} while using equations (4-68) and (4-73) we get i_{e0} thus,

$$v_{s-1}^{p} = \begin{bmatrix} M_2 U\left(x_s\left(3\right)\right) \\ M_1 U\left(x_s\left(3\right)\right) \\ x_s\left(4\right) \end{bmatrix} + \begin{bmatrix} \left(1-M_2\right) & 0 & 0 \\ -M_1 & 1 & 0 \\ 0 & 0 & 0 \end{bmatrix} v_s^p + \begin{bmatrix} M_3\left(1-M_2\right) & M_2 & 0 \\ -M_2 & M_1 & 0 \\ 0 & 0 & 0 \end{bmatrix} v_s^m \tag{4-76}$$

Using equations (4-69) and (4-73) we get i_{s1} while using equation (4-66) we get ϕ_{e2} thus,

$$\begin{aligned} v_{s+1}^{m} = & \begin{bmatrix} M_1 U\left(x_s\left(3\right)\right) \\ K_d K ln\left(x_s\left(4\right)\right) \\ x_s\left(4\right) \end{bmatrix} + \begin{bmatrix} -M_1 & 0 & 0 \\ 0 & M_4 & 0 \\ 0 & 0 & 0 \end{bmatrix} v_s^p \\ & + \begin{bmatrix} -\left(M_2-1\right) & M_1 & 0 \\ 0 & 1 & 0 \\ 0 & 0 & 0 \end{bmatrix} v_s^m + \begin{bmatrix} 0 \\ -K_d K ln\left(v_s^p\left(3\right)\right) \\ 0 \end{bmatrix} \end{aligned} \tag{4-77}$$

With this we complete the derivation of state-space model for a discretized part of positive / negative electrode in the desired form.

4-4-2 Separator

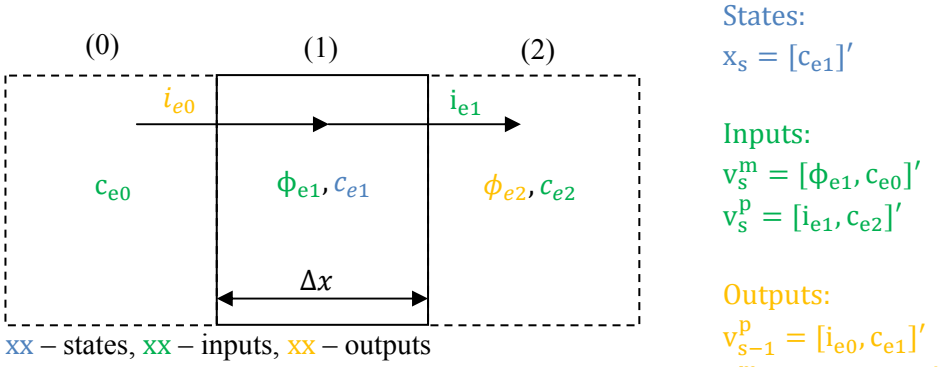

Figure 4-6: A single discretized part of separator, interconnected with neighboring blocks shown as dotted

A single discretized part of separator (Σ_{N_n+1} to $\Sigma_{N_n+N_s}$) is shown in Figure 4-6 with neighboring parts shown dotted. There is no solid active material particle in this block and there is only one state i.e. the electrolyte phase Li^+ ion concentration. We derive a non-linear state space model for this part. We first obtain the state equation for the model which arise from discretization of equation (4-13),

$$\dot{x}_s = \left[-\frac{2D_e^{eff}}{\epsilon_e \Delta x^2}\right] x_s + \left[\begin{array}{cc} 0 & \frac{D_e^{eff}}{\epsilon_e \Delta x^2} \end{array}\right] v_s^p + \left[\begin{array}{cc} 0 & \frac{D_e^{eff}}{\epsilon_e \Delta x^2} \end{array}\right] v_s^m \tag{4-78}$$

Now we obtain the output equations which arise from discretization of equations (4-9) and (4-66),

$$v_{s-1}^p = \left[\begin{array}{c} 0 \\ x_s \end{array}\right] + \left[\begin{array}{cc} 1 & 0 \\ 0 & 0 \end{array}\right] v_s^p + \left[\begin{array}{cc} 0 & 0 \\ 0 & 0 \end{array}\right] v_s^m \tag{4-79}$$

$$v_{s+1}^m = \left[\begin{array}{c} K_d K ln\left(x_s\right) \\ x_s \end{array}\right] + \left[\begin{array}{cc} -\frac{\Delta x}{\kappa^{eff}} & 0 \\ 0 & 0 \end{array}\right] v_s^p + \left[\begin{array}{cc} 1 & 0 \\ 0 & 0 \end{array}\right] v_s^m + \left[\begin{array}{c} -K_d K ln\left(v_s^p\left(2\right)\right) \\ 0 \end{array}\right] \tag{4-80}$$

This concludes the derivation of state-space model for a discretized part of separator in the desired form.

4-4-3 Boundary Elements

We need to impose the boundary conditions on four boundary elements. These are: terminal blocks of negative and positive electrodes and the blocks of positive and negative electrodes adjacent to the separator. This has to be done since the terminal block of negative electrode has no interconnecting inputs or outputs to the left. That is v_s^m and v_{s-1}^p do not exist for this block. They need to be evaluated using boundary conditions. Similarly inputs v_s^p and outputs v_{s+1}^m do not exist in the case of terminal block of positive electrode. While in the case of blocks of negative and positive electrodes just adjacent to the separator, there is size mismatch between the interconnecting inputs and outputs, which needs to be resolved by means of boundary conditions. We'll take the blocks one by one, impose the boundary conditions and then show the modified state-space representation of the model.

Negative Terminal:

For the negative terminal block (Σ_1), three inputs corresponding to the vector v_s^m do not exist. They are resolved using the following three boundary conditions.

$$\begin{aligned} i_{s0} &= \tfrac{I}{A} \\ i_{e0} &= 0 \\ c_{e0} &= c_{e1} \end{aligned} \tag{4-81}$$

Using the first boundary condition here, we obtain $v_s^m\left(1\right)$ while using the second boundary condition in equation for $v_{s-1}^p\left(2\right)$, (4-76) we eliminate $v_s^m\left(2\right)$ and from the third boundary condition, we obtain $v_s^m\left(3\right)$. Thus leading to state equation as,

$$\dot{x}_s = \begin{bmatrix} -\left(\frac{2D_s}{r_1\Delta r} + \frac{D_s}{\Delta r^2}\right) & +\left(\frac{2D_s}{r_1\Delta r} + \frac{D_s}{\Delta r^2}\right) & 0 & 0 \\ \frac{D_s}{\Delta r^2} & -\left(\frac{2D_s}{r_2\Delta r} + \frac{2D_s}{\Delta r^2}\right) & \left(\frac{2D_s}{r_2\Delta r} + \frac{D_s}{\Delta r^2}\right) & 0 \\ 0 & \frac{D_s}{\Delta r^2} & -\frac{D_s}{\Delta r^2} & 0 \\ 0 & 0 & 0 & -\frac{D_e^{eff}}{\epsilon_e \Delta x^2} \end{bmatrix} x_s + \begin{bmatrix} 0 & 0 & 0 \\ 0 & 0 & 0 \\ 0 & \frac{\Omega}{M_1} & 0 \\ 0 & \frac{\gamma}{M_1} & \frac{D_e^{eff}}{\epsilon_e \Delta x^2} \end{bmatrix} v_s^p + \begin{bmatrix} 0 \\ 0 \\ -\frac{\Omega M_2}{M_1} + \frac{\Omega \Delta x}{\sigma^{eff}} \\ -\frac{\gamma M_2}{M_1} + \frac{\gamma \Delta x}{\sigma^{eff}} \end{bmatrix} \frac{I}{A} \tag{4-82}$$

Here we also have an additional exogenous input dependent term. Similarly the output equations are,

$$v_{s+1}^m = \begin{bmatrix} 0 \\ -U\left(x_s\left(3\right)\right) + K_d K ln\left(x_s\left(4\right)\right) \\ x_s\left(4\right) \end{bmatrix} + \begin{bmatrix} 0 & -1 & 0 \\ 1 & M_4 - \frac{1}{M_1} & 0 \\ 0 & 0 & 0 \end{bmatrix} v_s^p + \begin{bmatrix} 1 \\ \frac{M_2}{M_1} \\ 0 \end{bmatrix} \frac{I}{A} + \begin{bmatrix} 0 \\ -K_d K ln\left(v_s^p\left(3\right)\right) \\ 0 \end{bmatrix} \tag{4-83}$$

The second set of output equations for v_{s-1}^p are not needed since there is no neighboring block on the left. However we are still interested in $v_{s-1}^p\left(1\right)$ as exogenous output. This is the solid phase potential at the negative terminal which is needed to obtain the terminal voltage.

$$y_1 = \left[0\right] x_s + \begin{bmatrix} 1 & -\frac{M_2}{M_1} & 0 \end{bmatrix} v_s^p + \left[M_3\left(1 - M_2\right) + \frac{\left(M_2\right)^2}{M_1}\right] \frac{I}{A} \tag{4-84}$$

It can be clearly seen that the state dependent part is zero which will lead to some observability problems as will be discussed later.

Negative - Separator:

For the block of negative electrode just adjacent to the separator (Σ_{N_n}), we have one boundary condition. This is used to resolve the size mismatch between the interconnecting variables of this block and the first block of the separator. The boundary condition is,

$$\phi_{s1} = \phi_{s2} \tag{4-85}$$

This can be used in the equation for $v_{s-1}^p\left(1\right)$, (4-76) to eliminate $v_s^p\left(1\right)$ since the input $v_s^p\left(1\right)$ is not provided by the separator block. However this is not done and an important assumption has to be made here. Since in this whole model, all solid phase potentials are given by difference equations in space, there are infinite number of combinations of potentials which hold true for the model equations. To resolve this, the solid phase potential of any one block has to be grounded and the value of other potentials considered with respect to it. If this

is not done, the interconnected system looses well posedness and cannot be simulated. Here assuming the solid phase potential of this block to be zero we get,

$$\phi_{s1} = \phi_{s2} = 0 \tag{4-86}$$

From this cell model, we are interested only in the potential difference between the terminal blocks, not individual potentials. Assuming any value of this potential does not make any difference in the terminal voltage given by the model.

Considering the interconnecting inputs and outputs with the separator as $v_s^p = [i_{e1},\ c_{e2}]^T$ and $v_{s+1}^m = [\phi_{e2},\ c_{e1}]^T$ we have modified the state and output equations as,

$$\begin{aligned}\dot{x}_s = &\begin{bmatrix} -\left(\frac{2D_s}{r_1\Delta r} + \frac{D_s}{\Delta r^2}\right) & +\left(\frac{2D_s}{r_1\Delta r} + \frac{D_s}{\Delta r^2}\right) & 0 & 0 \\ \frac{D_s}{\Delta r^2} & -\left(\frac{2D_s}{r_2\Delta r} + \frac{2D_s}{\Delta r^2}\right) & \left(\frac{2D_s}{r_2\Delta r} + \frac{D_s}{\Delta r^2}\right) & 0 \\ 0 & \frac{D_s}{\Delta r^2} & -\frac{D_s}{\Delta r^2} & 0 \\ 0 & 0 & 0 & -\frac{2D_e^{eff}}{\epsilon_e \Delta x^2} \end{bmatrix} x_s \\ &+ \begin{bmatrix} 0 \\ 0 \\ -\Omega\ U\left(x_s\left(3\right)\right) \\ -\gamma\ U\left(x_s\left(3\right)\right) \end{bmatrix} + \begin{bmatrix} 0 & 0 \\ 0 & 0 \\ 0 & 0 \\ 0 & \frac{D_e^{eff}}{\epsilon_e \Delta x^2} \end{bmatrix} v_s^p + \begin{bmatrix} 0 & 0 & 0 \\ 0 & 0 & 0 \\ \Omega\frac{\Delta x}{\sigma^{eff}} & -\Omega & 0 \\ \gamma\frac{\Delta x}{\sigma^{eff}} & -\gamma & \frac{D_e^{eff}}{\epsilon_e \Delta x^2} \end{bmatrix} v_s^m \end{aligned} \tag{4-87}$$

$$v_{s-1}^p = \begin{bmatrix} 0 \\ M_1 U\left(x_s\left(3\right)\right) \\ x_s\left(4\right) \end{bmatrix} + \begin{bmatrix} 0 & 0 \\ 1 & 0 \\ 0 & 0 \end{bmatrix} v_s^p + \begin{bmatrix} 0 & 0 & 0 \\ -M_2 & M_1 & 0 \\ 0 & 0 & 0 \end{bmatrix} v_s^m \tag{4-88}$$

$$\begin{aligned} v_{s+1}^m = &\begin{bmatrix} K_d K ln\left(x_s\left(4\right)\right) \\ x_s\left(4\right) \end{bmatrix} + \begin{bmatrix} M_4 & 0 \\ 0 & 0 \end{bmatrix} v_s^p \\ &+ \begin{bmatrix} 0 & 1 & 0 \\ 0 & 0 & 0 \end{bmatrix} v_s^m + \begin{bmatrix} -K_d K ln\left(v_s^p\left(2\right)\right) \\ 0 \end{bmatrix} \end{aligned} \tag{4-89}$$

Positive - Separator:

For the block of positive electrode just adjacent to the separator ($\Sigma_{N_n+N_s+1}$), we have one boundary condition. This is used to resolve the size mismatch between the interconnecting variables of this block and the last block of the separator. The boundary condition is,

$$i_{s0} = 0 \tag{4-90}$$

From this we eliminate the input $v_s^m\left(1\right)$ which is not provided by the separator block on the left. Now considering the interconnecting inputs and outputs with the separator as $v_s^m = [\phi_{e1},\ c_{e0}]^T$ and $v_{s-1}^p = [i_{e0},\ c_{e1}]^T$ we have modified the state and output equations as,

$$\dot{x}_s = \begin{bmatrix} -\left(\frac{2D_s}{r_1\Delta r} + \frac{D_s}{\Delta r^2}\right) & +\left(\frac{2D_s}{r_1\Delta r} + \frac{D_s}{\Delta r^2}\right) & 0 & 0 \\ \frac{D_s}{\Delta r^2} & -\left(\frac{2D_s}{r_2\Delta r} + \frac{2D_s}{\Delta r^2}\right) & \left(\frac{2D_s}{r_2\Delta r} + \frac{D_s}{\Delta r^2}\right) & 0 \\ 0 & \frac{D_s}{\Delta r^2} & -\frac{D_s}{\Delta r^2} & 0 \\ 0 & 0 & 0 & -\frac{2D_e^{eff}}{\epsilon_e \Delta x^2} \end{bmatrix} x_s + \begin{bmatrix} 0 \\ 0 \\ -\Omega\, U\left(x_s\left(3\right)\right) \\ -\gamma\, U\left(x_s\left(3\right)\right) \end{bmatrix} + \begin{bmatrix} 0 & 0 & 0 \\ 0 & 0 & 0 \\ \Omega & 0 & 0 \\ \gamma & 0 & \frac{D_e^{eff}}{\epsilon_e \Delta x^2} \end{bmatrix} v_s^p + \begin{bmatrix} 0 & 0 \\ 0 & 0 \\ -\Omega & 0 \\ -\gamma & \frac{D_e^{eff}}{\epsilon_e \Delta x^2} \end{bmatrix} v_s^m \tag{4-91}$$

$$v_{s-1}^p = \begin{bmatrix} M_1 U\left(x_s\left(3\right)\right) \\ x_s\left(4\right) \end{bmatrix} + \begin{bmatrix} -M_1 & 1 & 0 \\ 0 & 0 & 0 \end{bmatrix} v_s^p + \begin{bmatrix} M_1 & 0 \\ 0 & 0 \end{bmatrix} v_s^m \tag{4-92}$$

$$v_{s+1}^m = \begin{bmatrix} M_1 U\left(x_s\left(3\right)\right) \\ K_d K ln\left(x_s\left(4\right)\right) \\ x_s\left(4\right) \end{bmatrix} + \begin{bmatrix} -M_1 & 0 & 0 \\ 0 & M_4 & 0 \\ 0 & 0 & 0 \end{bmatrix} v_s^p + \begin{bmatrix} M_1 & 0 \\ 1 & 0 \\ 0 & 0 \end{bmatrix} v_s^m + \begin{bmatrix} 0 \\ -K_d K ln\left(v_s^p\left(3\right)\right) \\ 0 \end{bmatrix} \tag{4-93}$$

Positive Terminal:

For the last block of positive electrode at the terminal $\Sigma_{N_n+N_s+N_p}$, three inputs corresponding to the vector v_s^p do not exist. They are resolved using the following three boundary conditions.

$$\begin{aligned} i_{e1} &= 0 \\ i_{s1} &= \tfrac{I}{A} \\ c_{e2} &= c_{e1} \end{aligned} \tag{4-94}$$

Using the first boundary condition here, we obtain $v_s^p\left(2\right)$ while using the second boundary condition in equation for $v_{s+1}^m\left(1\right)$, (4-77) we eliminate $v_s^p\left(1\right)$ and from the third boundary condition, we obtain $v_s^p\left(3\right)$. Thus leading to state equation and output equations as,

$$\dot{x}_s = \begin{bmatrix} -\left(\frac{2D_s}{r_1\Delta r}+\frac{D_s}{\Delta r^2}\right) & +\left(\frac{2D_s}{r_1\Delta r}+\frac{D_s}{\Delta r^2}\right) & 0 & 0 \\ \frac{D_s}{\Delta r^2} & -\left(\frac{2D_s}{r_2\Delta r}+\frac{2D_s}{\Delta r^2}\right) & \left(\frac{2D_s}{r_2\Delta r}+\frac{D_s}{\Delta r^2}\right) & 0 \\ 0 & \frac{D_s}{\Delta r^2} & -\frac{D_s}{\Delta r^2} & 0 \\ 0 & 0 & 0 & -\frac{D_e^{eff}}{\epsilon_e \Delta x^2} \end{bmatrix} x_s + \begin{bmatrix} 0 & 0 & 0 \\ 0 & 0 & 0 \\ -\Omega\frac{M_2-1}{M_1}+\Omega\frac{\Delta x}{\sigma^{eff}} & 0 & 0 \\ -\gamma\frac{M_2-1}{M_1}+\gamma\frac{\Delta x}{\sigma^{eff}} & 0 & \frac{D_e^{eff}}{\epsilon_e\Delta x^2} \end{bmatrix} v_s^m + \begin{bmatrix} 0 \\ 0 \\ -\frac{\Omega}{M_1} \\ -\frac{\gamma}{M_1} \end{bmatrix} \frac{I}{A} \tag{4-95}$$

$$v_{s-1}^p = \begin{bmatrix} U\left(x_s\left(3\right)\right) \\ 0 \\ x_s\left(4\right) \end{bmatrix} + \begin{bmatrix} \left(1-M_2\right)\frac{M_1M_3-M_2+1}{M1} & 1 & 0 \\ -1 & 0 & 0 \\ 0 & 0 & 0 \end{bmatrix} v_s^m + \begin{bmatrix} \frac{\left(M_2-1\right)}{M_1} \\ 1 \\ 0 \end{bmatrix} \frac{I}{A} \tag{4-96}$$

The exogenous output here is $v_{s-1}^p\left(1\right)$. This is the solid phase potential at the positive terminal which is needed to obtain the terminal voltage.

$$y_N = \begin{bmatrix} U\left(x_s\left(3\right)\right) \end{bmatrix} + \begin{bmatrix} \left(1-M_2\right)\frac{M_1M_3-M_2+1}{M1} & 1 & 0 \end{bmatrix} v_s^m + \begin{bmatrix} \frac{\left(M_2-1\right)}{M_1} \end{bmatrix} \frac{I}{A} \tag{4-97}$$

Thus we obtained the state-space representation of each discretized part of the cell. The exogenous input is the current per unit area $\frac{I}{A}$ entering and leaving the terminals and the exogenous output is the terminal voltage,

$$V = y_N - y_1 - R_f\frac{I}{A} \tag{4-98}$$

4-5 Efficient Simulator

After having developed the model as string interconnected system, the next step is to simulate it. To efficiently simulate this system, we need each discretized part to be in the form as mentioned in section 3-2,

$$\begin{aligned} \dot{x}_s &= f_s\left(x_s, v_s^p, v_s^m, u_s\right) \\ v_{s-1}^p &= g_{s1}\left(x_s, u_s\right) + W_s^p v_s^p + Z_s^m v_s^m \\ v_{s+1}^m &= g_{s2}\left(x_s, u_s\right) + Z_s^p v_s^p + W_s^m v_s^m \\ y_s &= h_s\left(x_s, v_s^p, v_s^m, u_s\right) \end{aligned} \tag{4-99}$$

that is we clearly want a linear dependency between the interconnecting variables so that they can be evaluated in a centralized block at each time instant and then each sub-systems can

be simulated independently. However in the cell model, this linear dependency is not true for one term, for instance, refer to the last term of equation (4-77). Fortunately, that non-linear term is nothing but the state of the next neighboring block and can be evaluated directly. It is combined with the first term as,

$$\begin{aligned} v_{s+1}^{m} = & \begin{bmatrix} M_1 U\left(x_s\left(3\right)\right) \\ K_d K l n\left(x_s\left(4\right)\right) - K_d K l n\left(x_{s+1}\left(4\right)\right) \\ x_s\left(4\right) \end{bmatrix} + \begin{bmatrix} -M_1 & 0 & 0 \\ 0 & M_4 & 0 \\ 0 & 0 & 0 \end{bmatrix} v_s^p \\ & + \begin{bmatrix} -\left(M_2 - 1\right) & M_1 & 0 \\ 0 & 1 & 0 \\ 0 & 0 & 0 \end{bmatrix} v_s^m \end{aligned} \tag{4-100}$$

Where $x_{s+1}\left(4\right)$ is the fourth state of the next neighboring block whose value is available in the centralized block and can be evaluated. Same procedure is also applicable in the case of separator and boundary elements. Thus we arrive at the output equations in the desired form. As shown in section 3-2, the linear interconnecting variables dependent part of all the output equations is casted in a matrix E while all the state and input dependent terms are casted into a vector b and all the interconnecting variables are combined in the vector i thus forming,

$$\begin{aligned} Ei &= b \\ i &= E^{-1} b \end{aligned} \tag{4-101}$$

In this case the inverse of matrix E does exist and the system is well posed. However if the solid phase potential of one of the discretized part is not grounded, which was done in equation (4-86), the matrix E turns out to be rank deficient. Further as shown in section 3-2, the matrix E has Sequentially Semi Separable (SSS) structure and thus enabling efficient $O\left(N\right)$ inverse computation. The algorithm of the simulator is shown in Figure 4-7.

We initialize the state and define constant parameters and state-space matrices of the model. At each time instant, the state dependent parameters are updated. With this modeling approach, the spatial dependency of these parameters can be addressed very easily since each discretized element is defined in space. Also the non-linear model is updated based on the current state. The next step is to construct matrix E and vector b and then obtaining the interconnected variables i. After having obtained this, all the sub-systems can be simulated parallely using an ODE solver. Thus clearly a zero order hold scheme is used for the interconnecting variables. The sampling time chosen is say h seconds.

4-6 Simulation Results

This section will show various simulation results of the efficient cell simulator developed in the previous section. A 313^{th} order CFD model has been identified and validated in the literature against constant current and transient pulse current experimental data from that cell. Plots of this model with various current dis/charge profiles have been shown in [1]. The

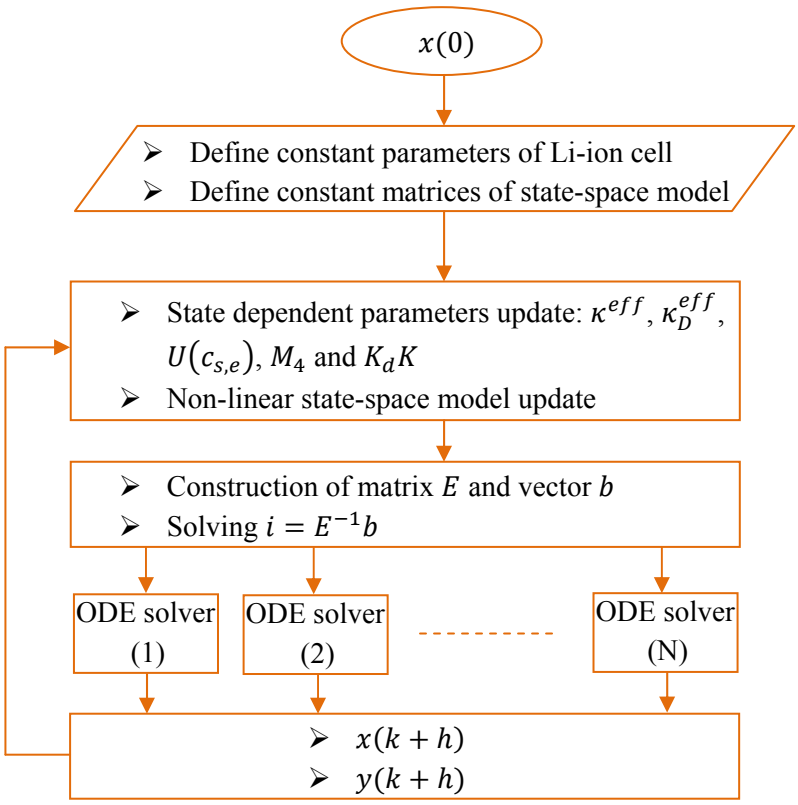

Figure 4-7: Li-ion cell simulator - algorithm

same model parameters are chosen and this higher order nonlinear CFD model is employed as a truth model for comparison with the model developed in this work. Thus a theoretical validation is done.

4-6-1 Model Order Selection

Before starting with the simulations, we need to decide the number of discretization points along the x and the r dimensions and thus the order of the model. The most critical choice is the discretization along the r dimension that is the number of discretized layers along the radial distance of the spherical active material particle. This is important to capture the solid phase diffusion phenomena of Li ions accurately. What happens is that during high rate dis/charge of the cell, the surface of the spherical active material particles become saturated or depleted of Li ions. Take for example the depletion case, which happens at the surface of active material particles of the negative electrode during high discharge currents. The depletion occurs since the Li ions are not diffused from inner regions to the surface fast enough to meet the demand of the reaction current at the surface. If we choose too few discretization points, this phenomena is not captured accurately. Say with 3 discretized

regions inside the sphere, the last region corresponding to the surface is large enough to supply Li ions for a long time before getting depleted. With increasing number of discretized regions we observe the depletion occurring faster and at the same time the transfer of Li ions from the previous inner region to the next region gets faster due to reducing widths of the regions and thus a point is reached when further discretization has little added value. We show the plots of terminal voltage and solid phase surface concentration $c_{s,e}$ obtained by simulating the model with different levels of discretization N_r of the spherical particles Figure 4-8. The input chosen is 10C (60A) of current for 20 seconds starting from 100% SoC followed by a period of rest. The negative electrode and positive electrode each is descretized into 5 parts and the separator into 3 parts. The second subplot of Figure 4-8 shows the surface concentration at 5 spherical active material particles of negative and positive electrode at time 20sec. The dimension x is normalized with respect to the total length of the cell L.

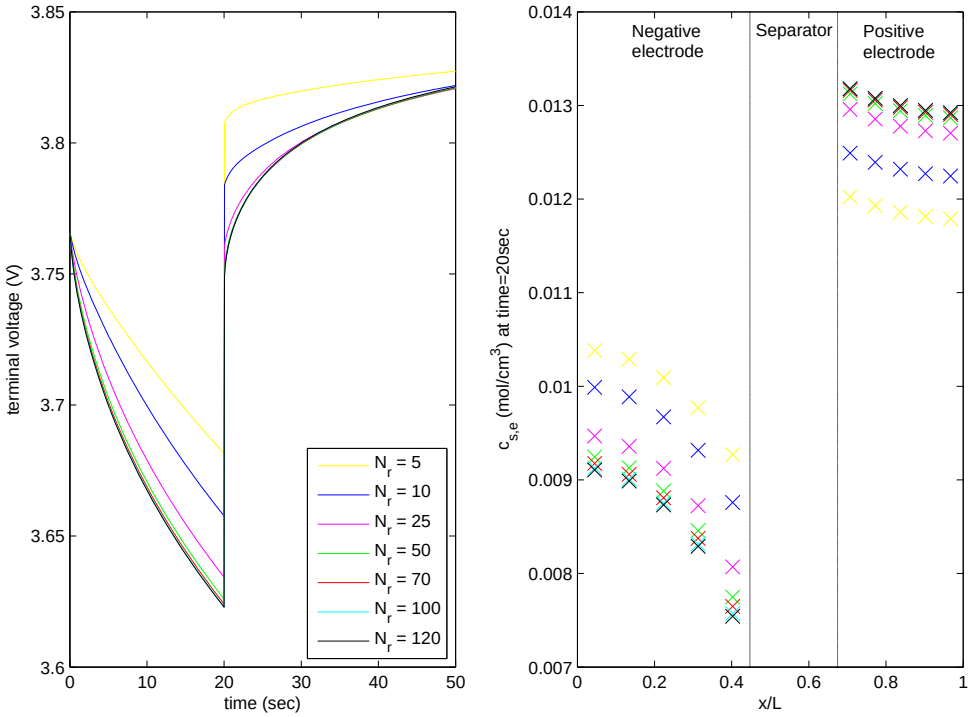

Figure 4-8: Effect of different levels of discretization of the spherical active material particle

We clearly observe that with finer discretization, the saturation / depletion at the surface is captured more accurately. However it also increases the order of the system thus a reasonable choice has to be made. Here we have chosen $N_r = 50$.

Also the discretization along the x dimension is important to capture the gradients formed in the electrolyte concentration with time. With discretizing the negative and positive electrode into 5 parts each and the separator into 3 parts we capture the gradients accurately as will be shown in the following sections.

4-6-2 Terminal Voltage Prediction

An important aspect of Li-ion cell model is its terminal voltage prediction capability. Here we show various plots of terminal voltage predicted by the model against the CFD model plots at various C-rates where C-rate is a standard way to represent the current with respect to the cell capacity. Here 1C is 6A of current since the nominal cell capacity is 6Ah, whereas 10C is ten times the current i.e. 60A.

A constant discharge current of 1C, 10C, 30C and 50C are applied to the model from 100% initial SoC condition and the terminal voltage is recorded against the Depth of Discharge (DoD) which is nothing but 100 minus the SoC of the cell Figure 4-9.

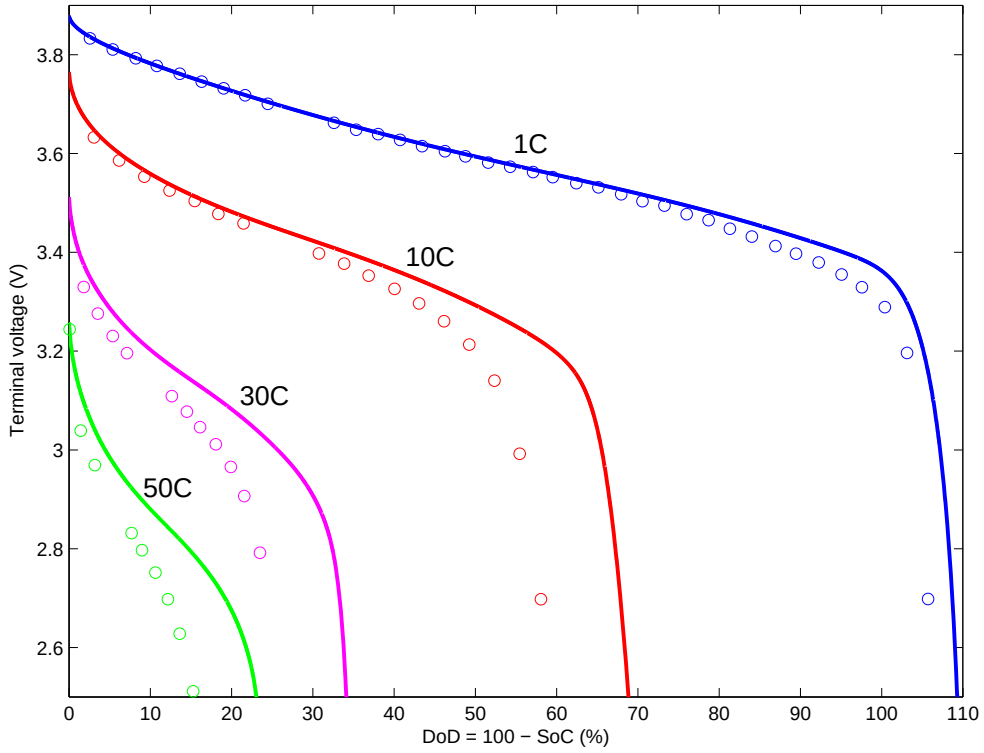

Figure 4-9: Terminal voltage prediction of model at different C-rates: (-) Discretized model, (o) CFD model

At low discharge current of 1C, it is observed that the cell can sustain this current even for more than 100% of its capacity i.e. the cell provides current of 1C for 1.1 hour. As the discharge current severity increases, the current is sustained only for a fraction of its capacity. That is say for extremely high discharge current of 50C (300A), the negative electrode surface gets depleted only within around 20% of depth of discharge. Though it does not mean that the cell is empty. If kept at rest for some time, the Li ions will diffuse from the inner regions to the surface and again current can be discharged from the cell.

The plot compares the model response with the CFD model, we observe that as current severity increases, we lose accuracy. This is attributed to two reasons, first being the level of

discretization of the spherical active material particles. With very high rate currents, when the solid phase surface concentration $c_{s,e}$ is driven to very low values quickly typically lower than 0.2 times $c_{s,max}$ the function $U(c_{s,e})$ increases very sharply. Thus very small errors in predicting $c_{s,e}$ will result into large errors in terminal voltage. It was shown in Figure 4-8 that with higher discretization, $c_{s,e}$ is predicted more accurately. The discharge current for that plot was chosen as 10C for 20sec and in that scenario, after $N_r = 50$ no much gain in accuracy was observed. However for sustained discharge at higher C rates, still higher discretization is needed to accurately predict the terminal voltage.

Secondly, the choice of the sampling time h also plays an important role. In the Figure 4-10 we have shown terminal voltage response at 50C discharge from 100% initial SoC condition at different sampling rates h. At the end of discharge, higher sampling results into more accurate plots. Also clearly there is a difference in $c_{s,e}$ prediction as shown in the second subplot.

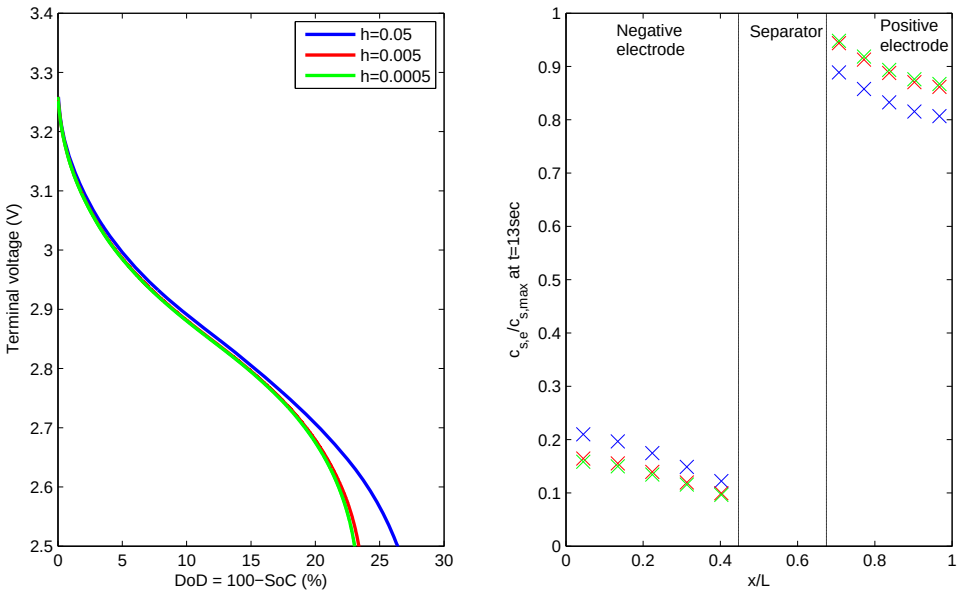

Figure 4-10: Terminal voltage and solid phase surface concentration prediction of model at different sampling rates

In the plots Figure 4-9 1C rate is simulated at 20Hz, 10C at 200Hz , 30C at 1000Hz and 50C at 2000Hz. In a vehicle application, very high discharge rates upto 50C are observed but they are only for a very short period of time. In the short time horizon of say 10% DoD the model predicts the terminal voltage accurately, less than 130mV even with 50C of discharge current and a miserly 20Hz of sampling. Thus this model can be considered acceptable for state-estimation application. Moreover, end of discharge is predicted in all the cases of Figure 4-9 within 10% SoC.

4-6-3 Gradients along x

The major motivation of developing this model is to capture the gradients of different quantities developed with time along the length of the cell, as we saw in previous plots, the distribution of solid phase surface concentration along L. The most important is the development of gradient of electrolyte phase concentration c_e, since some parameters are related to c_e which can be online updated along the length L and also the phenomena of electrolyte depletion can be estimated. The current cell under consideration does not experience electrolyte depletion at any current rate, however, other cells with less porous electrodes and separator may experience this limitation. To examine the development of gradients, the electrolyte diffusion coefficient was reduced by one order of magnitude in [1]. This was done for this model too and different quantities along L are compared with the CFD model as shown in Figure 4-11.

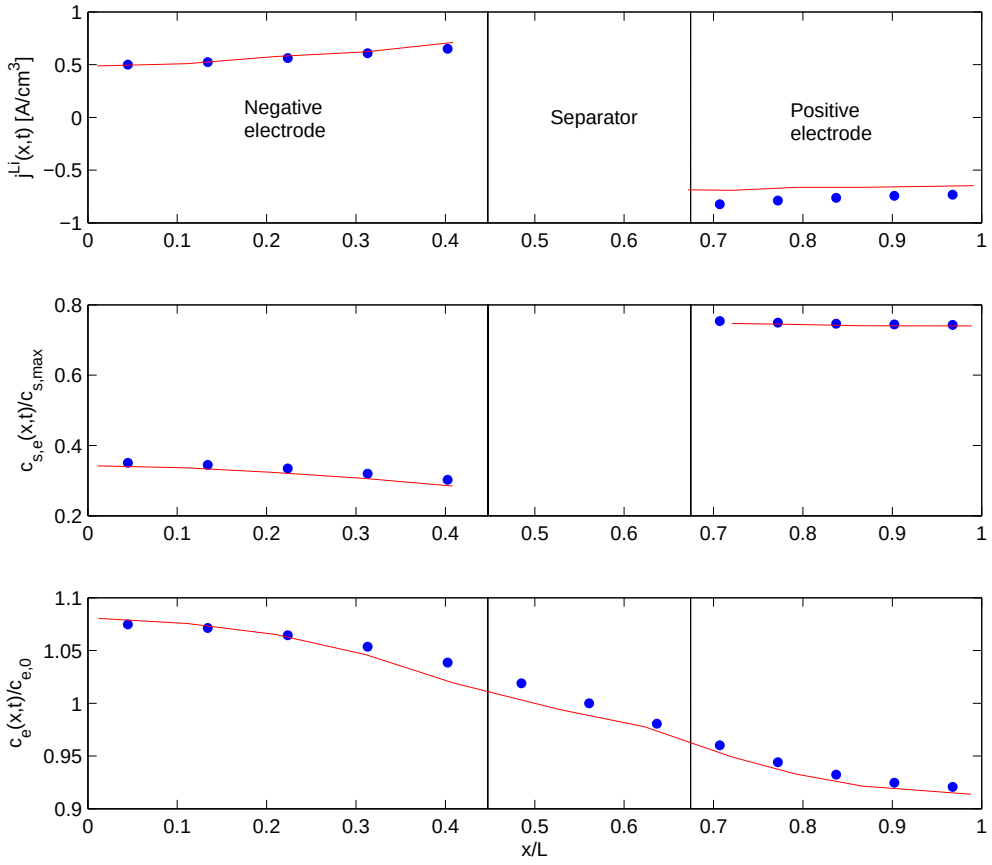

Figure 4-11: Gradient of different quantities formed along the length of the cell with 5C discharge current with 50% SoC initial condition at time = 20sec, Discretized model (*), CFD model (-)

It can be observed that the gradients are captured accurately by this model. The parameters κ^{eff} and κ_D^{eff} are a function of c_e which are very easily updated in each discretized part depending on the current value of c_e and thus this model can have significant advantage in cells

where such gradients are developed. Further the volumetric rate of electrochemical reaction at the solid/ electrolyte interface (j^{Li}) is coupled to c_e which is ignored in this model, however it can also be taken care very easily by updating the expression for j^{Li} in each discretized part based on c_e, which is expected to improve the model accuracy significantly especially in such cells. This is possible because of the structure of the model which preserves the spatial location of variables.

4-6-4 Response to Transient Current Profile

Apart from constant discharge currents, we need to test the model validity for sudden peaks of charge and discharge currents, which is normally the case in vehicle application. Here we show the terminal voltage response of the model with a very rate charge and discharge current profile against the voltage response from the CFD model, Figure 4-12.

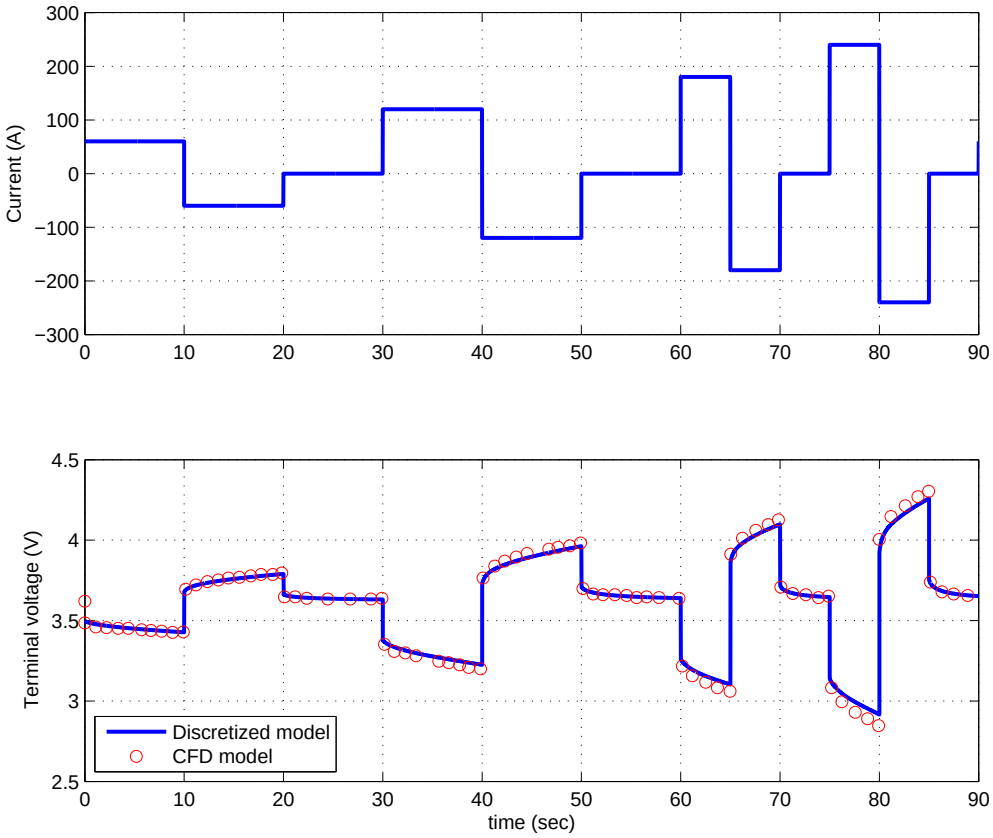

Figure 4-12: Voltage response of the model with high rate charge and discharge current profile

From 50% SoC initial condition with this current profile, we observe that the voltage response of the model has a maximum error of only 70mV at 40C charge pulse and its recovers very quickly in the following rest period.

4-6-5 Simulation Time

Here we'll show the simulation time taken by the model per step and also show how the simulation time grows with discretization. The simulations are performed on a 2.8GHz Intel Pentium 4 processor. Since the model is developed as spatially distributed string interconnected system, using the efficient simulation technique developed in section 3-2 we observe that the simulation time grows linearly $O(N)$ with increasing the number of discretization along x. First subplot of Figure 4-13 shows the simulation time with different discretization levels of positive electrode, negative electrode and separator keeping the discretization of spherical active material particle constant at 50. However in the case where the discretization level of positive electrode, negative electrode and separator are kept constant and the discretization level of spherical particle is increased, the simulation time does not grow linearly, since we have not exploited any structure in the r dimension. A two dimensional approach has the potential to give $O(N)$ simulation time in that dimension also. Nonetheless, it can be clearly seen that with the discretization of $N_r = 50$, $N_n = 5$, $N_p = 5$ and $N_s = 5$ only 0.13sec of computation time is required. Further the algorithm is fully parallelizable upto 10 times and with further optimization of code a real time implementation at 20-100Hz is possible.

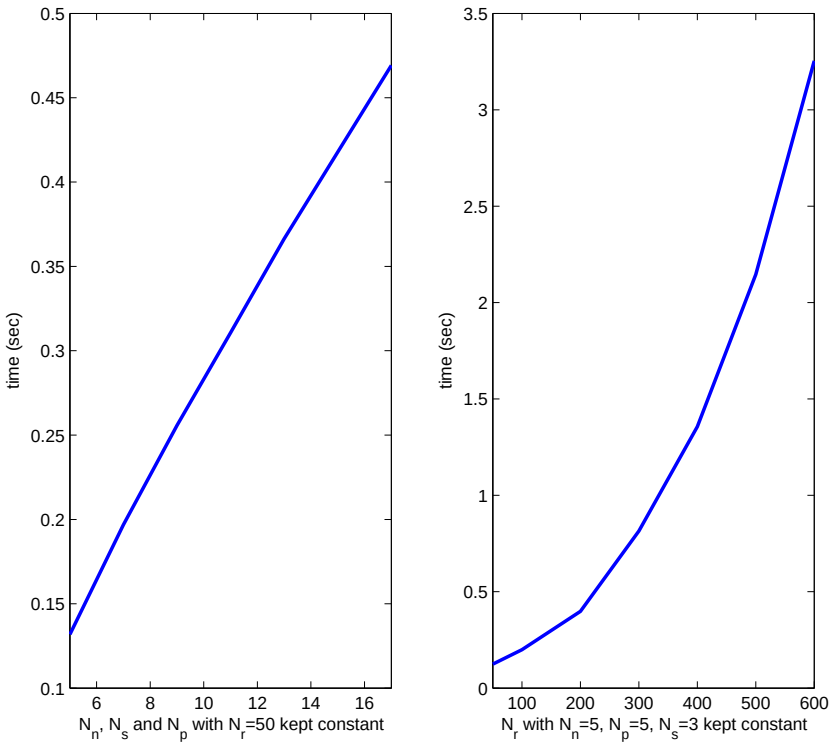

Figure 4-13: Simulation time per step for different discretization levels

4-7 Conclusion and Discussion

A Li-ion cell is modeled as spatially distributed string interconnected system and simulated efficiently in Matlab. The simulation results are compared against plots available in the literature which are based on a CFD model, identified and validated with experimental data from that cell. The results are found to be satisfactory with very high rates of constant as well as transient currents discharge as well as charge. The model is also able to predict the gradients developing along the length of the cell accurately which can be used for adapting some parameters at different points along the length of the cell. While investigating the simulation time per step required by the model, it was found that a real time implementation is possible. As a future development, a two dimensional structured approach is proposed wherein the structure of the model of each discretized part is also exploited. This may have great potential since the model of each discretized part is largely linear except the last two states. Thus each discretized part can be divided into two sub-parts, one non-linear of only order 2 and the other linear of order $N_r - 1$ where N_r is the level of discretization of spherical particle. The most time consuming step is non-linear simulation, which in this case will have to be performed only for a 2^{nd} order system. With this approach very high levels of discretization could be implemented in real-time gaining higher accuracy.

Chapter 5

SoC Estimation

In the last chapter, we developed a model of Lithium ion (Li-ion) cell as spatially distributed string interconnected system. In this chapter, we'll utilize this model to develop an efficient State of Charge (SoC) estimator based on Extended Kalman Filter (EKF) which was shown in chapter 3. The goal is to estimate the SoC of the cell based on measurement data of current and terminal voltage. First we analyze the observability of the model in section 5-1. We will find that the model with only one measurement is not observable. An innovative solution is proposed to solve this observability problem based on understanding of the internal processes taking place inside the cell. Using this approach, an SoC estimator is developed in section 5-2 and estimation results are shown in section 5-3.

5-1 Observability Analysis

The non-linear state-space model of Chapter 4 was first linearized at different equilibrium points. Since it is in the form of string interconnected system, each sub-system was linearized individually, converted to spatially strictly proper form and then lifted to obtain the lifted system matrices. It was found that these linear systems have three eigenvalues (λ) at the origin corresponding to integrator. All remaining eigenvalues are real and distributed along the negative real axis. Since this is a discretized model, we have finite number of eigenvalues while in reality, parabolic PDE systems, such as the three coupled diffusion problem considered here, are characterized by an infinite number of negative real eigenvalues. The Hautus test for observability [15] was used to check the observability of the model. It says that the pair (A, C) is observable if and only if the matrix,

$$\begin{bmatrix} A - \lambda I \\ C \end{bmatrix} \tag{5-1}$$

has full column rank for all $\lambda \in \mathbb{C}$. For this model, it was found that the three eigenvalues at the origin are not observable. To understand this loss of observability, let's understand the

processes inside the cell in a simplified manner. The Figure 5-1 shows the working of the cell in the most simplified manner, where the electrodes and the electrolyte are shown lumped.

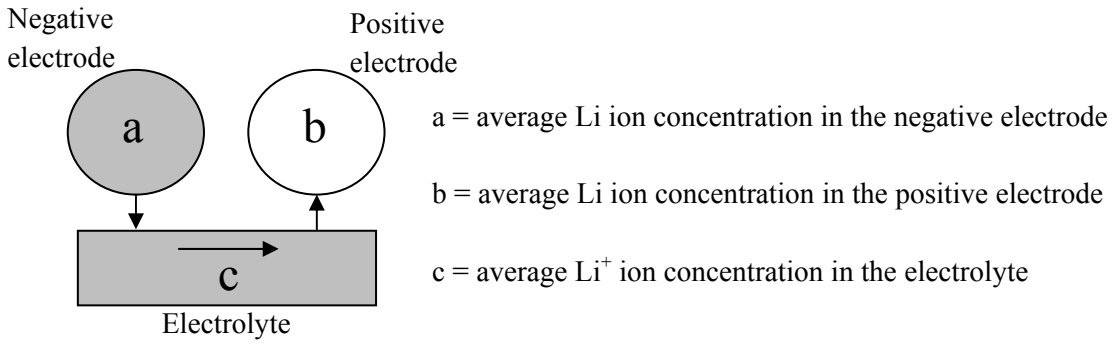

Figure 5-1: Simplified Li-ion cell schematic by lumping the electrodes and the electrolyte

Consider that the cell is fully charged. At this time, the value of a is maximum corresponding to 100% SoC say $c_{s,100-}$ while the value of b is minimum again corresponding to 100% SoC say $c_{s,100+}$. The value of c corresponds to the nominal value of Li^+ ion concentration in the electrolyte say $c_{e,0}$. During discharge, the Li ions convert from solid phase to liquid phase at the surface of the negative electrode, then they travel through the electrolyte to reach the positive electrode and at the positive electrode convert from liquid phase to solid phase. During high discharge, gradients are formed in the electrolyte and the electrodes as shown in Figure 5-2.

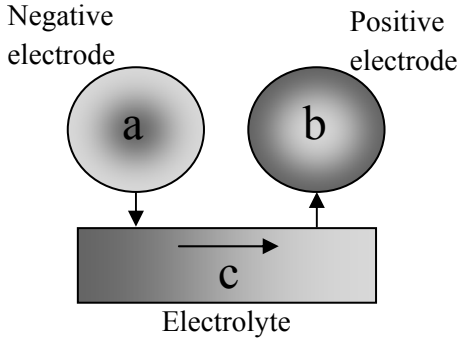

Figure 5-2: Simplified Li-ion cell schematic by lumping the electrodes and the electrolyte while getting discharged at high rate current

Thus during discharge, the value of a decreases while b increases. Gradients formed in the electrolyte are symmetric with respect to the centre of the length of the cell and thus the value of c remains close to its nominal value $c_{e,0}$. These three processes are happening inside the cell while the output is only one which is a function of a, b and c. In an observer we want to basically solve the inverse problem i.e. from the output to the estimates of a, b and c independently, which is not possible. To give an analogy, consider the electrodes and the electrolyte as three tanks filled with fluid. We want to estimate the level of fluid in each tank just by measuring the difference in level between two tanks b and a which is

not possible. However the interrelations between a, b and c can be utilized to solve the observability problem.

Assuming c to remain constant we can immediately observe that there is no addition or removal of Li ions from the electrolyte. Thus due to mass conservation law, the addition of Li ions in the positive electrode will be equal to the removal of Li ions from the negative electrode. In short,

$$vol_n \left(c_{s,100-} - a\right) = vol_p \left(b - c_{s,100+}\right) \tag{5-2}$$

will hold true at any time, where vol_n is the total volume of the solid negative electrode and vol_b is the total volume of the solid positive electrode. In our case where the electrodes are not lumped still this relationship can be used to obtain the solid phase Li ion concentration at the positive electrode ($c_{s,avg+}$) from the solid phase Li ion concentration of the negative electrode ($c_{s,avg-}$) as,

$$\begin{aligned} c_{s,avg+} &= \frac{\delta_- \epsilon_{s-}}{\delta_+ \epsilon_{s+}} \left(c_{s,100-} - c_{s,avg-}\right) + c_{s,100+} \\ \text{say,} \quad c_{s,avg+} &= f_c \left(c_{s,avg-}\right) \end{aligned} \tag{5-3}$$

However in reality, the assumption that c i.e. $c_{e,avg}$ remains constant is not true. It remains close to the constant value $c_{e,0}$, and thus the relation (5-3) holds true with some variance.

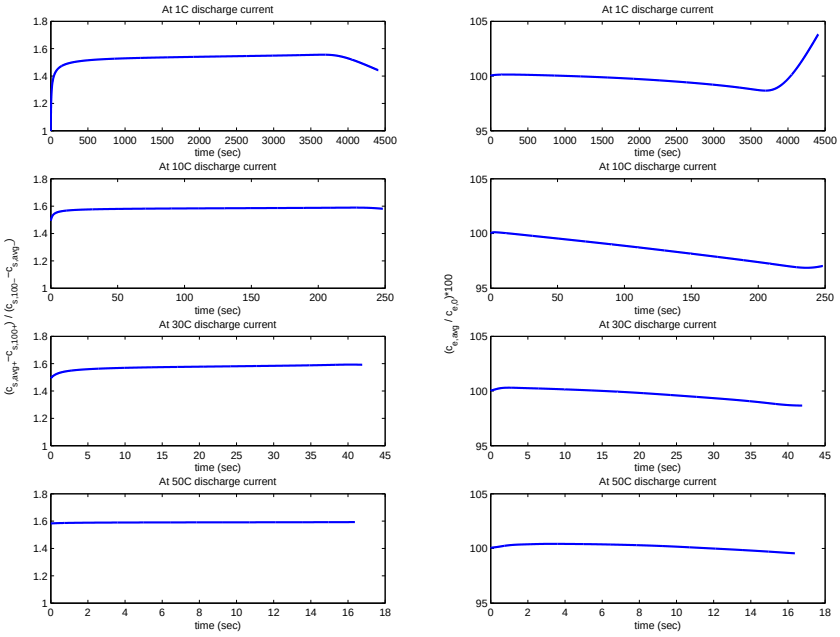

Figure 5-3: Co-relation between the solid phase average Li ion concentration of positive and negative electrode and percentage variance of electrolyte phase average Li^+ ion concentration about its nominal value

In a Kalman filter setting, these relations can be easily incorporated and the variance information can be utilized very easily, which will be shown in section 5-2, but first lets look at the validity of these relationships using simulations. We show in plots Figure 5-3 the ratio of $(c_{s,avg+} - c_{s,100+})$ to $(c_{s,100-} - c_{s,avg-})$ which should be equal to the ratio between the volume of solid active material particles at the negative electrode to the volume of solid active material particles at the positive electrode whose value is 1.5934 for the cell under consideration. Along with that the plots showing the percentage variance of $c_{e,avg}$ about its constant value are also shown.

From the plots we clearly observe that these are not hard relationships. If they were hard constrains, we would have used them at the modeling stage to either describe the model as a differential algebraic equation model or reduce the number of states by using these relations to obtain an observable model. In the next section we will use these relationships in open loop to add two fictitious sensors which makes the system observable and the variance of these sensors will be tuned using the variance of these relationships.

Further, the validity of these relationships is also tested with high rate charge and discharge current profile as shown in Figure 5-4. The ratio of $(c_{s,avg+} - c_{s,100+})$ to $(c_{s,100-} - c_{s,avg-})$ remains close to constant value in this case too. Note that its value is not shown in the rest periods inbetween. In these rest periods, since the SoC value reaches 100%, the numerator and the denominator terms of this ratio approach zero and thus the ratio of 0/0 has no validity in these regions. Again in this scenario we find that $c_{e,avg}$ remains close to its nominal value.

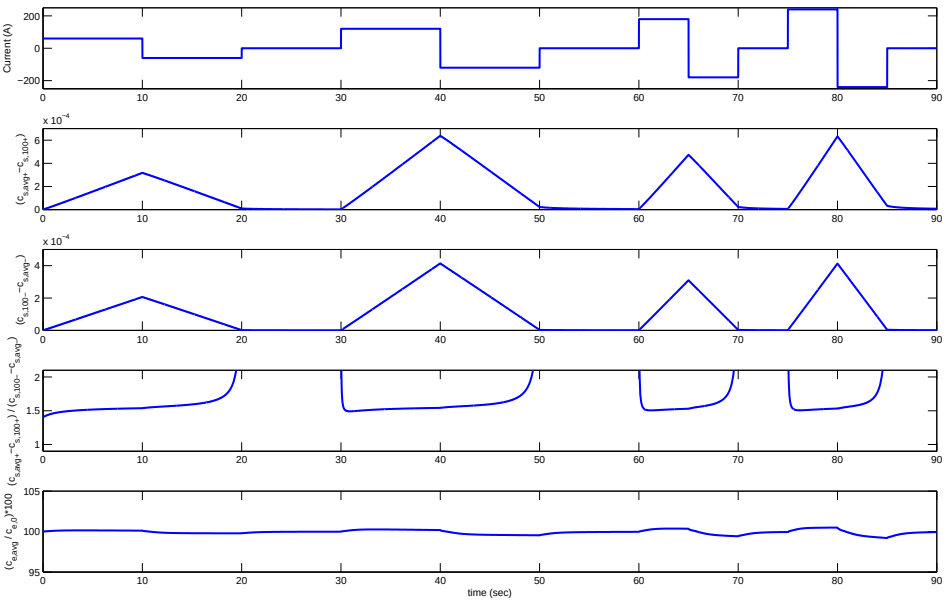

Figure 5-4: Co-relation between the solid phase average Li ion concentration of positive and negative electrode and percentage variance of electrolyte phase average Li^+ ion concentration about its nominal value for high rate dis/charge current profile

5-2 SoC Estimator

In this section, we'll develop an efficient SoC estimator utilizing the relationships developed in the last section to tackle the observability problem. The block diagram of the estimator is shown in Figure 5-5.

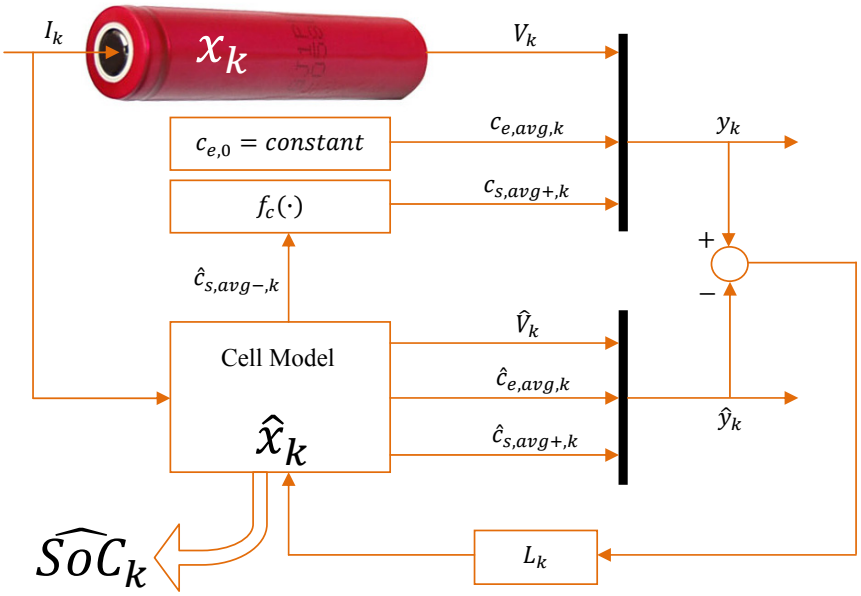

Figure 5-5: Block diagram of SoC estimator

From the cell, we only have one real measurable output that is the terminal voltage. An additional fictitious measurement can be considered as that of $c_{e,avg}$ which we know from the knowledge of the process to be near constant. Another additional fictitious measurement can be considered as $c_{s,avg+}$ which is derived from the one step ahead prediction of $c_{s,avg-}$ using the relation (5-3) in an open loop fashion. These three outputs are compared with the one step ahead prediction of the outputs from the model and the states are corrected using the optimal Kalman gain L_k. Using this three output approach, the system is fully observable (detectable in case of high discretizations) and an EKF does not diverge. This approach of fictitious measurements is nothing but adding relationships into the model in a different way, while keeping the actual measurement only one that is the terminal voltage.

Furthermore, the EKF algorithm used here is efficient $O(N)$ based on Chapter 3 shown in Figure 5-6. The algorithm starts with an initial estimate of state and error covariance $(\hat{x}_0^+, \Sigma_{\tilde{x},0}^+)$. Following that in the time update step, the model is simulated to generate an initial estimate of the next state and output $(\hat{x}_k^-, \hat{y}_k)$. Until now the steps are exactly similar to those shown in the previous chapter Figure 4-7 while simulating the cell model. Also at this

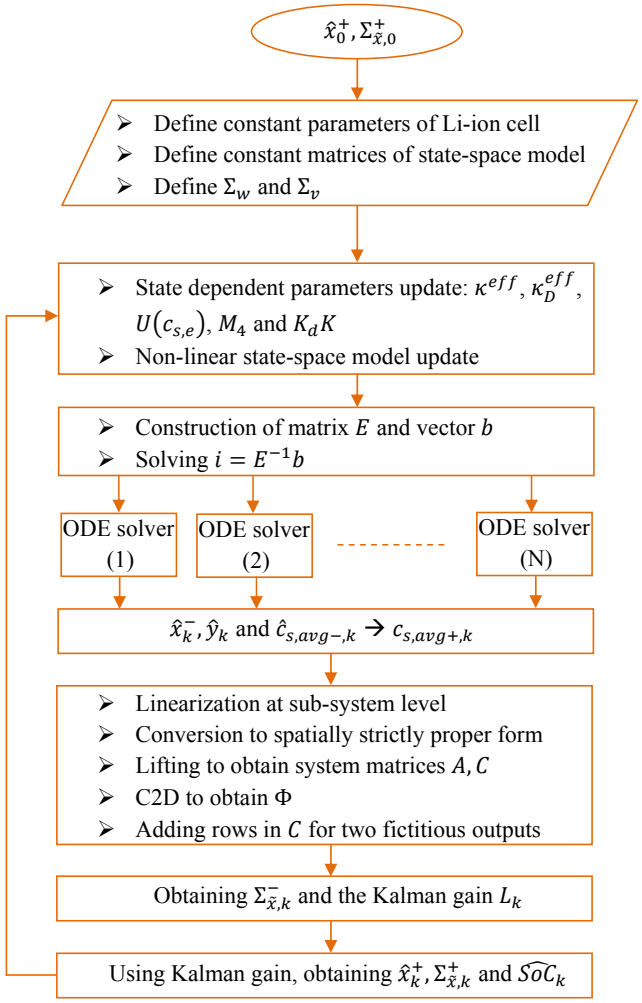

Figure 5-6: SoC estimation algorithm

step an estimate of $\hat{c}_{s,avg-,k}$ is made which is then used to obtain $c_{s,avg+,k}$ using relation (5-3). After this, linearization is performed at the sub-system level, the matrices are transformed to convert the linearized interconnected system as spatially strictly proper and then using these transformed matrices as generators, SSS form of lifted matrices A and C are obtained. Since the A matrix is obtained from linearization of continuous time state equation, it is converted to discrete time equivalent Φ using the structure preserving C2D conversion technique. Also additional rows are added to matrix C corresponding to the fictitious sensors: solid phase average Li ion concentration in the positive electrode and electrolyte phase average Li^+ ion concentration. Due to this the matrix C becomes unstructured however the "construct" function (section 2-4) of SSS Toolbox [13] is used to obtain an SSS structured representation of it. After obtaining the system matrices in SSS form, the EKF matrix computation steps are executed, first to obtain the Kalman gain L_k and then the corrected state estimate $\hat{x}_k^+$ along with its error covariance matrix $\Sigma_{\tilde{x},k}^+$. Finally an estimate of the state of charge $\widehat{SoC}_k$ is made from the corrected states. Here the SoC is derived using the equation (4-1) keeping the

positive electrode as reference since the equilibrium potential of positive electrode has more contribution in the measured output i.e. terminal voltage, leading to the states of positive electrode more observable than the states of negative electrode.

5-3 SoC Estimation Results

In this section, we will test the working of the SoC estimator and present the results. The simulator developed in the previous chapter is considered as a true system, used to obtain the measurement signal that is the terminal voltage and true SoC. The estimator is made to run in parallel with it. To test the validity of the estimator, the order of the simulator is chosen higher than that of the model used in the estimator. For the simulator, $N_r = 50$, $N_n = 5$, $N_p = 5$ and $N_s = 3$ while for the model in the estimator, $N_r = 40$, $N_n = 3$, $N_p = 3$ and $N_s = 3$. Further, the simulator is made to run at a higher frequency with $h = 0.005$ while the estimator is made to run with $h = 0.05$ thus the measurement signal is fed to the estimator every 10 samples. It was shown in section 4-6 that making these changes does have an effect on the output but the Kalman filter should be able to correct it. Apart from this model mismatch, an additive white Gaussian noise with a Signal to Noise ratio of 50dB is added to the measurement.

Tuning of the filter is done knowing the fact that $c_{e,avg}$ remains very close to $c_{e,0}$, maximum error of $\pm 3\%$ while the ratio of $(c_{s,avg+} - c_{s,100+})$ to $(c_{s,100-} - c_{s,avg-})$ varies a lot from its constant value, as high as $\pm 10\%$. The real measurement, terminal voltage is noisy but should be given more weight since it is the only real measurement from the system in this output injection scheme. Finally we choose Σ_v as $diag\left([1e0, 1e-3, 1e2]\right)$ where $y_k = [V_k, c_{e,avg,k}, c_{s,avg+,k}]^T$. The process noise is assumed to be low since the model is accurate and thus Σ_w is chosen as $1e-3 \times I$ while the initial state error covariance matrix is chosen high equal to $1e1 \times I$. We show here the results of estimation by applying a 10sec, 10C pulse discharge current profile starting from 100% SoC shown in Figure 5-7.

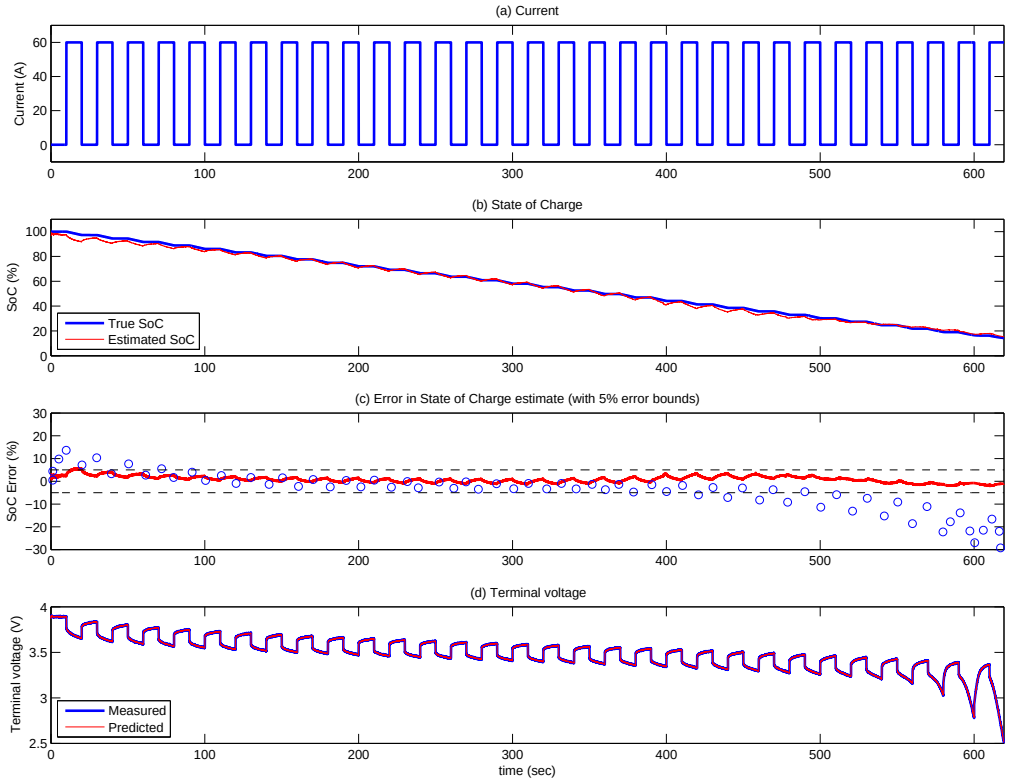

Figure 5-7: SoC estimation results with a 10sec, 10C pulse discharge current profile. Subplot (c) compares the SoC estimation error by this approach (-) against SoC estimation error from [8] with same current profile (o)

It can be observed that in the entire range, the SoC is estimated accurately. The RMS error in the entire range is only 1.63%. Here we started with an error in the initial condition of 3% and found that the filter converges in approximately 100sec. However since the number of states is very large, if started with larger difference in the initial condition, the convergence time will be higher. Though this is not a problem in the case of a battery, since during rest, when the gradients relax, the terminal voltage is directly a function of the SoC. This fact can be used to reset the filter following a rest period. These results seem very promising if we compare with the state of art. The same current profile was applied to an estimator developed in [8] based on the model found in [1]. It was found that the estimator is accurate ($\pm 5\%$) only in the middle SoC range as shown in subplot (c) of Figure 5-7. Moreover the estimator developed here even works with a very high dis/charge current profile as high as 50C shown in Figure 5-8.

In this whole range the RMS error of estimated SoC was found to be only 2.17% and the maximum error was found to be 5.5%. With this we show here the first ever SoC estimator developed to work accurately with dis/charge currents as high as 50C. Having found satisfactory results, in the following illustration, we investigate the time required per step by this EKF algorithm.

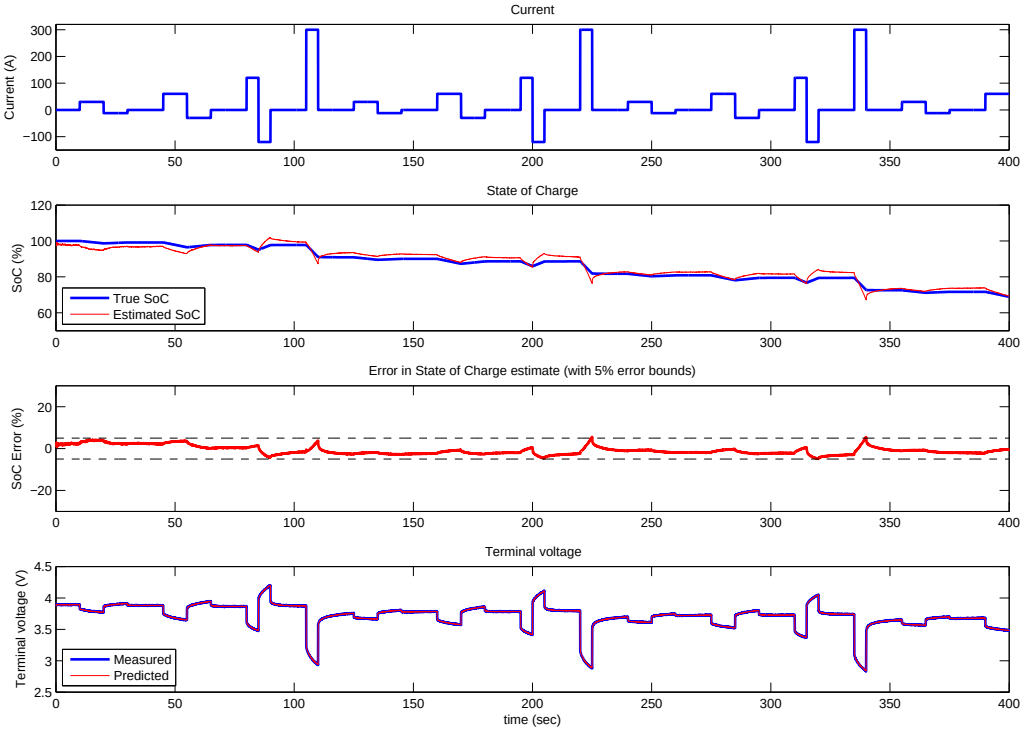

Figure 5-8: SoC estimation results with a transient dis/charge current profile upto 50C

It was found that the per step time required by this algorithm is 0.2sec. It was discussed in section 2-4 that at each SSS operation, the size of generator matrices increase, but the "reduce" function of the SSS toolbox [13] can be used to reduce the size with some loss of accuracy. This reduce function returns a compact SSS representation of a matrix. If this reduce function is not explicitly mentioned, after a few operations, a check is automatically applied to see if a reduction is necessary. If this is true, this function is called. However we can explicitly call the reduce function after each iteration to reduce the size of the generator matrices of the SSS matrix $\Sigma^{+}_{\tilde{x},k}$ before it is passed to the next time step. Here in this reduce function, a tolerance value can be set. It was found that setting this tolerance value high results into a more compact form representation with some loss of accuracy which results into lower accuracy of estimation results. By setting higher value of this tolerance, it was found that the convergence time of the estimated variable increases, but there is some gain in the computational cost. To show this effect, a high tolerance value of $5e3$ was set and the estimation of SoC was carried out with the same current profile as Figure 5-8. The SoC estimation accuracy in this case only changed marginally, with RMS error of 2% and maximum error of 8% while the computation time required per step reduced to 0.147sec. A comparison is shown in Figure 5-9.

It can be clearly observed that with a little loss of accuracy, a gain in computational cost can be achieved and the tolerance of the reduce function can be tuned to achieve a balance between computational cost and accuracy. With the current computational cost requirement, it can

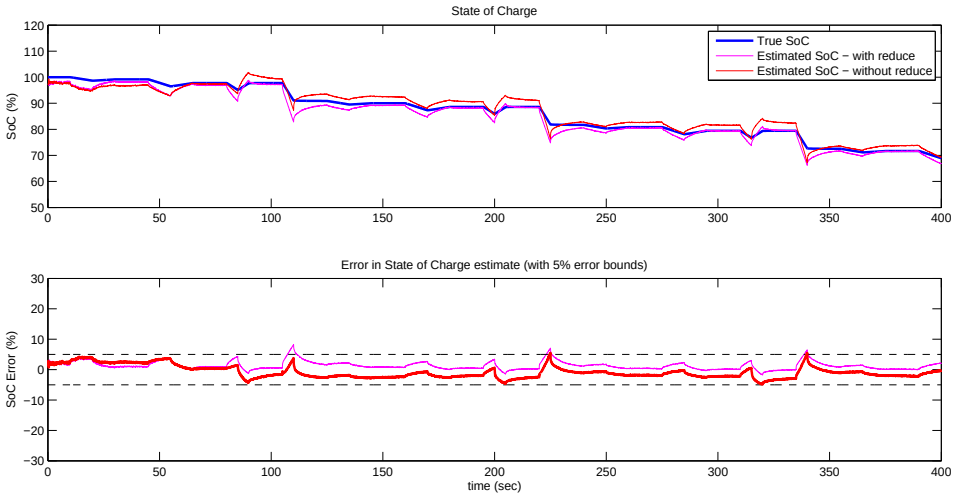

Figure 5-9: SoC estimation results with and without explicitly using the reduce function

be concluded that a real-time implementation is possible at 20Hz with the need for parallel processing which can be done since the algorithm is 6 times parallelizable. However with further optimization of software and utilizing the structure also within each sub-system, there is enough potential to reduce the computational cost further. We conclude this section by showing that the computational cost of this algorithm grows linearly with higher discretization along x in Figure 5-10, thus achieving a full $O(N)$ computational complexity EKF.

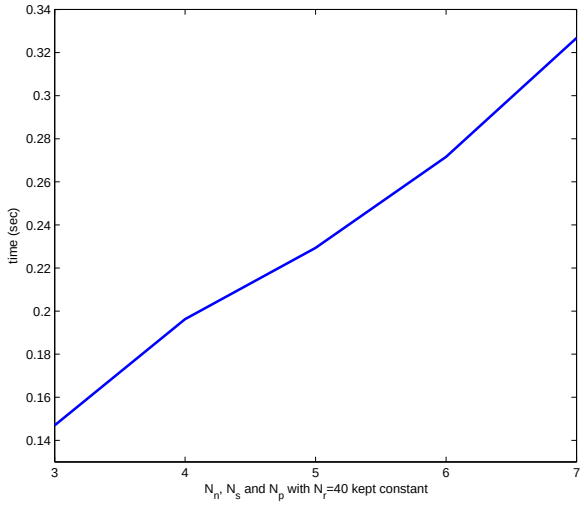

Figure 5-10: Computational cost per step required by the efficient EKF algorithm for different discretization levels

5-4 Conclusion and Discussion

We started with the observability analysis of the Li-ion cell modeled as spatially distributed string interconnected system and found loss of observability. However the problem was solved understanding the processes inside the cell and the inter-relation between variables. An efficient SoC Estimator was then developed based on Chapter 3 and the estimation results were found to be satisfactory. Even with a very high transient dis/charge current profile upto 50C, the RMS SoC estimation error was found to be only 2%. The model used in the estimator is of high order but still due to efficient techniques, the computational cost per step was found to reasonable enough for a real-time implementation at 20Hz and there is a scope of further improvement, using a 2D approach exploiting the structure also within each sub-system. With the Li-ion cell as an example, we developed and validated a full $O(N)$ computational complexity EKF algorithm which can be used for other spatially distributed string interconnected systems. For interconnected systems where the number of sub-systems is very high, this algorithm can have huge computational cost benefit.

Chapter 6

Conclusion and Recommendations

6-1 Conclusion

The main contribution of this thesis is the development of **new State of Charge (SoC) estimation algorithm** for a Lithium ion (Li-ion) cell based on fundamental electrochemical equations, which works accurately with high transient dis/charge current profiles and has a reasonable computational cost. This has been achieved by deriving an explicit non-linear state space representation of every element of a spatially discretized model of the cell. Then the cell is viewed as a spatially distributed string interconnected system with these elements as sub-systems exchanging information by means of interconnecting variables. Exploiting the structure of this system, efficient state-estimation algorithm has been developed to reduce the computational cost.

It was found from the literature review that discretization of the non-linear Partial Differential Equations (PDE) and then solution of the resulting set of ordinary differential equations can result in an accurate SoC estimate, however it is highly computationally expensive, slow and possibly non-convergent due to implicit relationships and thus prohibiting its real-time implementation. The model developed in this thesis is also based on discretization of PDEs and thus provides highly accurate SoC estimates, but at the same time since the model is developed as spatially distributed string interconnected system with each sub-system modeled in explicit state-space form, efficient state-estimation algorithm can be utilized resulting into low, fixed computation time. Thus achieving **high accuracy with low computational cost**. It is shown in [9] that iterative algorithms can take as high as 2.8sec of computation time in order to obtain the SoC at a particular time. The efficient algorithm developed in this thesis only requires less than 0.15sec of computation time per step. Further the algorithm is parallelizable up to 6 times and thus an online implementation up to 40Hz is possible. When tested at 20Hz with a very high transient dis/charge current profile up to 50C, an RMS SoC estimation error of around 2% was obtained.

Apart from accuracy and efficiency, another major advantage of this approach is that all the **variables have physical meaning** and their spatial position has been retained. This enables

the estimation of many other variables along with SoC, for instance the electrolyte phase Li ion concentration and its gradient along the length of the cell. With this the depletion of Li ion concentration in the electrolyte phase can be estimated and sudden loss of power can be avoided. Using these additional parameters a more effective battery management system can be built. It is mentioned in [20] that to avoid damaging side reactions, the solid/electrolyte phase potential difference must be maintained within constraints. The algorithm developed here can be used to estimate this potential difference as well, along the whole length of the cell and this information can be fed to a battery management system in order to develop strategies to increase the life of the battery pack.

Taking Li-ion cell as an example, it is shown that the efficient state-estimation algorithm developed in this thesis has $O(N)$ computational complexity. This **efficient state-estimation algorithm can be used for many other PDE systems** or systems which are inherently spatially distributed in a string interconnected form. The gain in computational cost will be higher as the number of sub-systems N grow, since traditional unstructured algorithms approach $O(N^3)$ computational complexity. Also an efficient simulation scheme is shown for such interconnected systems which even works with systems whose representation is not spatially strictly proper, under certain assumptions. $O(N)$ computational complexity of this simulation scheme is also shown.

6-2 Recommendations

Many recommendations for further research, to improve this approach will be discussed. Also the potential application of some techniques developed here will be shown.

1. To further improve the efficiency of this algorithm, a **two dimensional structured approach** is proposed wherein the structure of the model of each sub-system in the interconnected scheme is also exploited. This may have great potential in the case of a Li-ion cell since the model of each discretized part is largely linear except the last two states as discussed in section 4-7.

2. While developing efficient time update step of an Extended Kalman Filter (EKF), zero order hold of the interconnecting variables was assumed in section 3-2. As an improvement, a first or higher order hold scheme can be utilized.

3. Here we propose a centralized kalman filter scheme to estimate the states. Since the sub-systems are decoupled and the interconnecting variables are only evaluated at each time instance, a distributed kalman filter implementation can also be done. With this approach, utilizing the structure within each sub-system can become simple.

4. The measurement update step was implemented in section 3-4 using classical EKF algorithm however a **square root algorithm** as shown in [14] can be more efficient. An implementation of square root algorithm utilizing the Sequentially Semi Separable (SSS) structure needs to be investigated.

5. The volumetric rate of electrochemical reaction at the solid/ electrolyte interface (j^{Li}) is coupled to c_e which is ignored in this model. As an improvement, the expression for j^{Li}

in each discretized part can be updated based on c_e. This can have major improvement in cells where large gradient of electrolyte phase Li^+ ion concentration is formed.

6. The **effect of temperature and State of Health (SoH)** of the cell are not considered in this work. Energy balance equations [18] can be added to the model to incorporate temperature information. Additionally a temperature sensor can be proposed for the cell along with a sensor for terminal voltage. Further, model parameters can be adapted to take into account the ageing of the cell, counting the number of dis/charge cycles that the cell has undergone using some intelligent logic.

7. The EKF used in this work is based on relationships between some variables in open loop to tackle observability issues as discussed in section 5-1. These are not hard relationships and thus **robust or adaptive kalman filter** schemes can be developed to improve the SoC estimates.

8. The tuning of this filter was done on ad-hoc basis however a more optimized tuning can be done to improve the noise rejection capability and decrease the convergence time of the estimates.

9. All the timing analysis were done in Matlab, however for accurate timing analysis, an embedded processor with a real-time operation system is recommended. There is a lot of scope for software optimization and reduction of computational cost further, for instance, look-up tables can be used for some computationally expensive non-linear functions. Further, dedicated hardware like a dedicated processer for fast SSS computation can be implemented on a real system.

10. In this whole work, a One Dimensional (1D) electrochemical model is considered. This work can be extended to 2D or 3D electrochemical models. A structured approach for these high dimensional systems need to be developed.

11. Some steps of this efficient EKF algorithm like the time update step can even be used in Sigma Point Kalman Filter or the Particle Filters. Non-linear simulation is the first step of all these state estimation algorithms which can be done efficiently using the technique presented here. However the further steps differ and more research needs to be done to make them efficient for interconnected systems.

Appendix A

Conversion to Spatially Strictly Proper Form

Here we show how to convert a linear interconnected system into spatially strictly proper form. This technique has been taken from [11] and is extended with exogenous inputs and outputs.

The technique of change of variables is shown in [11] for autonomous systems with state-space realization as,

$$\Sigma_s : \quad \begin{bmatrix} \dot{x}_s \\ v^p_{s-1} \\ v^m_{s+1} \end{bmatrix} = \begin{bmatrix} A_s & B^p_s & B^m_s \\ C^p_s & W^p_s & Z^m_s \\ C^m_s & Z^p_s & W^m_s \end{bmatrix} \begin{bmatrix} x_s \\ v^p_s \\ v^m_s \end{bmatrix} \tag{A-1}$$

First Z^p_s term is eliminated through a change of variable and also transformation of system matrices, then Z^m_s is eliminated through another change of variables. To use the same technique with exogenous inputs and outputs as well, we augment the state vector with inputs and derivative of state vector with outputs,

$$\Sigma_s : \quad \begin{bmatrix} \begin{bmatrix} \dot{x}_s \\ y_s \end{bmatrix} \\ v^p_{s-1} \\ v^m_{s+1} \end{bmatrix} = \begin{bmatrix} \begin{bmatrix} A_s & B^2_s \\ C^2_s & D^{22}_s \end{bmatrix} & \begin{bmatrix} B^p_s \\ H^p_s \end{bmatrix} & \begin{bmatrix} B^m_s \\ H^m_s \end{bmatrix} \\ \begin{bmatrix} C^p_s & V^p_s \end{bmatrix} & W^p_s & Z^m_s \\ \begin{bmatrix} C^m_s & V^m_s \end{bmatrix} & Z^p_s & W^m_s \end{bmatrix} \begin{bmatrix} \begin{bmatrix} x_s \\ u_s \end{bmatrix} \\ v^p_s \\ v^m_s \end{bmatrix} \tag{A-2}$$

then the same transformation steps are applied on these block matrices. The algebra works in this situation as well, since we have grouped together the variables that will remain unchanged

during this transformation on the left hand side as well as on the right hand side of the equation. We illustrate the steps here.

First do forward iteration to obtain $\tilde{Q}_s \ \forall s \in \{1, 2, \ldots, N-1\}$ using,

$$\begin{gathered} \tilde{Q}_{s+1} = Z_s^p + W_s^m \Big(I - \tilde{Q}_s Z_s^m\Big)^{-1} \tilde{Q}_s W_s^p \\ \text{with initial condition, } \ \tilde{Q}_1 = 0 \end{gathered} \tag{A-3}$$

During this iteration, the inverse of $\Big(I - \tilde{Q}_s Z_s^m\Big)$ will exist only if the system is "well posed".

Then define $\tilde{Z}_s^m = \Big(I - \tilde{Q}_s Z_s^m\Big)^{-1}$ and $\tilde{Z}_s^p = \Big(I - Z_s^m \tilde{Q}_s\Big)^{-1}$.

Now performing first round of change of variables,

$$\acute{\Sigma}_s : \begin{bmatrix} \begin{bmatrix} \dot{x}_s \\ y_s \end{bmatrix} \\ v_{s-1}^p \\ \acute{v}_{s+1}^m \end{bmatrix} = \begin{bmatrix} \begin{bmatrix} \acute{A}_s & \acute{B}_s^2 \\ \acute{C}_s^2 & \acute{D}_s^{22} \end{bmatrix} & \begin{bmatrix} \acute{B}_s^p \\ \acute{H}_s^p \end{bmatrix} & \begin{bmatrix} \acute{B}_s^m \\ \acute{H}_s^m \end{bmatrix} \\ \begin{bmatrix} \acute{C}_s^p & \acute{V}_s^p \end{bmatrix} & \acute{W}_s^p & \acute{Z}_s^m \\ \begin{bmatrix} \acute{C}_s^m & \acute{V}_s^m \end{bmatrix} & 0 & \acute{W}_s^m \end{bmatrix} \begin{bmatrix} \begin{bmatrix} x_s \\ u_s \end{bmatrix} \\ v_s^p \\ \acute{v}_s^m \end{bmatrix}$$

$$\text{where, } \ \acute{A}_s = \Big[A_s + B_s^m \tilde{Z}_s^m \tilde{Q}_s C_s^p\Big], \ \ \acute{B}_s^2 = \Big[B_s^2 + B_s^m \tilde{Z}_s^m \tilde{Q}_s V_s^p\Big], \ \ \acute{C}_s^2 = \Big[C_s^2 + H_s^m \tilde{Z}_s^m \tilde{Q}_s C_s^p\Big],$$

$$\acute{D}_s^{22} = \Big[D_s^{22} + H_s^m \tilde{Z}_s^m \tilde{Q}_s V_s^p\Big], \ \ \acute{B}_s^p = \Big[B_s^p + B_s^m \tilde{Z}_s^m \tilde{Q}_s W_s^p\Big], \ \ \acute{H}_s^p = \Big[H_s^p + H_s^m \tilde{Z}_s^m \tilde{Q}_s W_s^p\Big],$$

$$\acute{C}_s^m = \Big[C_s^m + W_s^m \tilde{Z}_s^m \tilde{Q}_s C_s^p\Big], \ \ \acute{V}_s^m = \Big[V_s^m + W_s^m \tilde{Z}_s^m \tilde{Q}_s V_s^p\Big], \ \ \acute{B}_s^m = B_s^m \tilde{Z}_s^m, \ \ \acute{H}_s^m = H_s^m \tilde{Z}_s^m,$$

$$\acute{C}_s^p = \tilde{Z}_s^p C_s^p, \ \ \acute{V}_s^p = \tilde{Z}_s^p V_s^p, \ \ \acute{Z}_s^m = \tilde{Z}_s^p Z_s^m, \ \ \acute{W}_s^p = \tilde{Z}_s^p W_s^p, \ \ \acute{W}_s^m = W_s^m \tilde{Z}_s^m \tag{A-4}$$

With this conversion, the system is spatially strictly proper in one direction. Now perform the backward Stein iteration[1] $\forall i \in \{N, N-1, \ldots, 2\}$,

$$\begin{gathered} \breve{Z}_{i-1} = \acute{Z}_i^m + \acute{W}_i^p \breve{Z}_i \acute{W}_i^m \\ \text{with initial condition, } \ \breve{Z}_N = 0 \end{gathered} \tag{A-5}$$

Now performing second round of change of variables,

[1] Note that there is a typographical error in the subscripts of this iteration in [11] which is corrected here

$$\hat{\Sigma}_s : \begin{bmatrix} \begin{bmatrix} \dot{x}_s \\ y_s \end{bmatrix} \\ \hat{v}^p_{s-1} \\ \hat{v}^m_{s+1} \end{bmatrix} = \begin{bmatrix} \begin{bmatrix} \hat{A}_s & \hat{B}^2_s \\ \hat{C}^2_s & \hat{D}^{22}_s \end{bmatrix} & \begin{bmatrix} \hat{B}^p_s \\ \hat{H}^p_s \end{bmatrix} & \begin{bmatrix} \hat{B}^m_s \\ \hat{H}^m_s \end{bmatrix} \\ \begin{bmatrix} \hat{C}^p_s & \hat{V}^p_s \end{bmatrix} & \hat{W}^p_s & 0 \\ \begin{bmatrix} \hat{C}^m_s & \hat{V}^m_s \end{bmatrix} & 0 & \hat{W}^m_s \end{bmatrix} \begin{bmatrix} \begin{bmatrix} x_s \\ u_s \end{bmatrix} \\ \hat{v}^p_s \\ \hat{v}^m_s \end{bmatrix} \tag{A-6}$$

where, $\hat{A}_s = \acute{A}_s + \acute{B}^p_s \breve{Z}_s \acute{C}^m_s$, $\hat{B}^2_s = \acute{B}^2_s + \acute{B}^p_s \breve{Z}_s \acute{V}^m_s$, $\hat{C}^2_s = \acute{C}^2_s + \acute{H}^p_s \breve{Z}_s \acute{C}^m_s$,

$\hat{D}^{22}_s = \acute{D}^{22}_s + \acute{H}^p_s \breve{Z}_s \acute{V}^m_s$, $\hat{B}^m_s = \acute{B}^m_s + \acute{B}^p_s \breve{Z}_s \acute{W}^m_s$, $\hat{H}^m_s = \acute{H}^m_s + \acute{H}^p_s \breve{Z}_s \acute{W}^m_s$,

$\hat{C}^p_s = \acute{C}^p_s + \acute{W}^p_s \breve{Z}_s \acute{C}^m_s$, $\hat{V}^p_s = \acute{V}^p_s + \acute{W}^p_s \breve{Z}_s \acute{V}^m_s$, $\hat{B}^p_s = \acute{B}^p_s$, $\hat{H}^p_s = \acute{H}^p_s$,

$\hat{C}^m_s = \acute{C}^m_s$, $\hat{V}^m_s = \acute{V}^m_s$, $\hat{W}^p_s = \acute{W}^p_s$, $\hat{W}^m_s = \acute{W}^m_s$,

Thus leading to a spatially strictly proper form.

Appendix B

Model Parameters for Li-ion Cell

(a) Universal constants:

Faraday's constant, F (C/mol)	$96,487$
Universal gas constant, R (J/mol K)	8.3143

(b) Discretization, geometry and volume fractions:

Parameter	**Negative electrode**	**Separator**	**Positive electrode**
Number of discretized parts along x	N_n	N_s	N_p
Number of discretized parts along r	N_{r_-}		N_{r_+}
Thickness, δ (cm)	50×10^{-4}	25.4×10^{-4}	36.4×10^{-4}
Particle radius, R_s (cm)	1×10^{-4}		1×10^{-4}
Thickness of a discretized part of the sphere, Δr (cm)	R_{s_-}/N_{r_-}		R_{s_+}/N_{r_+}
Active material volume fraction, ϵ_s	0.58		0.5
Electrolyte phase volume fraction, ϵ_e	0.332	0.5	0.330
Thickness of a discretized part along x, Δx (cm)	$R_{s_-}\left(\frac{4\pi}{3\epsilon_{s_-}}\right)^{1/3}$	$\frac{\delta_{sep}}{N_s}$	$R_{s_+}\left(\frac{4\pi}{3\epsilon_{s_+}}\right)^{1/3}$
Interfacial surface area, a_s (cm^{-1})	$\left(\frac{\delta_-}{N_n \Delta x_-}\right)\left(\frac{3\epsilon_{s_-}}{R_{s_-}}\right)$		$\left(\frac{\delta_+}{N_p \Delta x_+}\right)\left(\frac{3\epsilon_{s_+}}{R_{s_+}}\right)$

Note: At the negative and positive electrode, Δx represents the average distance between spherical active material particles. Its value is calculated here by fitting the volume of a cube of length Δx times the active material volume fraction to the volume of a sphere of radius R_s assuming uniform distribution of spherical particles in all three dimensions.

(c) Li^+ concentrations:

Parameter	**Negative electrode**	**Separator**	**Positive electrode**
Maximum solid phase concentration, $c_{s,max}$ (mol cm^{-3})	16.1×10^{-3}		23.9×10^{-3}
Stoichiometry at 0% SoC, $\theta_{0\%}$	0.126		0.936
Stoichiometry at 100% SoC, $\theta_{100\%}$	0.676		0.442
Average electrolyte concentration, c_e (mol cm^{-3})	1.2×10^{-3}		

(d) Kinetic and transport properties:

Parameter	**Negative electrode**	**Separator**	**Positive electrode**
Exchange current density, j_0 (A cm^{-2})	3.6×10^{-3}		2.6×10^{-3}
Charge-transfer coefficients, $\alpha_a,\ \alpha_c$	0.5, 0.5		0.5, 0.5
Solid phase Li diffusion coefficient, D_s (cm^2 s^{-1})	2×10^{-12}		3.7×10^{-12}
Solid phase conductivity, σ (S cm^{-1})	1.0		0.1
Solid phase effective conductivity, σ^{eff} (S cm^{-1})	$\sigma_- \epsilon_{s_-}$		$\sigma_+ \epsilon_{s_+}$
Bruggeman porosity exponent, p	1.5	1.5	1.5
Electrolyte phase Li^+ diffusion coefficient, D_e (cm^2 s^{-1})	2.6×10^{-6}		
Electrolyte phase effective diffusion coefficient, D_e^{eff} (cm^2 s^{-1})	$D_e \epsilon_{e_-}^{p_-}$	$D_e \epsilon_{e_{sep}}^{p_{sep}}$	$D_e \epsilon_{e_+}^{p_+}$
Electrolyte phase ionic conductivity, κ (S cm^{-1})	$\kappa = 15.8\ c_e\ exp[0.85(1000 c_e)^{1.4}]$		
Electrolyte phase effective ionic conductivity, κ^{eff} (S cm^{-1})	$\kappa \epsilon_{e_-}^{p_-}$	$\kappa \epsilon_{e_{sep}}^{p_{sep}}$	$\kappa \epsilon_{e_+}^{p_+}$
Li^+ transference number, t_+^0	0.363		
Effective diffusional conductivity, κ_D^{eff}	$\frac{2\left(t_+^0 - 1\right) RT \kappa_-^{eff}}{F}$	$\frac{2\left(t_+^0 - 1\right) RT \kappa_{sep}^{eff}}{F}$	$\frac{2\left(t_+^0 - 1\right) RT \kappa_+^{eff}}{F}$

(e) Plate area-specific parameters and temperature:

Electrode plate area, A (cm^2)	$10,452$
Current collector contact resistance, R_f (Ω cm^2)	20
Temperature, T (K)	298

Bibliography

[1] K. A. Smith, C. D. Rahn, and C.-Y. Wang, "Control oriented 1D electrochemical model of lithium ion battery," *Energy Conversion and Management*, vol. 48, no. 9, pp. 2565 – 2578, 2007.

[2] F. Codecà, *Analysis and Development of Electric Vehicles: Modeling of Li-ion Batteries and Control of Vehicle Dynamics*. PhD thesis, Politecnico di Milano, 2008.

[3] F. Zhang, G. Liu, and L. Fang, "A battery state of charge estimation method with extended kalman filter," *IEEE/ASME International Conference on Advanced Intelligent Mechatronics*, pp. 1008 – 1013, Jul 2008.

[4] J. Lee, O. Nam, and B. Cho, "Li-ion battery SoC estimation method based on the reduced order extended kalman filtering," *Journal of Power Sources*, vol. 174, no. 1, pp. 9 – 15, 2007.

[5] A. J. Salkind, C. Fennie, P. Singh, T. Atwater, and D. E. Reisner, "Determination of state-of-charge and state-of-health of batteries by fuzzy logic methodology," *Journal of Power Sources*, vol. 80, no. 1-2, pp. 293 – 300, 1999.

[6] G. L. Plett, "Kalman-filter SoC estimation for LiPB HEV cells," *CD-ROM Proceedings of the 19th Electric Vehicle Symposium (EVS19), Busan Korea,*, Oct 2002.

[7] G. L. Plett, "Extended kalman filtering for battery management systems of LiPB-based HEV battery packs: Part 3. state and parameter estimation," *Journal of Power Sources*, vol. 134, no. 2, pp. 277 – 292, 2004.

[8] K. A. Smith, C. D. Rahn, and C.-Y. Wang, "Model-based electrochemical estimation of lithium-ion batteries," *17th IEEE International Conference on Control Applications*, pp. 714 – 719, Sep 2008.

[9] S. Santhanagopalan and R. E. White, "State of charge estimation using an unscented filter for high power lithium ion cells," *International Journal of Energy Research*, vol. 34, no. 2, pp. 152 – 163, Feb 2010.

[10] J. Rice, *Efficient Algorithms for Distributed Control: A Structured Matrix Approach*. PhD thesis, Delft University of Technology, 2010.

[11] J. K. Rice and M. Verhaegen, "Distributed control: A sequentially semi-separable approach for spatially heterogeneous linear systems," *IEEE Transactions on Automatic Control*, vol. 54, no. 6, pp. 1270 – 1283, Jun 2009.

[12] R. D'Andrea and G. E. Dullerud, "Distributed control design for spatially interconnected systems," *IEEE Transactions on Automatic Control*, vol. 48, no. 9, pp. 1478 – 1495, 2003.

[13] DCSC, TU Delft, "Sequentially semi-separable matrix toolbox (version 0.8, 20-may-2011)." Available at http://www.dcsc.tudelft.nl/~datadriven/sss/ssstoolbox_product_page.html Last accessed: Jun 11, 2011.

[14] M. Verhaegen and V. Verdult, *Filtering and System Identification, A Least Squares Approach*. Cambridge University Press, 2007.

[15] C. Scherer, "Control theory - lecture slides." Delft Center for Systems and Control (DCSC), Delft University of Technology.

[16] T. F. Fuller, M. Doyle, and J. Newman, "Simulation and optimization of the dual lithium ion insertion cell," *Journal of the Electrochemical Society*, vol. 141, pp. 1 – 10, 1994. Selected papers presented at the 11th International Meeting on Lithium Batteries.

[17] D. D. Domenico, G. Fiengo, and A. Stefanopoulou, "Lithium-ion battery state of charge estimation with a kalman filter based on a electrochemical model," *IEEE International Conference on Control Applications*, pp. 702 – 707, 2008.

[18] W. Gu and C. Wang, "Thermal and electrochemical coupled modeling of a lithium-ion cell, in lithium batteries," *ECS Proceedings*, vol. 99 - 25 (1), pp. 748–762, 2000.

[19] S. Santhanagopalan, Q. Zhang, K. Kumaresan, and R. E. White, "Parameter estimation and life modeling of lithium-ion cells," *Journal of the Electrochemical Society*, vol. 155, no. 4, pp. A345 – A353, 2008.

[20] K. A. Smith, C. D. Rahn, and C.-Y. Wang, "Model-based electrochemical estimation and constraint management for pulse operation of lithium ion batteries," *IEEE Transactions on Control Systems Technology*, vol. 18, pp. 654 – 663, May 2010.

Glossary

List of Acronyms

DCSC	Delft Center for Systems and Control
Li-ion	Lithium ion
SoC	State of Charge
SSS	Sequentially Semi Separable
1D	One Dimensional
EKF	Extended Kalman Filter
RMS	Root Mean Square
SoH	State of Health
PDE	Partial Differential Equation
SISO	Single Input Single Output
LTV	Linear Time Varying
DoD	Depth of Discharge